相対性理論

アインシュタインはどこまで正しいのか

１．序論
２．特殊相対性理論
　時間の進み方は観測者によって異なる　　干渉計
　$E=mc^2$，原子核反応，星の一生　　GPS
３．一般相対性理論　　光格子時計
　時間の進み方は重力によって異なる
　ブラックホール，重力波，重力波のデータ解析

真貝寿明（しんかい ひさあき）
大阪工業大学 情報科学部 教授
武庫川女子大学 非常勤講師
理化学研究所 客員研究員
http://www.oit.ac.jp/is/shinkai/

references

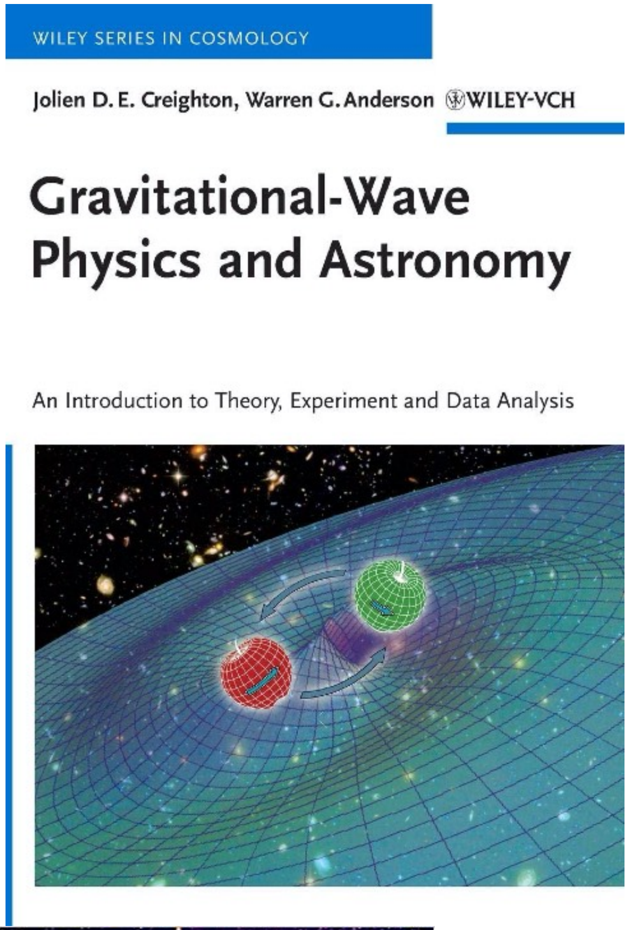

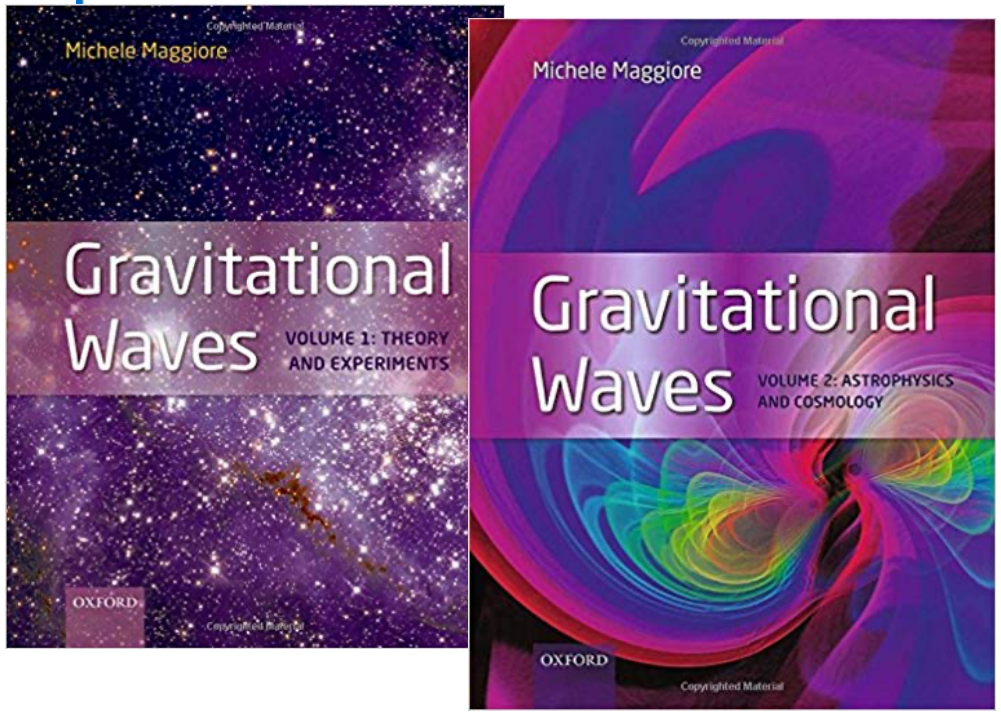

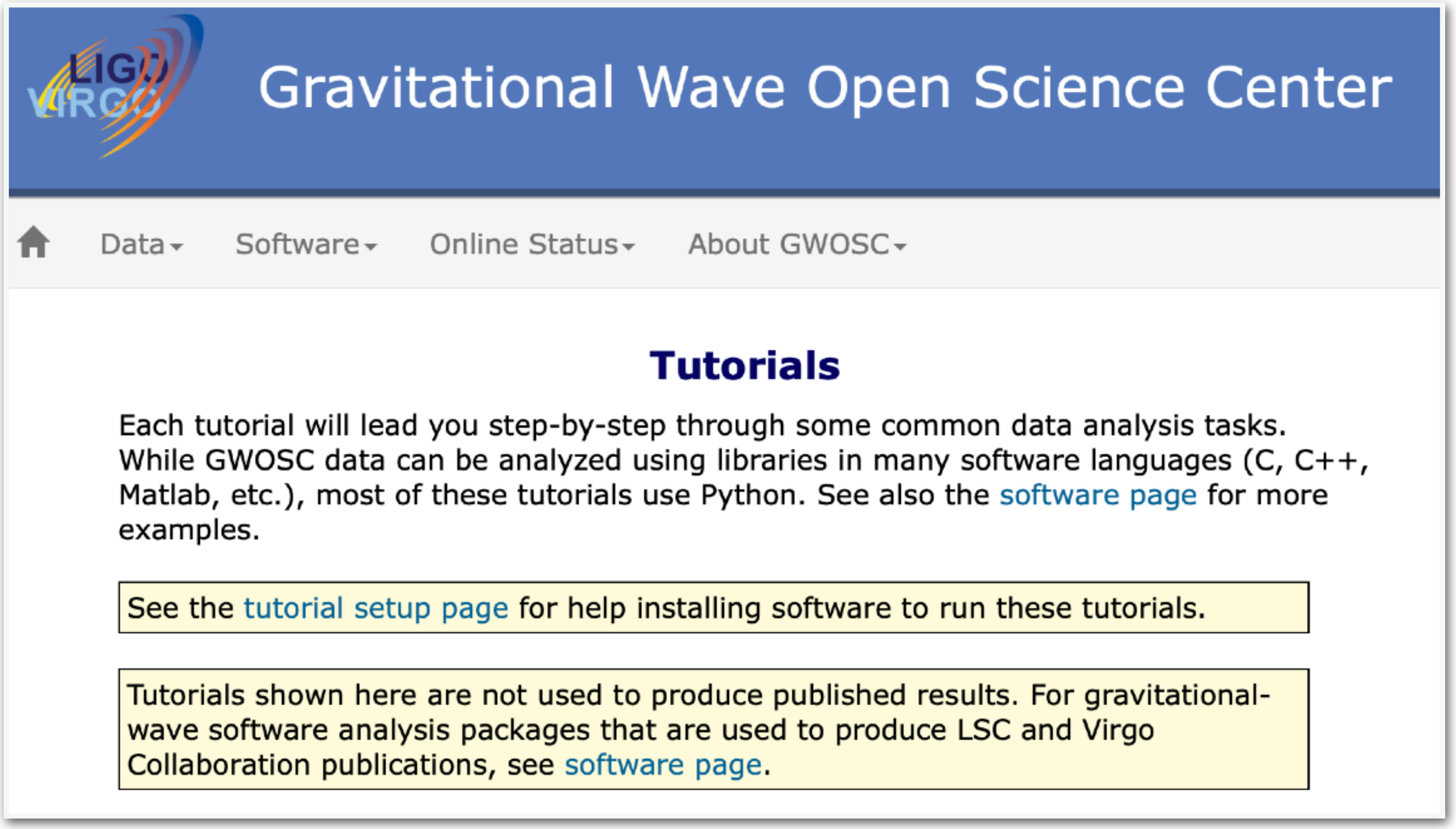

https://www.gw-openscience.org/tutorials/

references

370 システム/制御/情報，Vol. 62, No. 9, pp. 370–375, 2018

解　説

重力波の直接検出とデータ解析

真貝　寿明*

一般社団法人
ISCIE システム制御情報学会
The Institute of Systems, Control and Information Engineers

https://www.iscie.or.jp/pub/journal

http://www.oit.ac.jp/is/shinkai/

◆◆◆◆ **解説** ◆◆◆◆

重力波の観測とデータ解析

日本物理学会誌　Vol. 72, No. 3, 2017

田 越 秀 行
大阪市立大学大学院理学研究科
tagoshi@sci.osaka-cu.ac.jp

伊 藤 洋 介
東京大学大学院理学系研究科附属ビッグバン宇宙国際研究センター
yousuke_itoh@resceu.s.u-tokyo.ac.jp

端 山 和 大
東京大学宇宙線研究所重力波観測研究施設
hayama@icrr.u-tokyo.ac.jp

428 | 情報処理 Vol.57 No.5 May 2016

特別解説

重力波の初検出と情報処理技術

—LIGO と KAGRA で活用されている情報処理技術—

Kipp Cannon [*1]　端山和大 [*1]　伊藤洋介 [*1]　高橋弘毅 [*2]
[*1] 東京大学
[*2] 長岡技術科学大学

重力波
Gravitational Wave

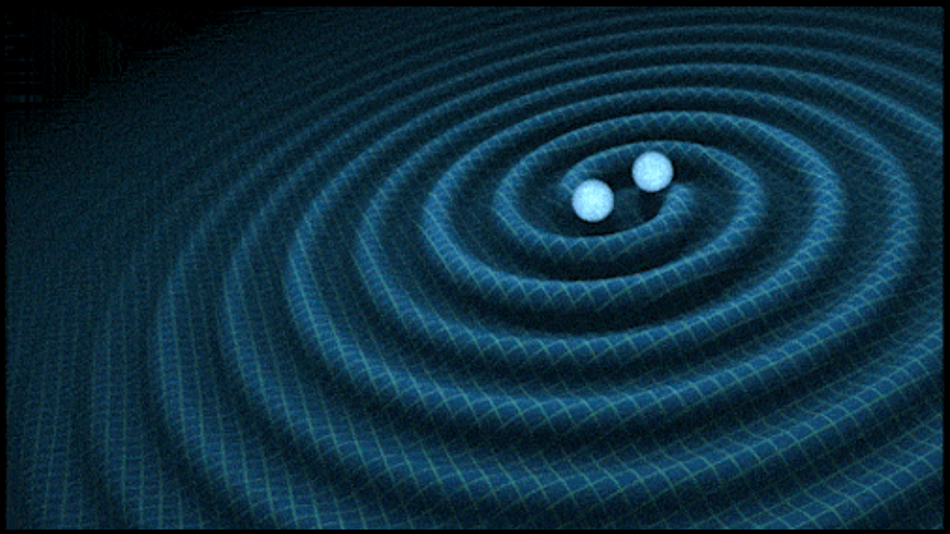

- アインシュタインは，電磁波との類推から重力波の存在を予言した．しかし，後に重力波は存在しないかも，という論文を書きかけた．
- 1968年，ウェーバーによる重力波検出は幻とされた．
- 1974年，連星中性子星の発見によって，重力波の存在が間接的に証明された．
- 100年経った2015年，ブラックホールが連星を形成して合体することが，重力波によって確認された．

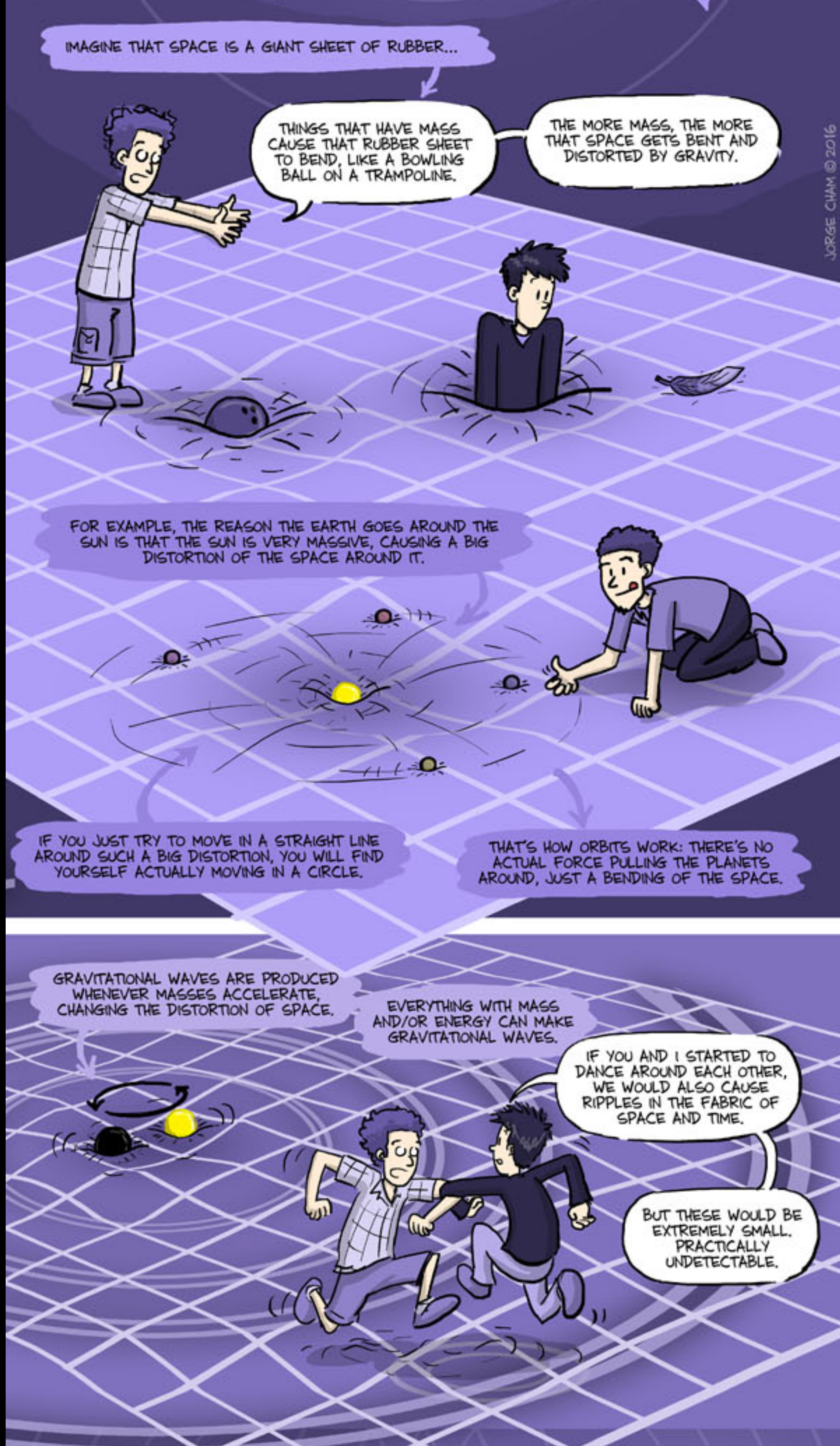

重力＝時空のゆがみ

質点が加速度運動 ＝ 重力波発生

大質量の天体が激しく加速度運動
＝ 観測できる重力波が発生

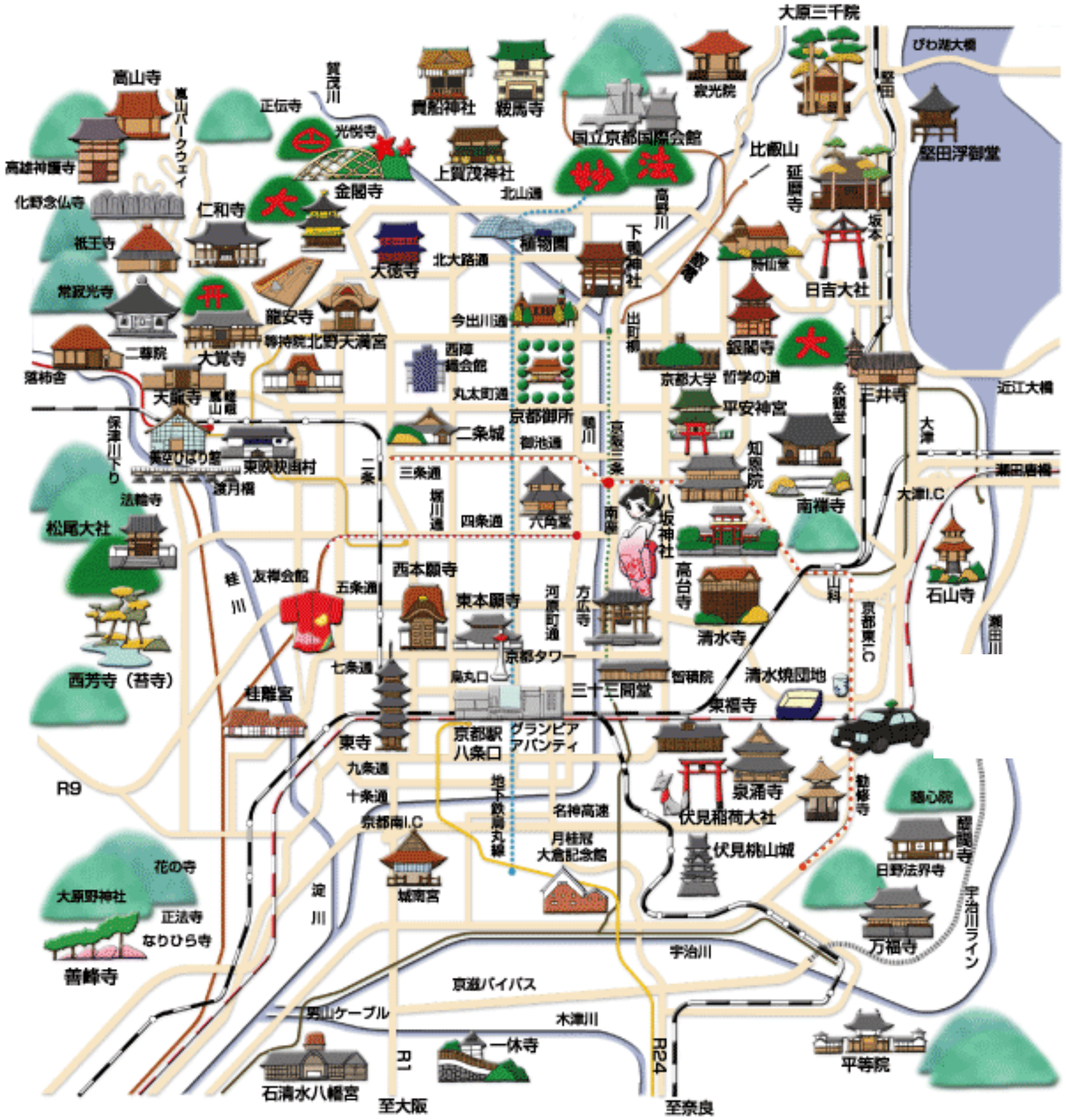
大原三千院
びわ湖大橋
高山寺
正伝寺
光悦寺
貴船神社
鞍馬寺
寂光院
国立京都国際会館
堅田浮御堂
高雄神護寺
化野念仏寺
金閣寺
上賀茂神社
比叡山
延暦寺
仁和寺
祇王寺
常寂光寺
大徳寺
北大路通
植物園
日吉大社
龍安寺
等持院
北野天満宮
今出川通
銀閣寺
二尊院
大覚寺
京都大学
哲学の道
落柿舎
丸太町通
京都御所
平安神宮
大河内山荘
三井寺
二条城
御池通
近江大橋
東映太秦映画村
渡月橋
三条通
四条通
南禅寺
法輪寺
松尾大社
六角堂
八坂神社
知恩院
大津I.C
瀬田唐橋
友禅会館
五条通
西本願寺
東本願寺
高台寺
清水寺
石山寺
七条通
京都タワー
智積院
清水焼団地
西芳寺（苔寺）
桂離宮
三十三間堂
東福寺
東寺
京都駅
八条口
グランビア
アバンティ
九条通
十条通
泉涌寺
随心院
京都南I.C
名神高速
伏見稲荷大社
伏見桃山城
醍醐寺
月桂冠
大倉記念館
日野法界寺
花の寺
大原野神社
正法寺
なりひら寺
城南宮
万福寺
善峰寺
宇治川
京滋バイパス
木津川
一休寺
平等院
石清水八幡宮
至大阪
至奈良
R9
R1
R24


除夜の鐘
1年間の煩悩を払いのけ、新たな年を迎えます。

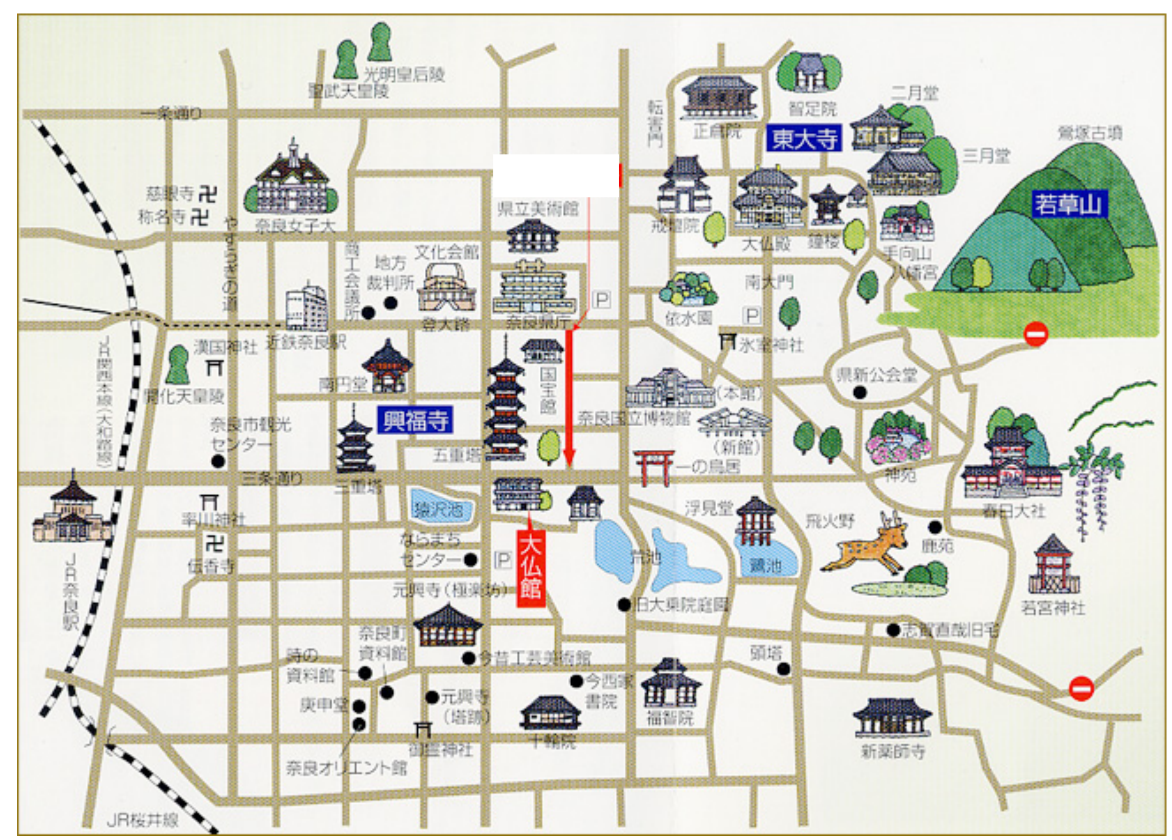
光明皇后陵
聖武天皇陵
一条通り
正倉院
東大寺
二月堂
三月堂
鶯塚古墳
若草山
奈良女子大
県立美術館
戒壇院
大仏殿
手向山八幡宮
文化会館
地方裁判所
依水園
南大門
奈良県庁
氷室神社
近鉄奈良駅
漢国神社
県新公会堂
国宝館
興福寺
奈良国立博物館
開化天皇陵
奈良市観光センター
五重塔
一の鳥居
三条通り
猿沢池
浮見堂
飛火野
鹿苑
春日大社
率川神社
ならまちセンター
大仏館
元興寺（極楽坊）
旧大乗院庭園
志賀直哉旧宅
若宮神社
頭塔
奈良町資料館
今西家書院
福智院
元興寺（塔跡）
十輪院
新薬師寺
御霊神社
奈良オリエント館
JR桜井線
JR奈良駅

重力波の波源 (GW sources)

http://gwcenter.icrr.u-tokyo.ac.jp

supernovae | **pulsars** | **black hole** | **binary neutron stars**

超新星爆発（写真出典:NASA）

パルサー（写真出典:NASA）

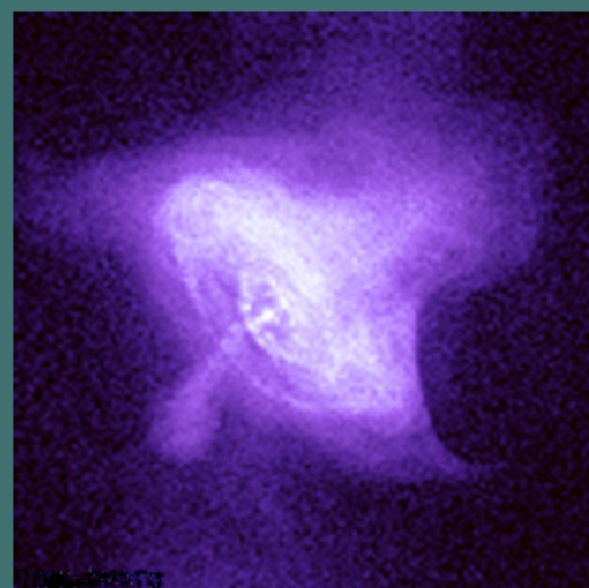

ブラックホール（想像図）

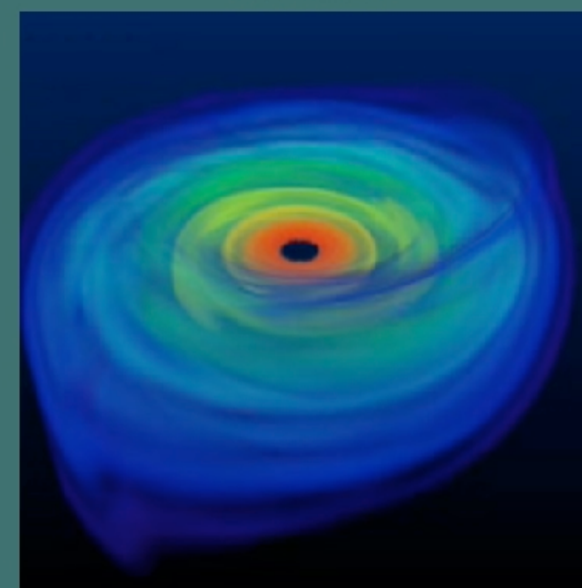

連星中性子星合体（想像図）

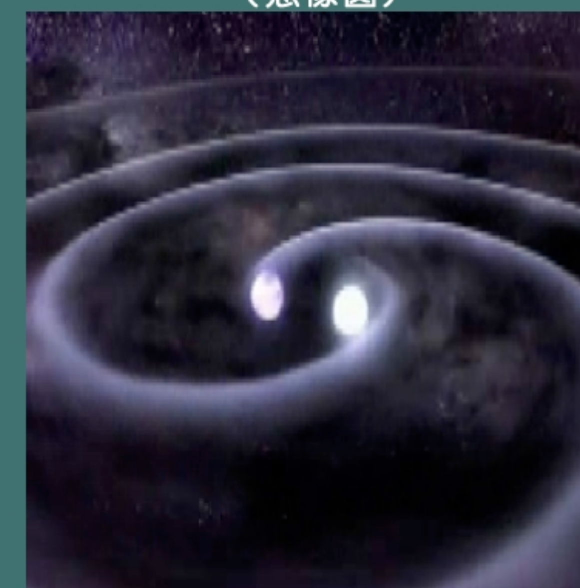

予測が難しい

hard to predict

振幅が小さい

too small amplitude

振幅が小さい

too small amplitude

連星合体をターゲットに

binary coalescence

重力波の分類 (GW classification)

	sources	waveform prediction	data analysis	projects/codes
連星合体 CBC **compact binary coalescence**	**binary BHBH/ NSNS/BHNS**	so so	so so	LALInference pyCBC, gstLAL BayesWave
バースト **Burst**	**supernovae**	hard	unknown	cWB
連続 CW **continuous wave**	**pulsars, rotating stars**	easy	hard	Einstein@Home
ランダム **Stochastic**	**cosmological**	model dependent	hard	
未知 **Unknown**	**unknown**	unknown	unknown	

What we can learn from GW? (重力波観測によって解明できること)

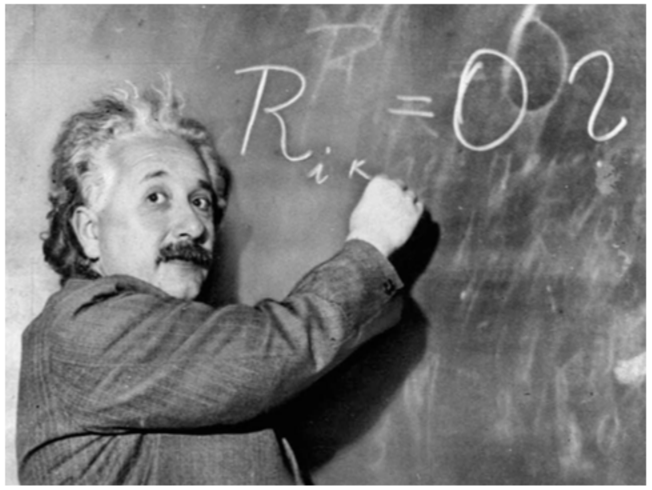

Test of GR at strong gravity region.

一般相対性理論は正しいか？

強い重力場で重力理論の検証ができる

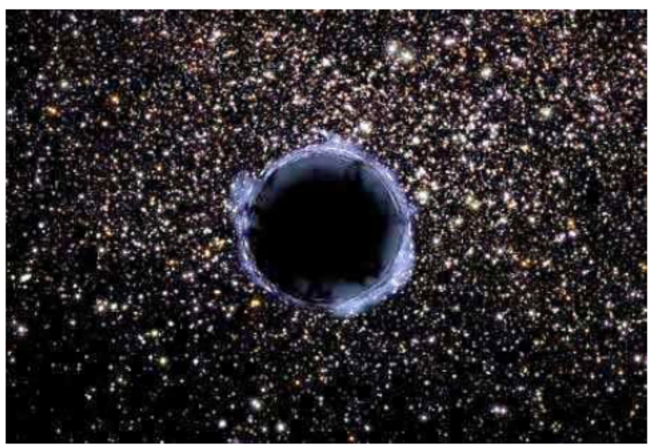

Test of BH no-hair theory

ブラックホール合体後のふるまいは？

no hair になるか.

（質量，角運動量，電荷の3物理量のみか？）

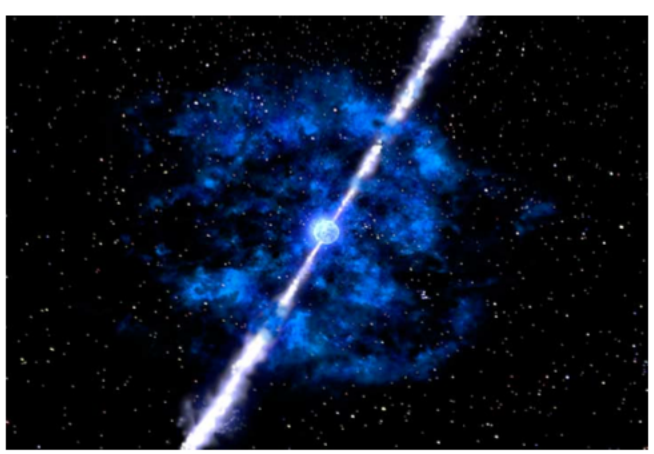

Sources of Gamma-ray bursts

ガンマ線バースト現象の起源は？

加速メカニズムは？

What we can learn from GW? (重力波観測によって解明できること)

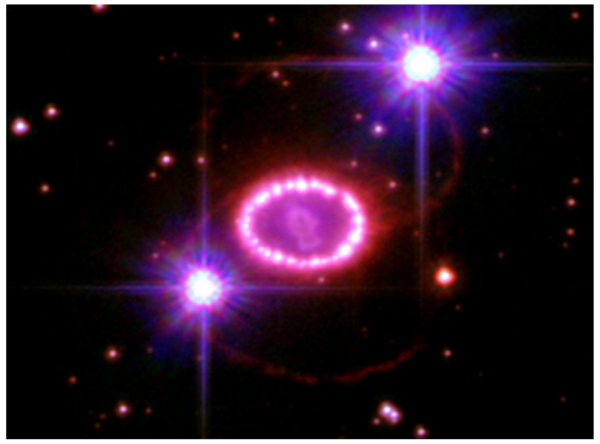

Mechanism of Supernovae

超新星爆発のメカニズムは？

ブラックホールと中性子星の質量差？

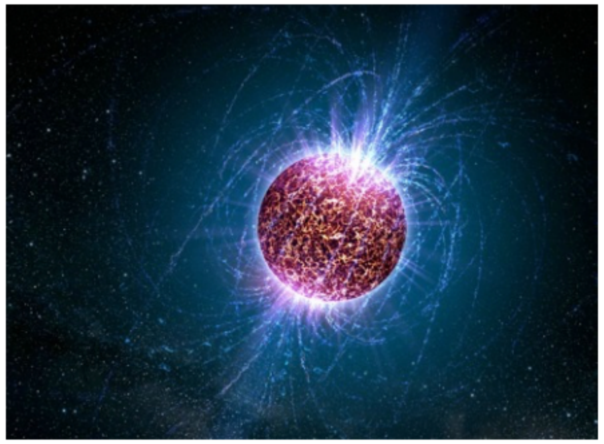

Equation of State of nuclear matter

中性子星の最大質量は？

高密度物質の状態方程式は？

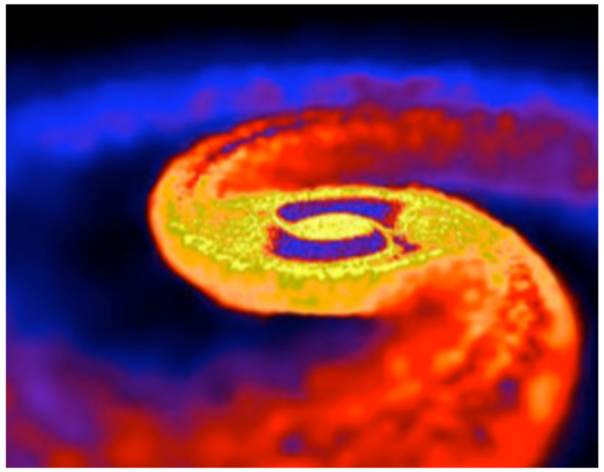

Origin of heavy elements

重元素の起源？

r-processは充分に発生するか？

What we can learn from GW? (重力波観測によって解明できること)

Origin of Supermassive Blackholes

銀河中心の超巨大ブラックホールの起源は？

合体成長か，初期にできていたか？

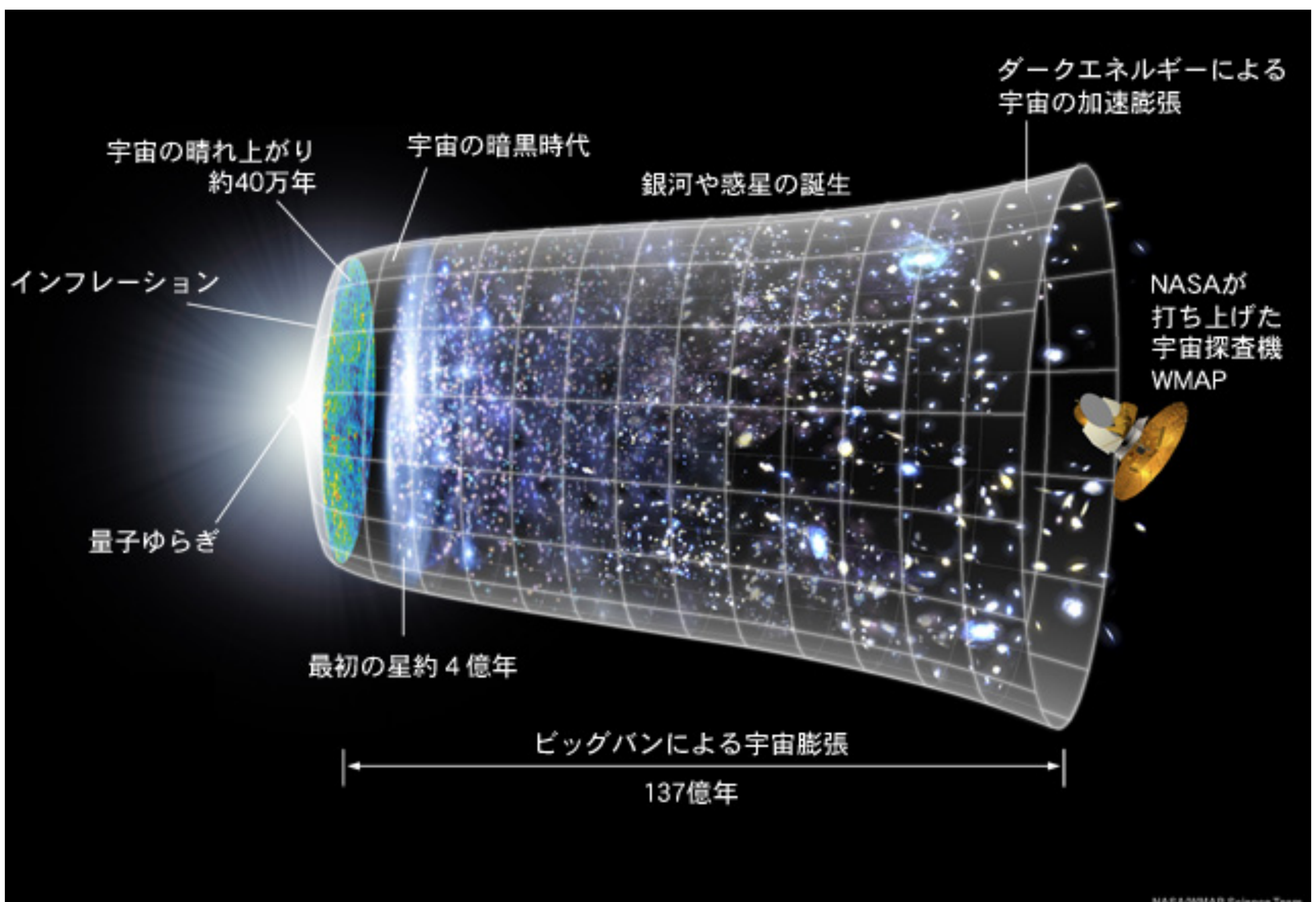

Cosmological Parameters

宇宙の膨張速度の測定

Stellar formation scenario

星形成モデルの特定

Early Universe before CMB

CMB以前の初期宇宙の解明

What we can learn from GW? (重力波観測によって解明できること)

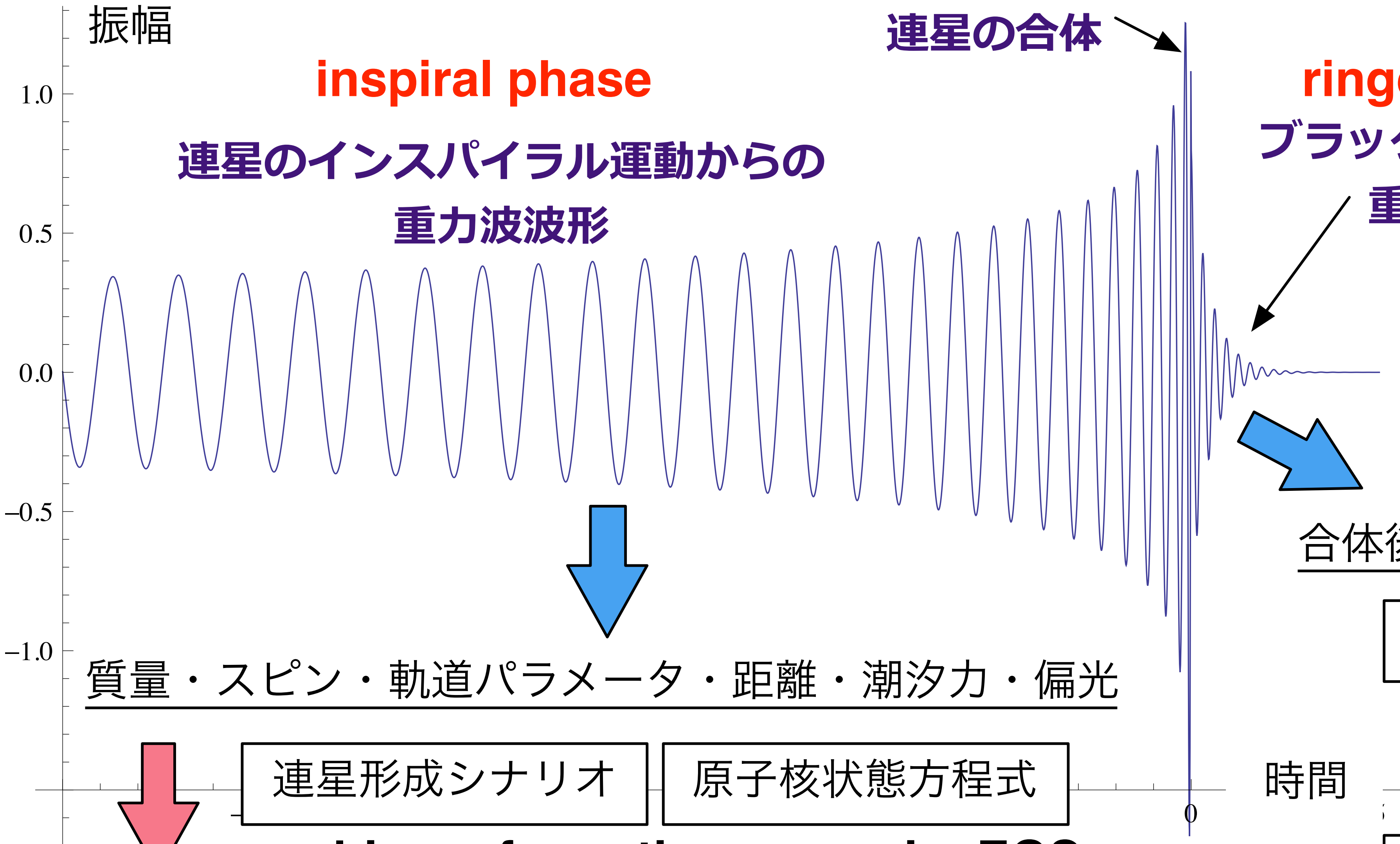

merger phase
連星の合体

inspiral phase
連星のインスパイラル運動からの重力波波形

ringdown phase
ブラックホール形成の重力波波形

質量・スピン・軌道パラメータ・距離・潮汐力・偏光

統計

statistics

連星形成シナリオ　原子核状態方程式

binary formation scenario, EOS

宇宙論パラメータ　銀河形成シナリオ

cosmological parameters, galaxy formation scenario

合体後の質量・角運動量

重力理論の検証

test of GR

究極理論の構築

unified theory

O3b (2019/11/1 - 2020/3/27)

After O3b：GWTC3 (2021/11/7 released)

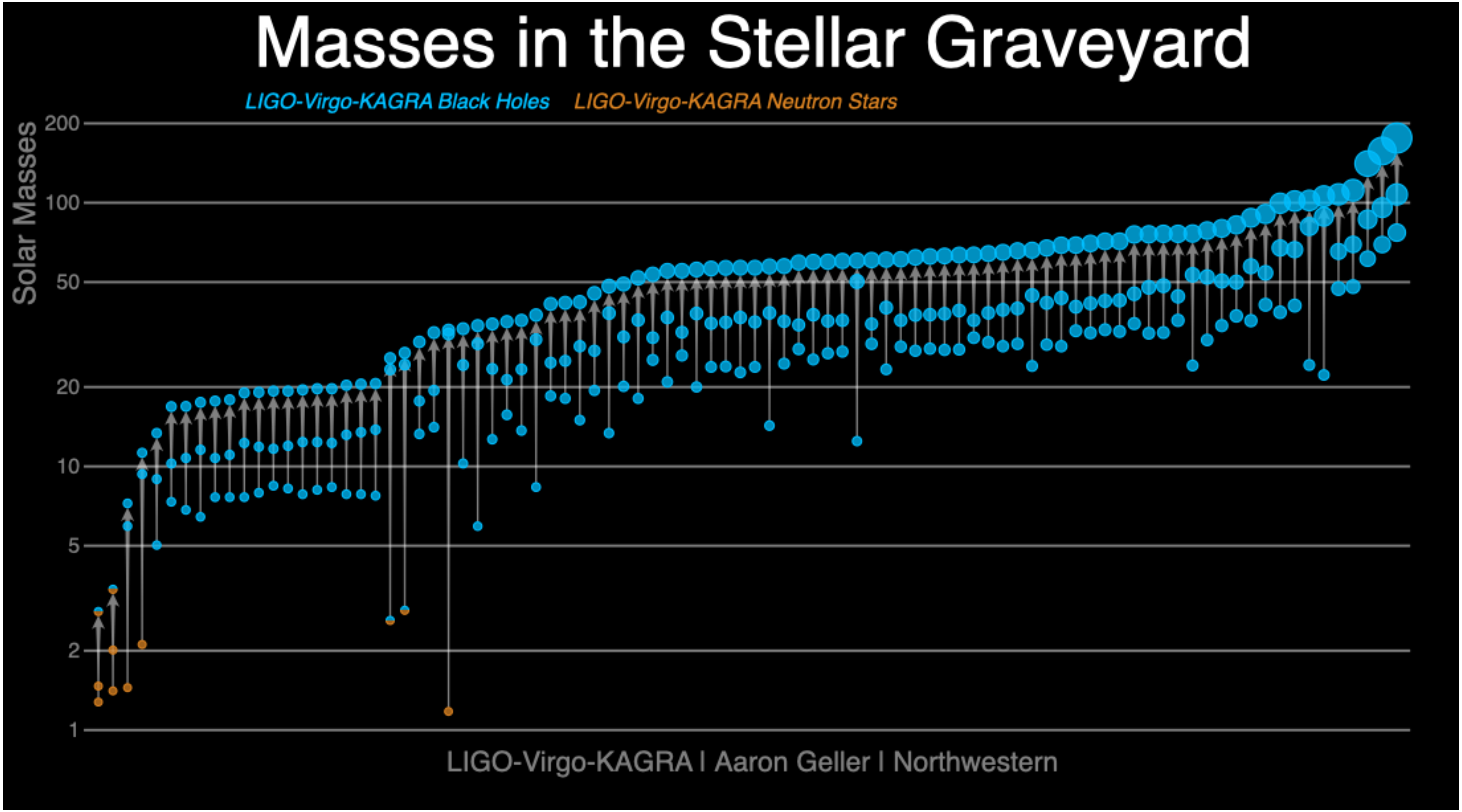

この現状をどう説明する？

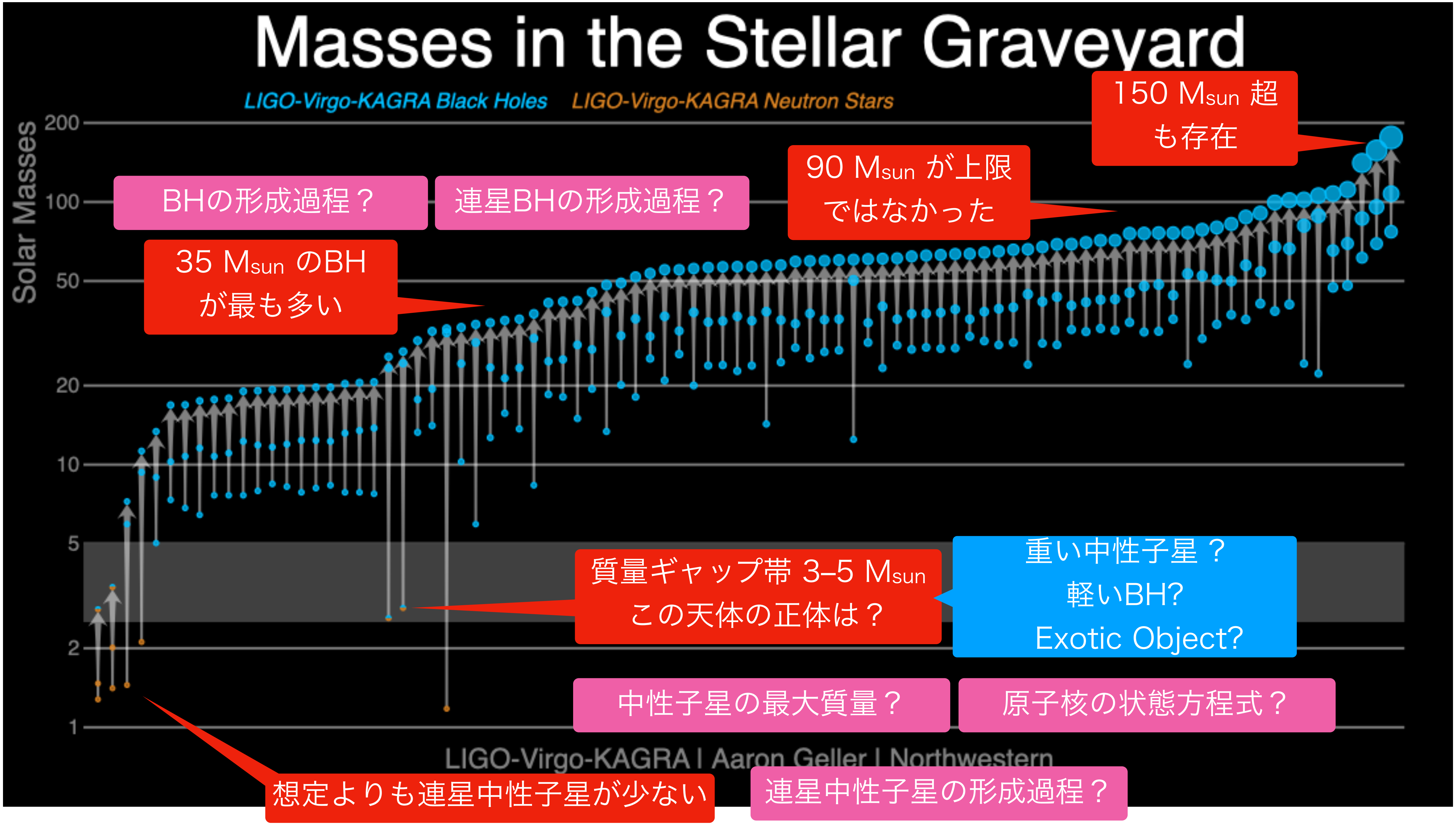

CBC: compact binary coalescence

連星系のパラメータ．　$\boldsymbol{s}_1, \boldsymbol{s}_2, \boldsymbol{n}$ はベクトル量

2 つの天体の質量	m_1, m_2
2 つの天体の回転角運動量	$\boldsymbol{s}_1, \boldsymbol{s}_2$
連星軌道面の傾斜角	ι
合体時刻と合体時の位相	$t_c,\ \varphi_c$
観測地点からの波源方向	$-\hat{\boldsymbol{n}}$
2 つの重力波モードの偏角	ψ
観測地点からの距離	r

GW151226　(S/N=13.0)

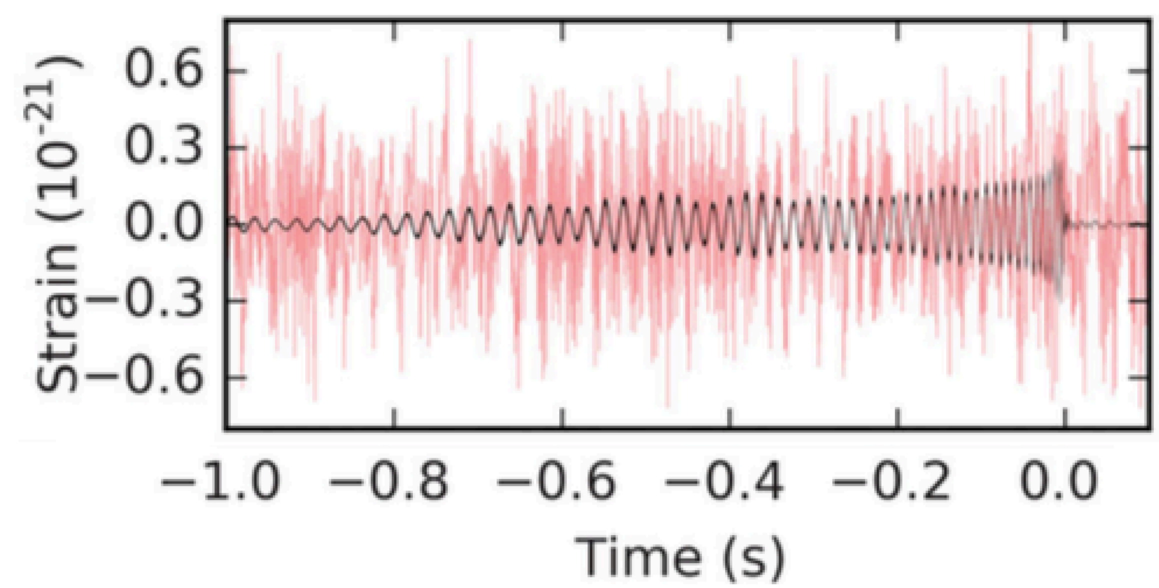

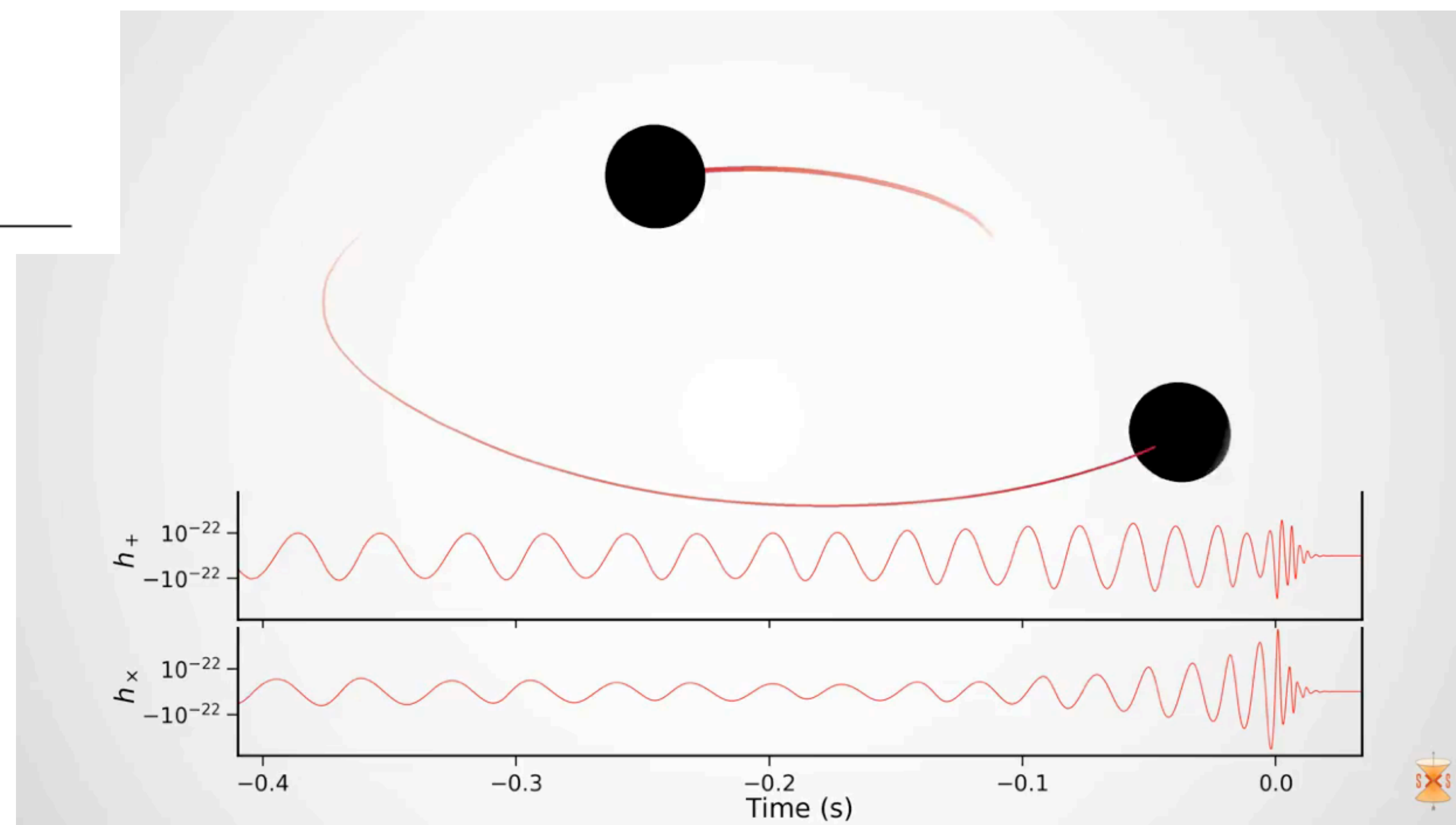

http://ligo.org/detections/GW170104.php

CBC: compact binary coalescence

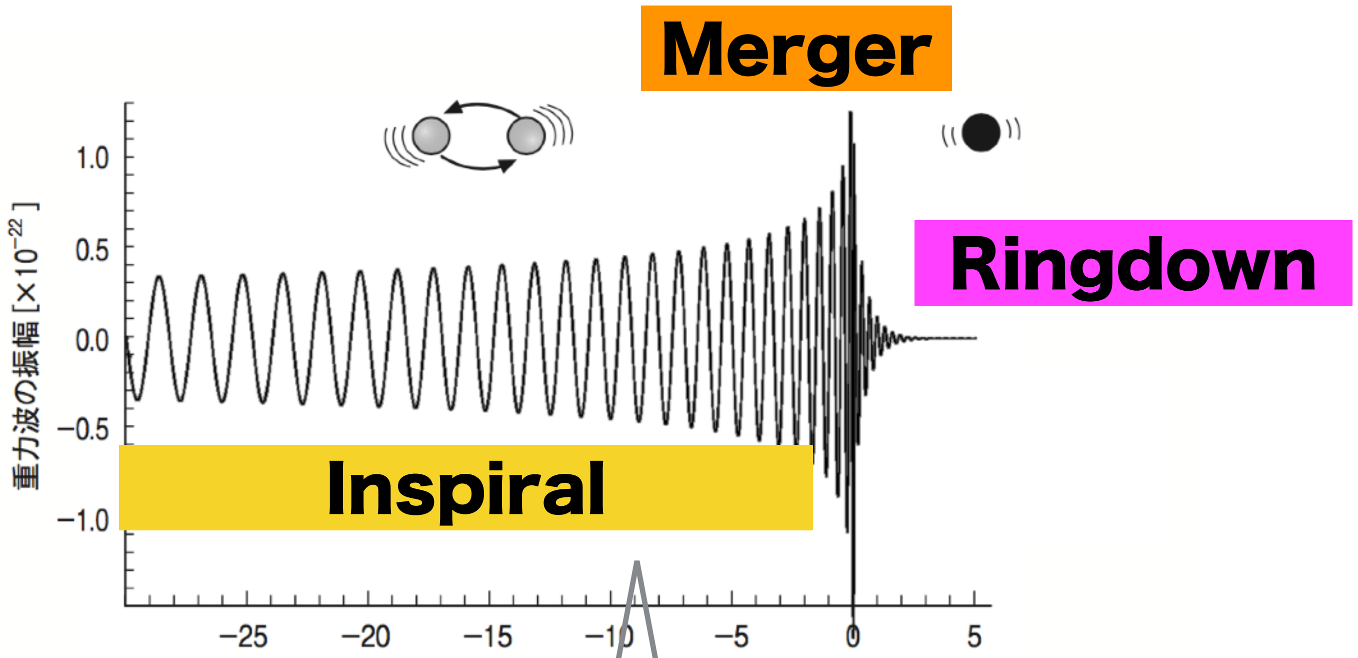

quadrupole formula

$$h_+(t) = -\frac{G\mathcal{M}}{c^2 r}\frac{1+\cos^2\iota}{2}\left(\frac{t_c - t}{5G\mathcal{M}/c^3}\right)^{-1/4}\cos 2\varphi$$

$$h_\times(t) = -\frac{G\mathcal{M}}{c^2 r}\cos\iota\left(\frac{t_c - t}{5G\mathcal{M}/c^3}\right)^{-1/4}\sin 2\varphi$$

chirp mass

$$\mathcal{M} = \frac{(m_1 m_2)^{3/5}}{(m_1+m_2)^{1/5}}$$

$$h(t+\tau) = F_+(\hat{\boldsymbol{n}},\psi)\,h_+(t) + F_\times(\hat{\boldsymbol{n}},\psi)\,h_\times(t)$$

$$h(t) = -\frac{G\mathcal{M}}{c^2 D}\left(\frac{t_c - t}{5G\mathcal{M}/c^3}\right)^{-1/4}\cos 2[\varphi(t)+\Delta\varphi]$$

where

$$D \equiv r\left[F_+^2\left(\frac{1+\cos^2\iota}{2}\right)^2 + F_\times^2\,\cos^2\iota\right]^{-1/2}$$

and

$$2\Delta\varphi \equiv -\tan^{-1}\left(\frac{F_\times}{F_+}\frac{2\cos\iota}{1+\cos^2\iota}\right)$$

CBC: compact binary coalescence

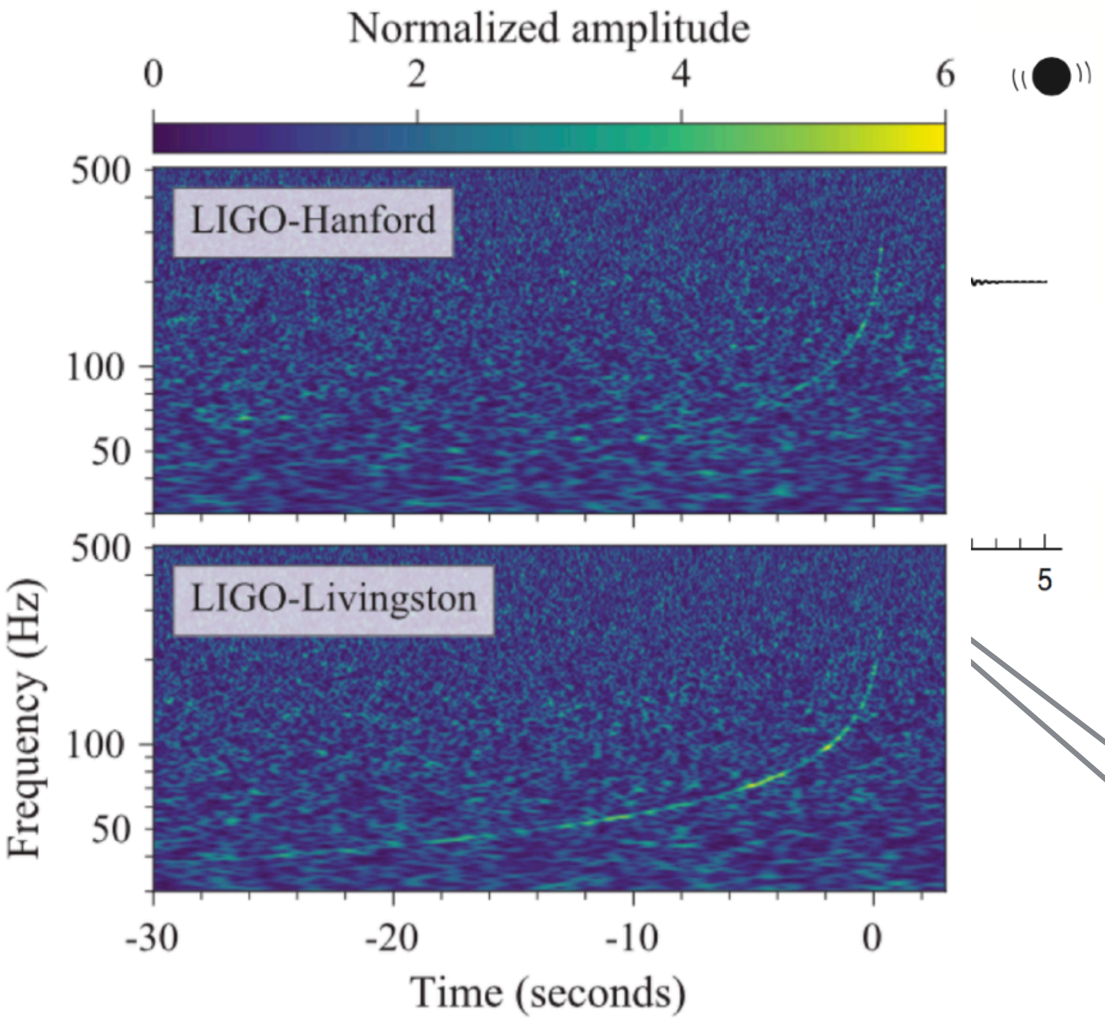

spectrogram

2nd PN 近似までで,

$$\tilde{g}(f) = -\sqrt{\frac{5\pi}{24}}\frac{G^2\mathcal{M}^2}{c^5}\left(\frac{\pi G\mathcal{M}f}{c^3}\right)^{-7/6} e^{-i\Psi(f)}$$

where

$$\Psi(f) = -\frac{\pi}{4} + \frac{3}{128\eta}\left[x^{-5/2} + \left(\frac{3715}{756} + \frac{55}{9}\eta\right)x^{-3/2} - 16\pi x^{-1} + \left(\frac{15293365}{508032} + \frac{27145}{504}\eta + \frac{3085}{72}\eta^2\right)x^{-1/2}\right]$$

$$h(t+\tau) = F_+(\hat{\boldsymbol{n}},\psi)\,h_+(t) + F_\times(\hat{\boldsymbol{n}},\psi)\,h_\times(t)$$

$$h(t) = -\frac{G\mathcal{M}}{c^2 D}\left(\frac{t_c - t}{5G\mathcal{M}/c^3}\right)^{-1/4}\cos 2[\varphi(t) + \Delta\varphi]$$

where

$$D \equiv r\left[F_+^2\left(\frac{1+\cos^2\iota}{2}\right)^2 + F_\times^2\,\cos^2\iota\right]^{-1/2}$$

and

$$2\Delta\varphi \equiv -\tan^{-1}\left(\frac{F_\times}{F_+}\frac{2\cos\iota}{1+\cos^2\iota}\right)$$

Fourier Transform

$$\begin{cases} \tilde{x}(f) = \displaystyle\int_{-\infty}^{\infty} x(t)\,e^{-2\pi i f t}\,dt \\ x(t) = \displaystyle\int_{-\infty}^{\infty} \tilde{x}(f)\,e^{2\pi i f t}\,df \end{cases}$$

Sensitivity curves

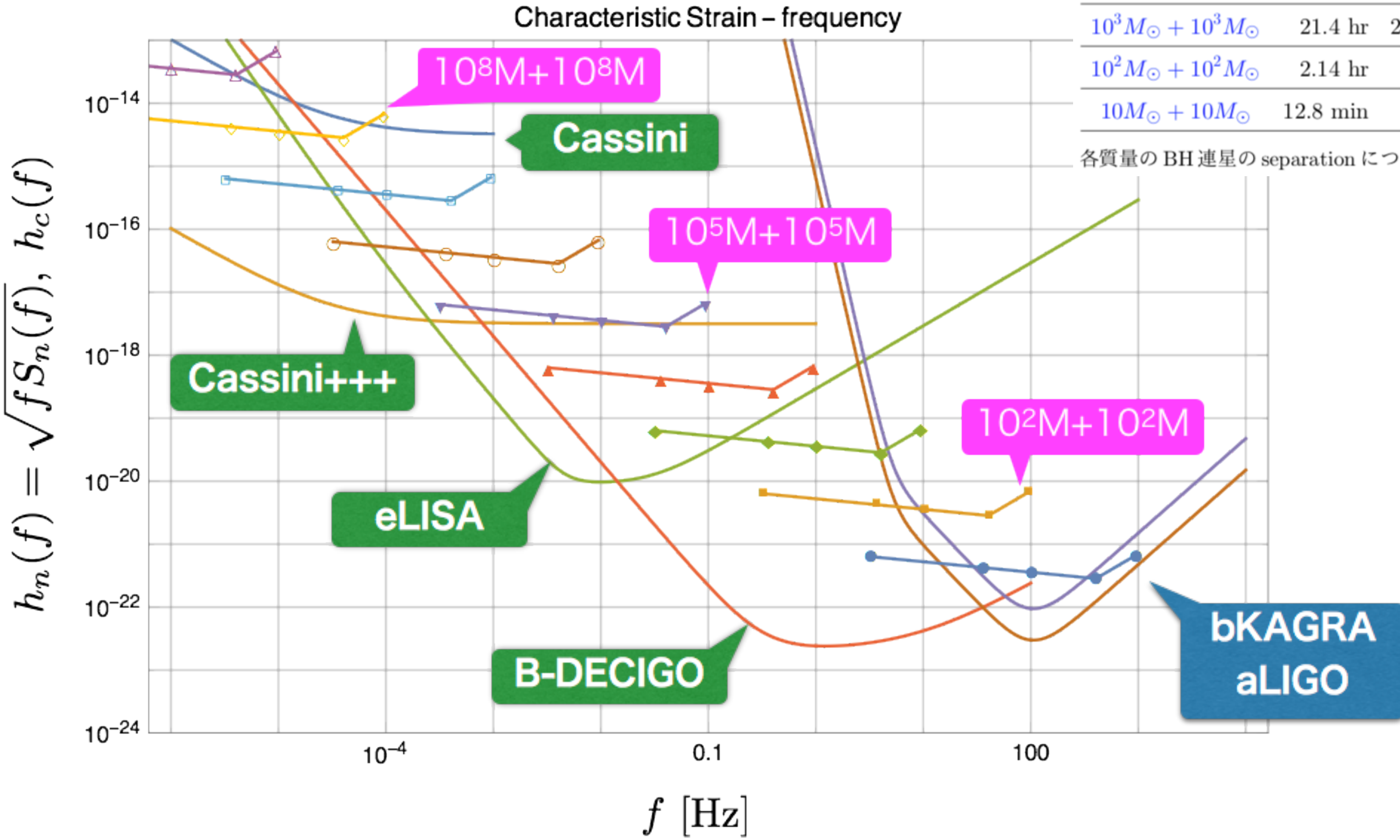

BH-BH 質量	$50R_g$	$10R_g$	$5R_g$
$10^8 M_\odot + 10^8 M_\odot$	244 yr	142 day	8.91 day
$10^7 M_\odot + 10^7 M_\odot$	24.4 yr	14.3 day	21.4 hr
$10^6 M_\odot + 10^6 M_\odot$	2.44 yr	1.43 day	2.14 hr
$10^5 M_\odot + 10^5 M_\odot$	89.1 day	3.42 hr	12.8 min
$10^4 M_\odot + 10^4 M_\odot$	8.91 day	20.5 min	77.0 sec
$10^3 M_\odot + 10^3 M_\odot$	21.4 hr	2.05 min	7.70 sec
$10^2 M_\odot + 10^2 M_\odot$	2.14 hr	12.3 sec	0.77 sec
$10 M_\odot + 10 M_\odot$	12.8 min	1.23 sec	77 msec

各質量の BH 連星の separation について，合体までの時間を

Moore, Cole, & Berry, CQG 32(2015) 015014

Sensitivity curve with characteristic strain

http://gwplotter.com

(dimensionless)

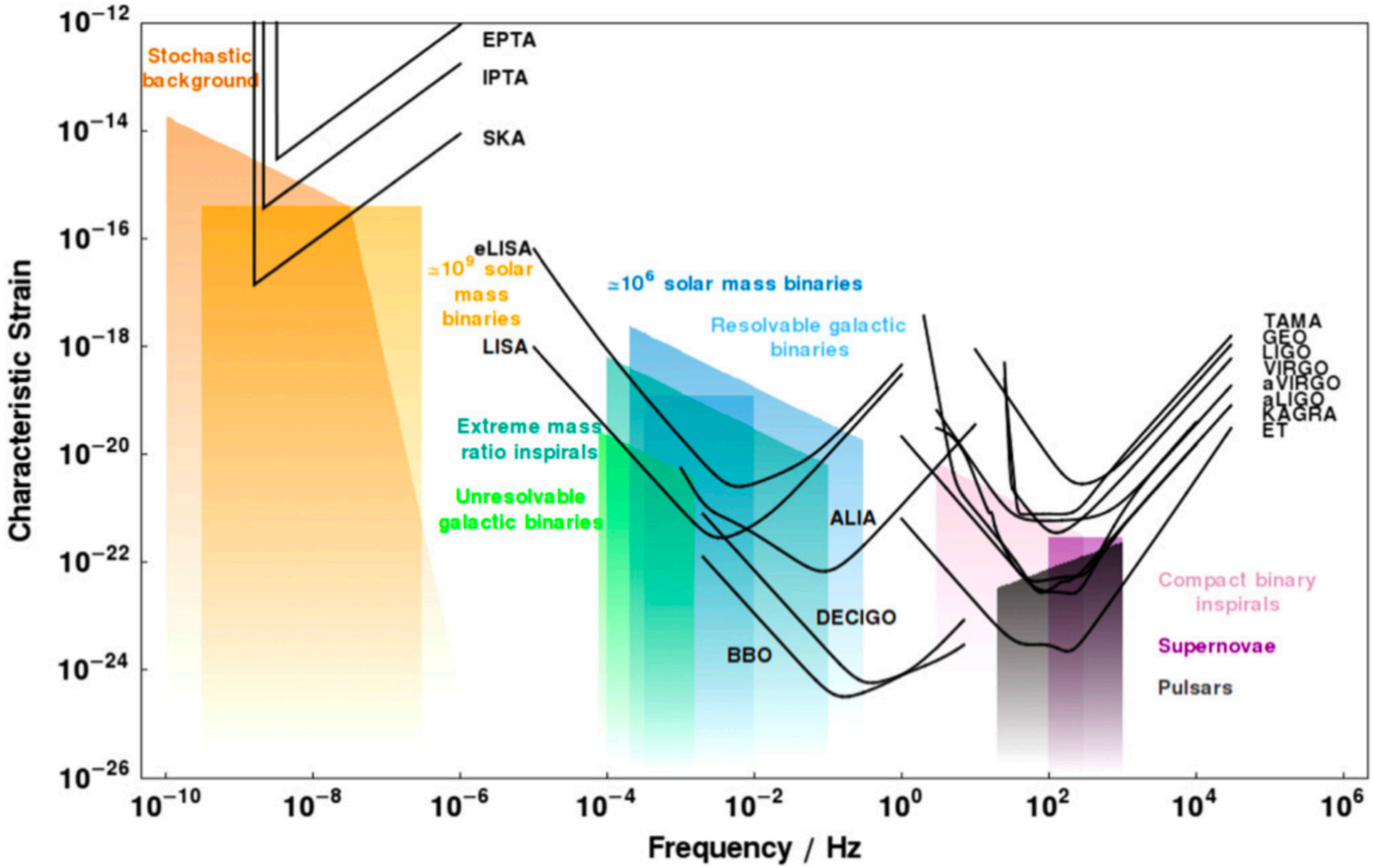

Figure A1. A plot of characteristic strain against frequency for a variety of detectors and sources.

Sensitivity curve with Power Spectral Density

http://gwplotter.com

/sqrt(Hz)

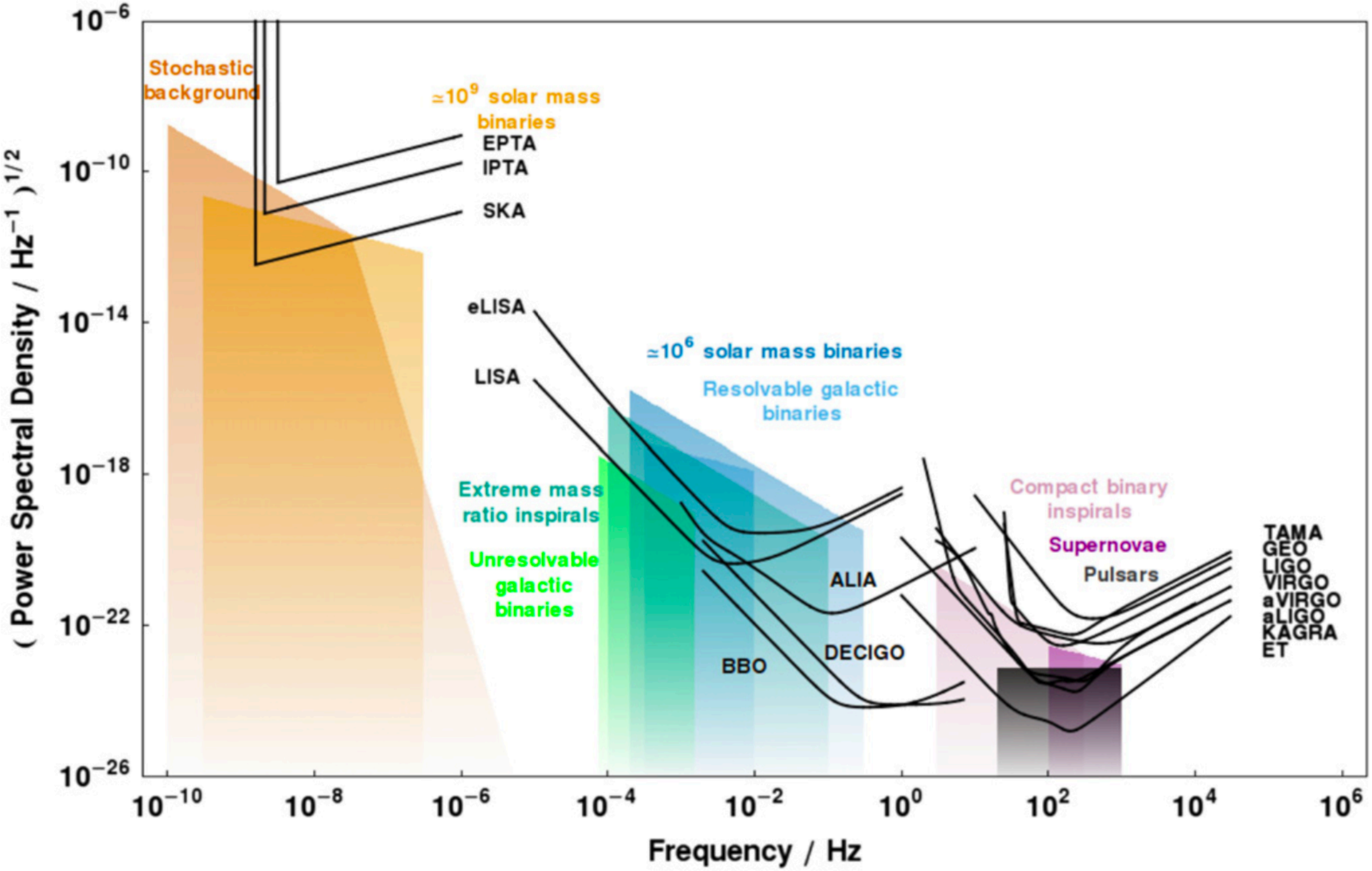

Figure A2. A plot of the square root of PSD against frequency for a variety of detectors and sources.

Sensitivity curve with dimensionless energy density

http://gwplotter.com

(dimensionless)

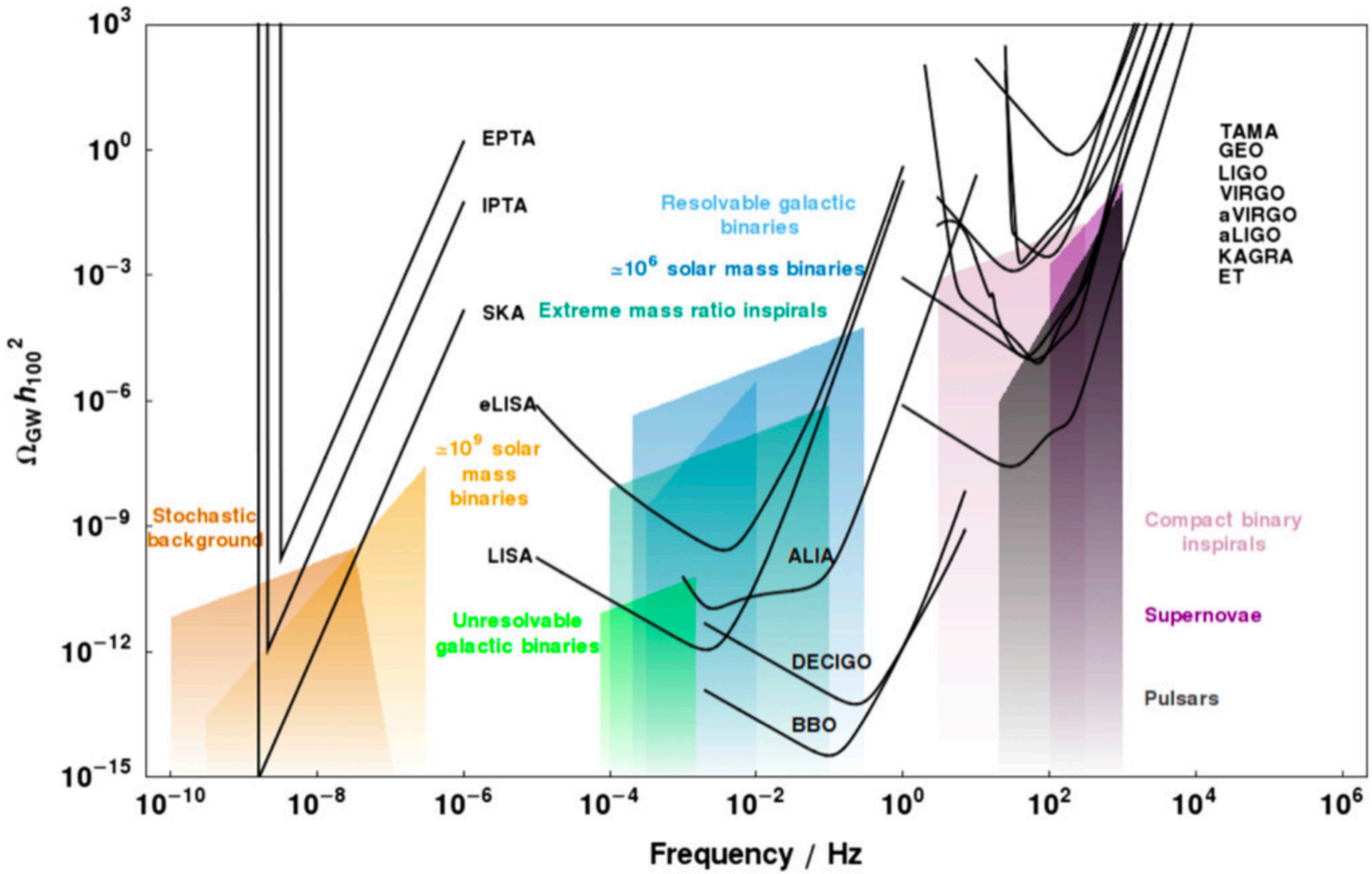

Figure A3. A plot of the dimensionless energy density in GWs against frequency for a variety of detectors and sources.

Ideal vs Reality (Theory vs Data Analysis)

GW150914 (S/N=23.7)

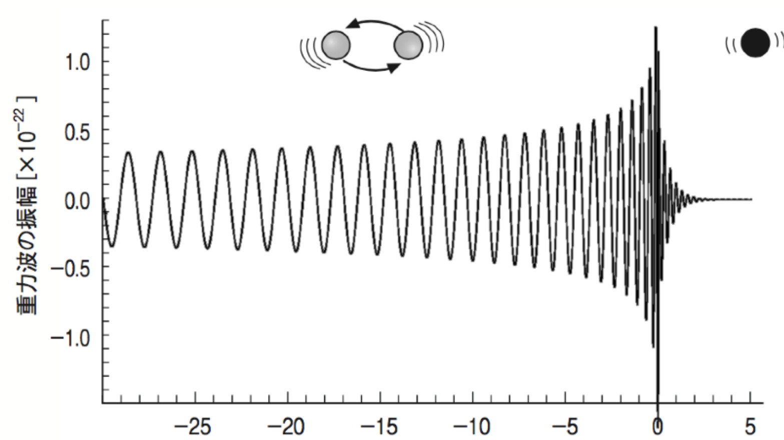

h(t)

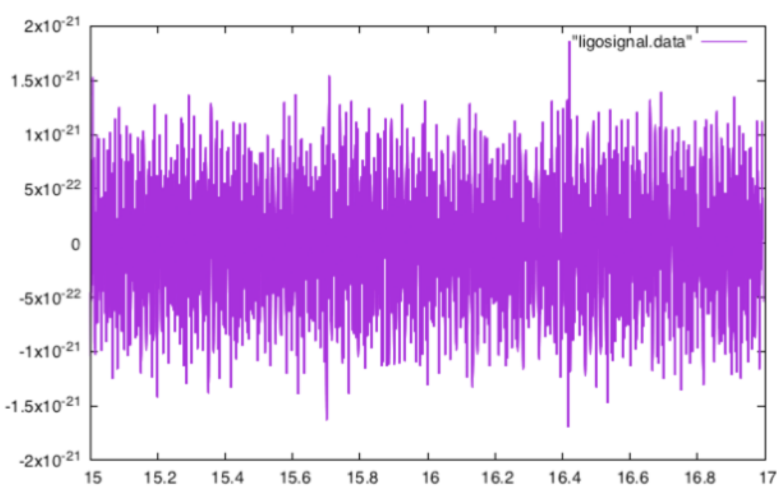

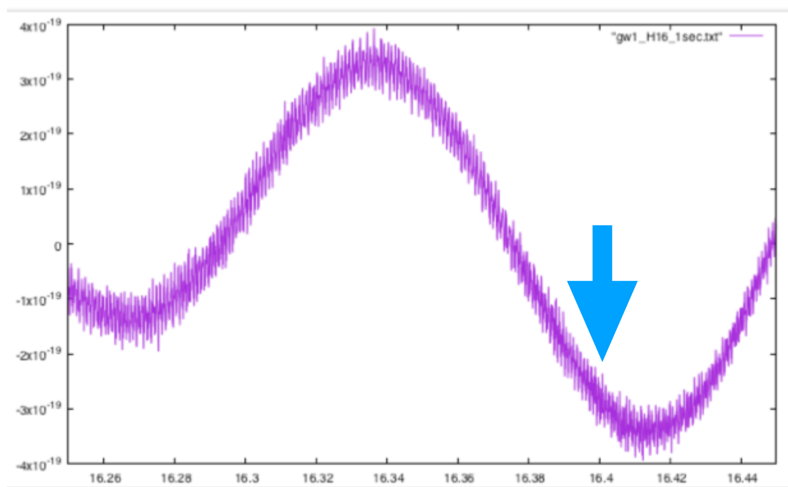

16.25 16.45

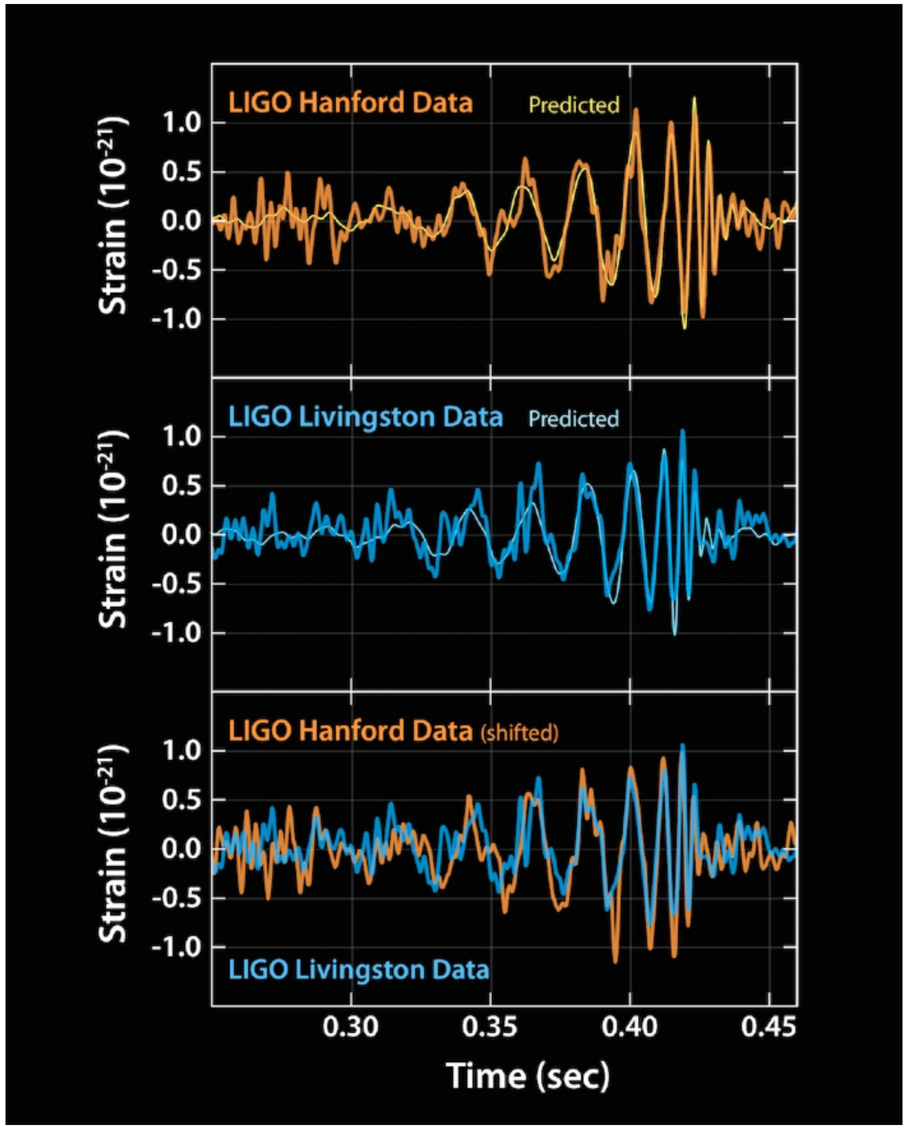

challenging for data analysis

GW data is with noise

signal quickly decays

(M=60Msun, a=0.75 —> 300Hz, tau = 3 ms)

Power spectrum of Noise

Parseval id.▶ $$\int_{-\infty}^{\infty}[x(t)]^2\,dt=\int_{-\infty}^{\infty}[\tilde{x}(f)]^2\,df$$

power spectrum density

$$\langle x^2\rangle=\lim_{T\to\infty}\frac{1}{T}\int_{-T/2}^{T/2}[x(t)]^2\,dt=\int_{-\infty}^{\infty}P(f)df$$

$$P(f)=\lim_{T\to\infty}\frac{1}{T}\left[\tilde{x}(f)\tilde{x}^*(f)\right]$$

if stationary prob. process

Wiener-Khinchin theorem ▶ $$P(f)=\int_{-\infty}^{\infty}R_x(\tau)e^{-2\pi i f\tau}\,d\tau$$

$$R_x(\tau)=\langle x(t)\,x(t+\tau)\rangle=\lim_{T\to\infty}\frac{1}{T}\int_{-T/2}^{T/2}x(t)x(t+\tau)\,dt$$

auto-correlation func.

$$\langle x^2\rangle=2\int_0^{\infty}P(f)\,df=\int_0^{\infty}S_x(f)\,df$$

if noise is Gaussian

$$S_x(f)=2\int_{-\infty}^{\infty}R_x(\tau)e^{-2\pi i f\tau}\,d\tau=\lim_{\Delta t\to 0}2\sigma^2\Delta t$$

Power spectrum of Noise

$$\langle x^2 \rangle = 2\int_0^\infty P(f)\,df = \int_0^\infty S_x(f)\,df$$

if noise is Gaussian

$$S_x(f) = 2\int_{-\infty}^{\infty} R_x(\tau) e^{-2\pi i f \tau}\,d\tau = \lim_{\Delta t \to 0} 2\sigma^2 \Delta t$$

Power spectrum of Noise

$$\langle x^2 \rangle = 2\int_0^\infty P(f)\,df = \int_0^\infty S_x(f)\,df$$

if noise is Gaussian

$$S_x(f) = 2\int_{-\infty}^{\infty} R_x(\tau)e^{-2\pi i f\tau}\,d\tau = \lim_{\Delta t\to 0} 2\sigma^2\Delta t$$

$$p_x[x(t)] \propto \exp\left[-\frac{1}{2\sigma^2}\sum_j x_j^2\right] \propto \exp\left[-\int_{-\infty}^{\infty}\frac{|\tilde{x}(f)|^2}{S_x}\,df\right]$$

$$p_x[x(t)] \propto e^{-(x,x)/2}$$

define the noise-weighed inner product

$$\begin{aligned}(a,b) &\equiv 4\,\mathcal{R}e\int_0^\infty \frac{\tilde{a}(f)\,\tilde{b}^*(f)}{S(f)}df \\ &= 2\int_{-\infty}^{\infty}\frac{\tilde{a}(f)\,\tilde{b}^*(f)}{S(|f|)}df \\ &= \int_{-\infty}^{\infty}\frac{\tilde{a}(f)\,\tilde{b}^*(f)+\tilde{a}^*(f)\,\tilde{b}(f)}{S(|f|)}df\end{aligned}$$

Matched Filter

帰無仮説 $\mathcal{H}_0 : \quad s(t) = n(t)$

対立仮説 $\mathcal{H}_1 : \quad s(t) = n(t) + h(t)$

signal = gw + noise

$$s(t) = h(t) + n(t)$$

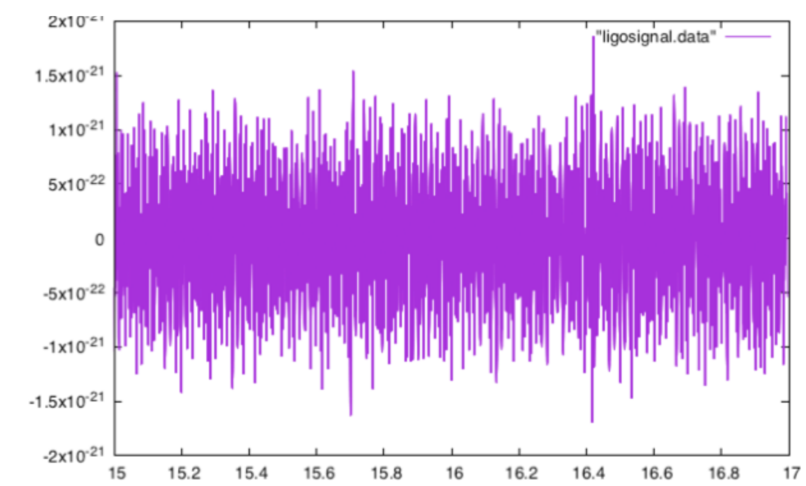

Odds Ratio

$$O(\mathcal{H}_1|s) = \frac{P(\mathcal{H}_1|s)}{P(\mathcal{H}_0|s)}$$

Likelihood

$$\Lambda(\mathbf{B}|\mathbf{A}) = \frac{P(\mathbf{A}|\mathbf{B})}{P(\mathbf{A}|\overline{\mathbf{B}})}$$

$$\Lambda(\mathcal{H}_1|s) = \frac{p(s|\mathcal{H}_1)}{p(s|\mathcal{H}_0)}$$

$$p(s|\mathcal{H}_1) = p_n[s(t) - h(t)] \propto e^{-(s-h,s-h)/2}$$

$$p(s|\mathcal{H}_0) = p_n[s(t)] \propto e^{-(s,s)/2}$$

$$\Lambda(\mathcal{H}_1|s) = \frac{e^{-(s-h,s-h)/2}}{e^{-(s,s)/2}} = e^{(s,h)} e^{-(h,h)/2}$$

Matched Filter (signal-noise ratio)

$$(s,h) = 4\,\mathcal{R}e \int_0^\infty \frac{\tilde{s}(f)\,\tilde{h}^*(f)}{S_n(f)}\,df$$

Bayes Theorem

conditional probability

$$P(B_k|A) = \frac{P(A \cap B_k)}{P(A)}$$

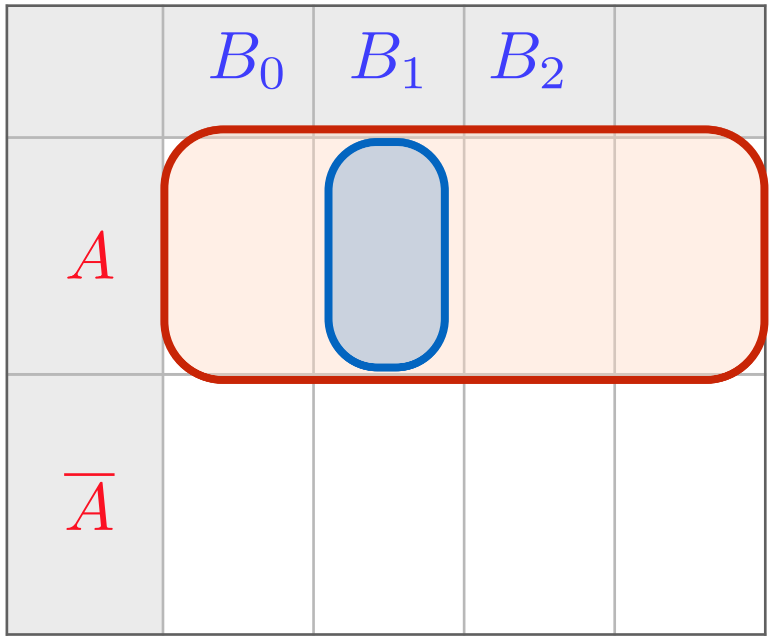

$$P(A \cap B_k) = P(A|B_k)P(B_k)$$

$$P(A) = \sum_k P(A \cap B_k)$$

$$P(B_k|A) = \frac{P(A|B_k)P(B_k)}{\sum_k P(A|B_k)P(B_k)}$$

A→B
原因→結果

B→A
結果→原因

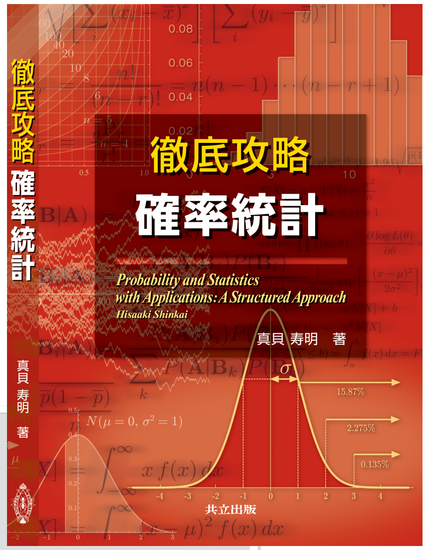

応用例

インターネットでの個別広告の実現
　本屋や音楽ダウンロードサイトで「おすすめ」
迷惑メールフィルタ
　ユーザに合わせた設定

少年が嘘つきの場合（事象 $\mathbf{A}$），「オオカミがいる」と言ったとき，オオカミが発見される（事象 $\mathbf{B}$）確率を 20%，発見できない（事象 $\overline{\mathbf{B}}$）確率を 80%とする．少年が嘘つきでない場合（事象 $\overline{\mathbf{A}}$），「オオカミがいる」と言ったとき，オオカミが発見される確率を 70%，発見できない確率を 30%とする．事前確率として，少年が嘘つきの可能性を 10%とする．(15 点)

	オオカミ発見 $\mathbf{B}$	発見できない $\overline{\mathbf{B}}$
少年が嘘つき　$\mathbf{A}$	20 %	80 %
少年が正直者　$\overline{\mathbf{A}}$	70 %	30 %

(1) 1 度目，少年が「オオカミがいる」と言ったが，オオカミは発見されなかった．少年が嘘つきと考えられる事後確率 $P(\mathbf{A}|\overline{\mathbf{B}})$ を求めよ．
引き続いて 2 度目，少年が「オオカミがいる」と言ったが，オオカミは発見されなかった．少年が嘘つきと考えられる事後確率を求めよ．

(2) 1 度目，少年が「オオカミがいる」と言い，オオカミが発見された．少年が嘘つきと考えられる事後確率を求めよ．

(1) 1度目 22.9%，2度目 44.2%
嘘が続いた時の嘘つき確率は右グラフ

(2) 3.1%

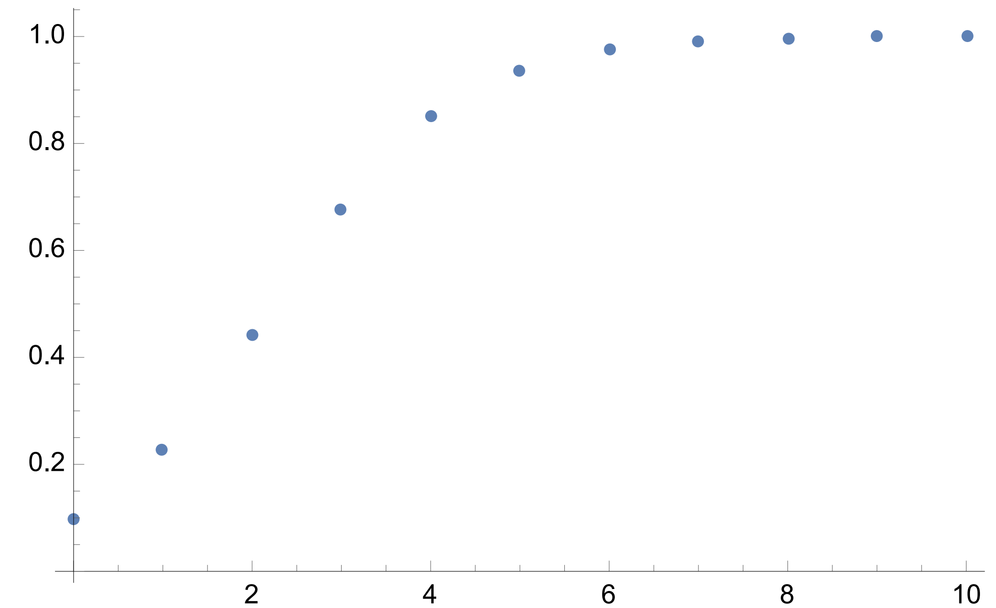

Matched Filter

signal = gw + noise

$$s(t) = h(t) + n(t)$$

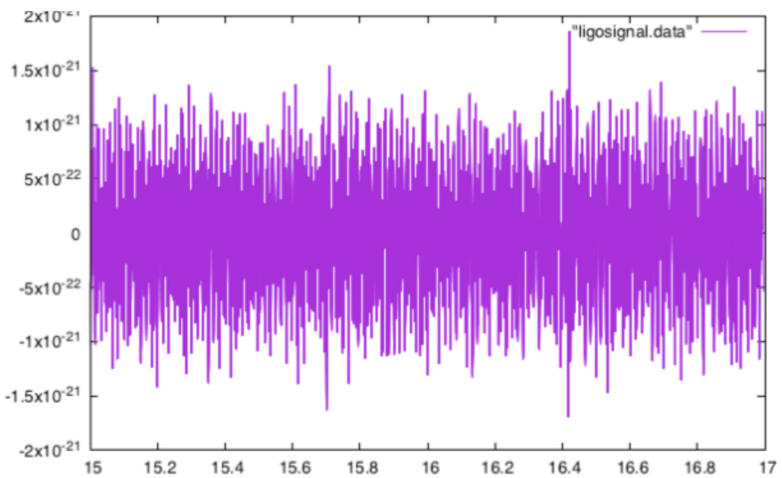

gw template

$$h(t)$$

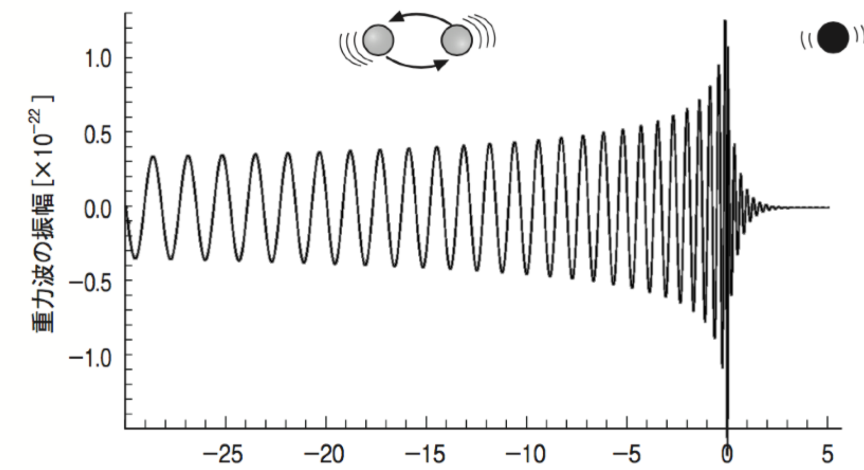

$$\rho = 2\int_{-\infty}^{\infty} \frac{\tilde{s}(f)\tilde{h}^*(f)}{S_h(|h|)}df$$

signal/noise ratio

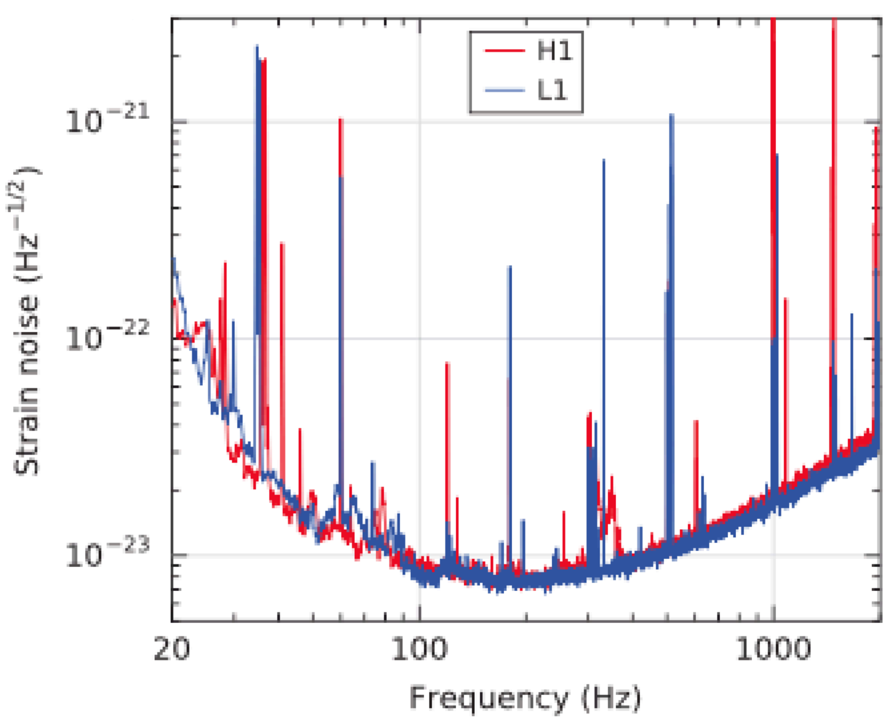

GW151226 (S/N=13.0)

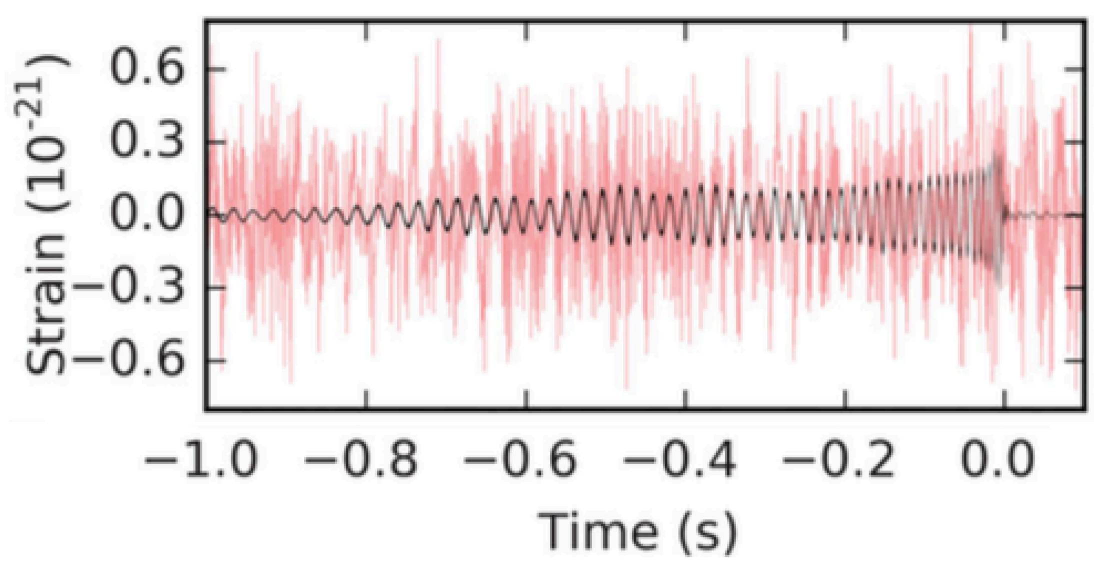

Parameter Estimation

Likelihood

$$\Lambda(\mathcal{H}_1|s) = \frac{p(s|\mathcal{H}_1)}{p(s|\mathcal{H}_0)}$$

$$s(t) = n(t) + h_\theta(t)$$

パラメータ θ^i

$$\Lambda(\mathcal{H}_\theta|s) = \frac{p(s|\mathcal{H}_\theta)}{p(s|\mathcal{H}_0)}$$

連星系のパラメータ． $\boldsymbol{s}_1, \boldsymbol{s}_2, \boldsymbol{n}$ はベクトル量

2 つの天体の質量	m_1, m_2
2 つの天体の回転角運動量	$\boldsymbol{s}_1, \boldsymbol{s}_2$
連星軌道面の傾斜角	ι
合体時刻と合体時の位相	$t_c,\ \varphi_c$
観測地点からの波源方向	$-\hat{\boldsymbol{n}}$
2 つの重力波モードの偏角	ψ
観測地点からの距離	r

$$\log \Lambda(\mathcal{H}_\theta|s) = (s, h_\theta) - \frac{1}{2}(h_\theta, h_\theta)$$

deriv. local max

$$\left.(s - h_\theta, \frac{\partial}{\partial \theta^i} h_\theta)\right|_{\theta=\theta_{\max}} = 0$$

Fisher matrix

$$\Gamma_{ij} \equiv \overline{v_i v_j} = \overline{(n, \frac{\partial h_{\theta_{\max}}}{\partial \theta^i})(\frac{\partial h_{\theta_{\max}}}{\partial \theta^j}, n)} = (\frac{\partial h_{\theta_{\max}}}{\partial \theta^i}, \frac{\partial h_{\theta_{\max}}}{\partial \theta^j}) \qquad v_i \equiv (n, \frac{\partial h_{\theta_{\max}}}{\partial \theta^i})$$

$$p(\boldsymbol{v}) = \frac{1}{\sqrt{2\pi \det \Gamma}} \exp\left[-\frac{1}{2} V^{ij} v_i v_j\right]$$

$$V^{ij} \equiv (\Gamma^{-1})^{ij}$$

uncertainty

$$(\Delta\theta^i)_{\rm rms} = \sqrt{V^{ii}} \quad \text{(no summation)}$$

correlation coef.

$$c_{ij} = \frac{\overline{\Delta\theta^i \Delta\theta^j}}{V^{ii} V^{jj}} = \frac{V^{ij}}{\sqrt{V^{ii} V^{jj}}}$$

Markov Chain Monte Carlo (MCMC)

Column

コンピューターで大進化を遂げ重力波観測に貢献するベイズ

今年2月、米国を中心とした国際チームによって、アインシュタインの予測した「重力波」が史上初めて観測されたことが明らかになった。

米国の観測装置は、13億年前に二つのブラックホールが衝突、合体したことで生じた重力波を捉えた。それが事前に予想された波形と見事に合致したのである。

そんな科学の大きな進歩につながる歴史的な発見に、実はベイズの理論が大きく貢献していた。詳細は統計専門誌「SIGNIFICANCE（4月号）」に譲るが、約250年前に発見されて〝追放〟された理論が今、再び脚光を浴びている。

その理由をひもとくのが、「マルコフ連鎖モンテカルロ法（MCMC）」と呼ばれる確率分布を求める手法だ。

そもそも、ベイズの理論は数学を基礎としており理論的に完成度が高かった。だが、実際に応用するとなると、あまりに高度な積分計算をしなければ解けない。そのため、複雑なモデルを組むことができず、1980年代まで注目されなかった。

その壁を越えたのが、MCMCとコンピューターの力であった。

ここでMCMCの原理について数式を使わずに触れよう。

左図に「山田君が洞穴に落ちてそこが真っ暗な場合、穴の場所をどう推定するか」という事例を掲載した。

確率分布を見つける力業

マルコフ連鎖モンテカルロ法（MCMC）の考え方

問題発生

山田君は誤って大きな洞穴に落ちて気を失ってしまった。気付けば夜で、中は真っ暗に。落ちた穴をどう見つければいいのか。

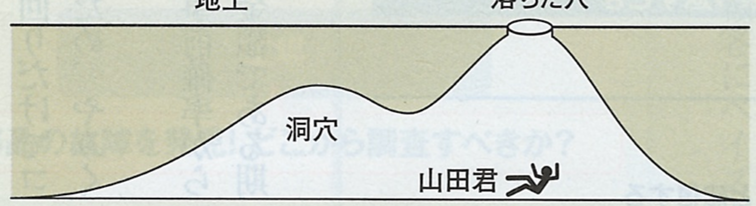

ランダムに歩いて（乱数発生）、小石を投げる（計測）

そこで山田君は、ランダムに歩き、近くの小石を拾って真上に投げ、小石が天井にぶつかり落ちてくる時間を測った。「ここが高いな」と思ったら、その付近に集中的に小石を投げた。合計で20回小石を投げ上げた。

足跡を数える（確率分布〈P（x）〉の推測）

暗闇の中、山田君が注目したのは足元だった。スマートフォンの明かりで足跡を調べ、その分布を見て洞穴の形状を推測。右から2番目の足跡までの確率を2／20、すなわち0.1とみた。

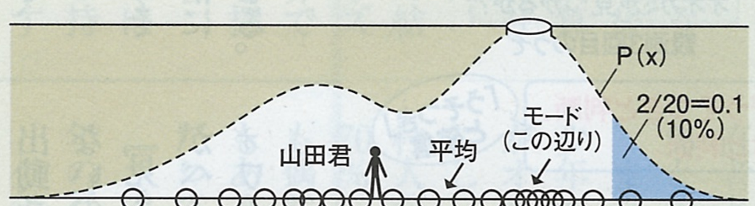

本質

天井ではなく足元を見る。これがMCMCの発想だ。小石を投げる回数を20回から1000回にすれば、推測の精度は上がる。体力勝負の力業であり、コンピューターとの相性が抜群だ

＊藤田一弥・フォワードネットワーク代表への取材を基に本誌編集部作成

LIGO Computing Latencies

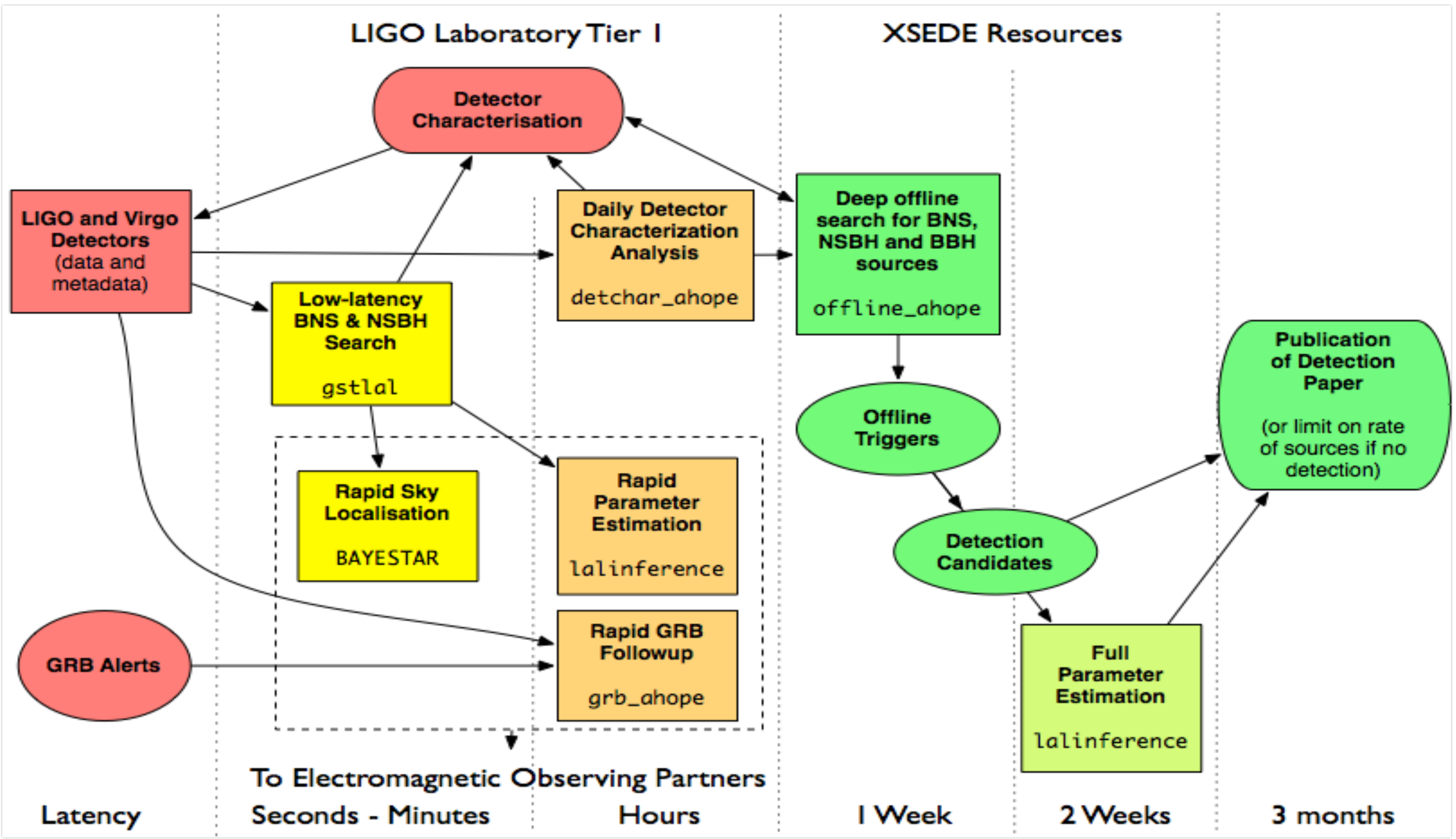

Sharon Brunett, 2015/10

CBC: compact binary coalescence

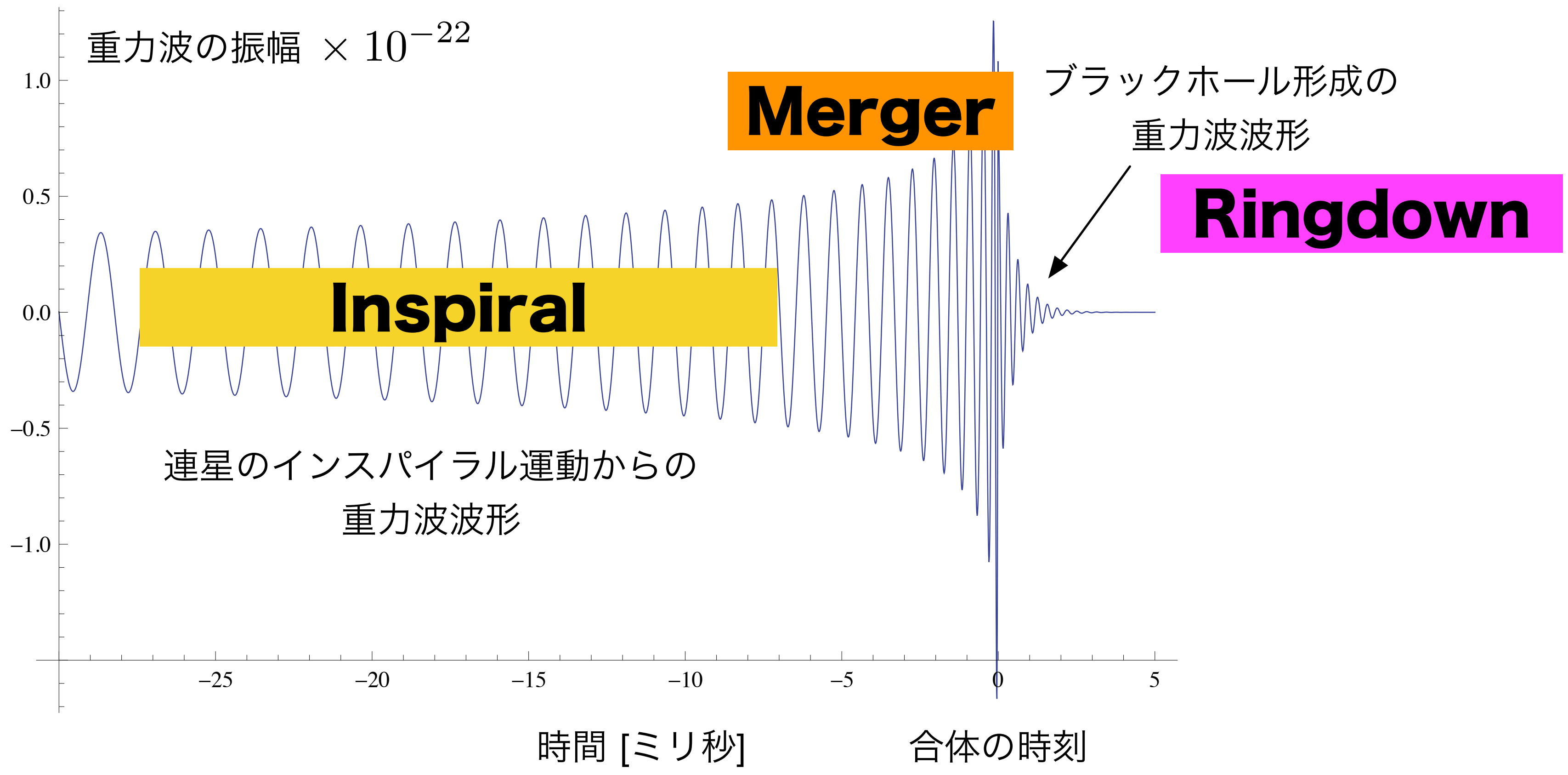

$$h(t) = -\frac{G\mathcal{M}}{c^2 D}\left(\frac{t_c - t}{5G\mathcal{M}/c^3}\right)^{-1/4} \cos 2[\varphi(t) + \Delta\varphi]$$

where

$$D \equiv r\left[F_+^2\left(\frac{1+\cos^2\iota}{2}\right)^2 + F_\times^2\ \cos^2\iota\right]^{-1/2}$$

and

$$2\Delta\varphi \equiv -\tan^{-1}\left(\frac{F_\times}{F_+}\frac{2\cos\iota}{1+\cos^2\iota}\right)$$

Horizon distance (Observational range)

$$D_{\mathrm{horizon}} = \frac{2}{5}\sqrt{\frac{5}{6}}\frac{c}{\pi^{2/3}}\left(\frac{G\mathcal{M}}{c^3}\right)^{5/6}\left[\int_{f_{\min}}^{f_{\max}}\frac{f^{7/3}}{S_n(f)}df\right]^{1/2}\frac{1}{\rho}$$

Horizon distance

LVK, 1304.0670 (2020/1 update)

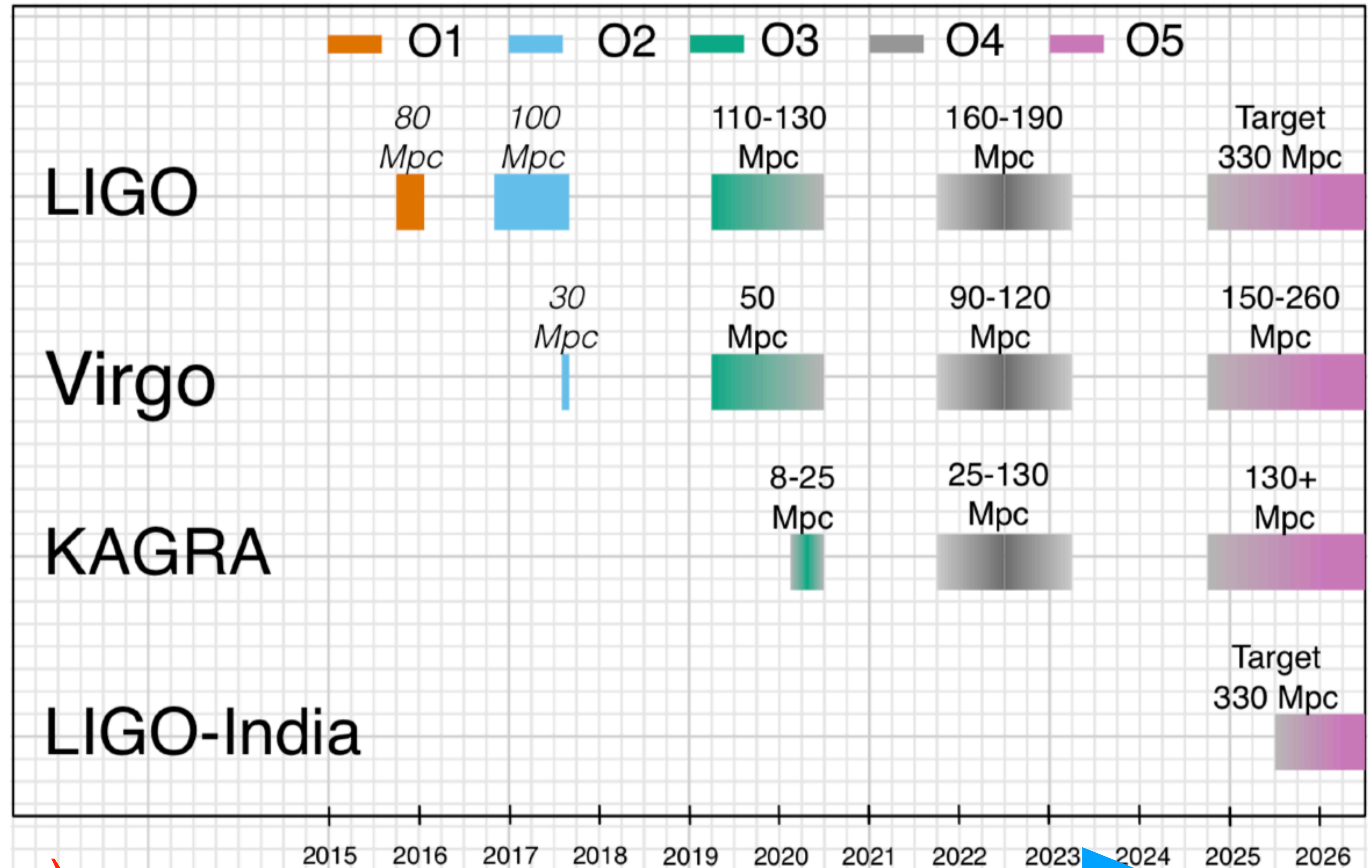

遅

Horizon distance (Observational range)

		O1	O2	O3	O4	O5
BNS Range (Mpc)	aLIGO	80	100	110 – 130	160 – 190	330
	AdV	-	30	50	90 – 120	150 – 260
	KAGRA	-	-	8 – 25	25 – 130	130+
BBH Range (Mpc)	aLIGO	740	910	990 – 1200	1400 – 1600	2500
	AdV	-	270	500	860 – 1100	1300 – 2100
	KAGRA	-	-	80 – 260	260 – 1200	1200+
NSBH Range (Mpc)	aLIGO	140	180	190 – 240	300 – 330	590
	AdV	-	50	90	170 – 220	270 – 480
	KAGRA	-	-	15 – 45	45 – 290	290+
Burst Range (Mpc)	aLIGO	50	60	80 – 90	110 – 120	210
$[E_{\rm GW}=10^{-2}M_\odot c^2]$	AdV	-	25	35	65 – 80	100 – 155
	KAGRA	-	-	5 – 25	25 – 95	95+
Burst Range (kpc)	aLIGO	15	20	25 – 30	35 – 40	70
$[E_{\rm GW}=10^{-9}M_\odot c^2]$	AdV	-	10	10	20 – 25	35 – 50
	KAGRA	-	-	0 – 10	10 – 30	30+

Table 2 Achieved and projected detector sensitivities for a $1.4M_\odot$+$1.4M_\odot$ BNS system, a $30M_\odot$+$30M_\odot$ BBH system, a $1.4M_\odot$+$10M_\odot$ NSBH system, and for an unmodeled burst signal. The quoted ranges correspond to the orientation-averaged spacetime volumes surveyed per unit detector time. For the burst ranges, we assume an emitted energy in GWs at 140 Hz of $E_{\rm GW}=10^{-2}M_\odot c^2$ and of $E_{\rm GW}=10^{-9}M_\odot c^2$. The later is consistent with the order of magnitude of the energy expected from core-collapse of massive stars (see footnote 4). Both CBC and burst ranges are obtained using a single-detector SNR threshold of 8. The O1 and O2 numbers are representative of the best ranges for the LIGO detectors: Hanford in O1 and Livingston in O2. The O3 numbers for aLIGO and AdV reflect recent average performance of each of the three detectors. Range intervals are quoted for future observing runs due to uncertainty about the sequence and impact of upgrades.

rho=8

$$D_{\rm horizon}=\frac{2}{5}\sqrt{\frac{5}{6}\frac{c}{\pi^{2/3}}}\left(\frac{G\mathcal{M}}{c^3}\right)^{5/6}\left[\int_{f_{\rm min}}^{f_{\rm max}}\frac{f^{7/3}}{S_n(f)}df\right]^{1/2}\frac{1}{\rho}$$

CBC: compact binary coalescence

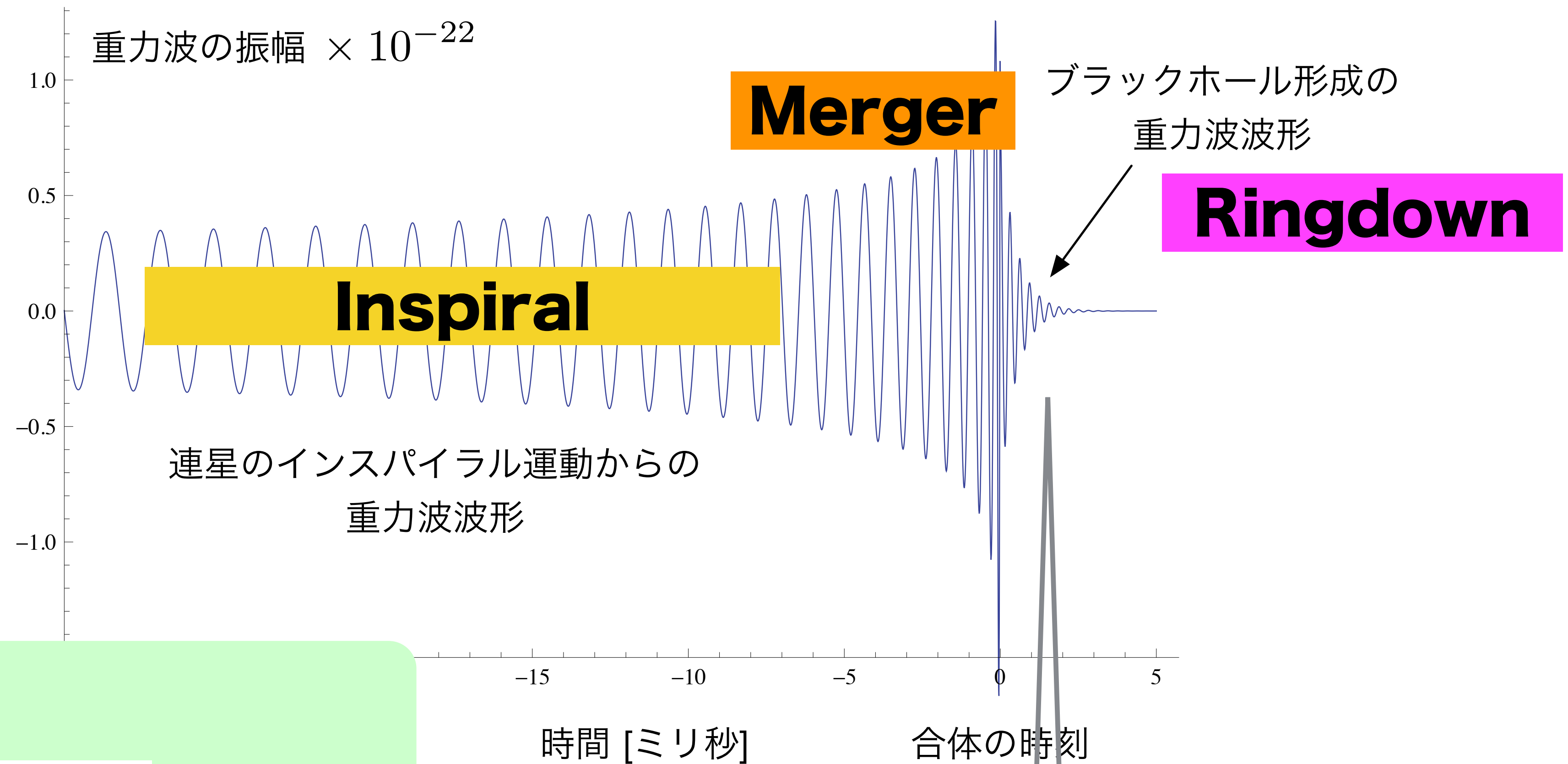

Fitting formula

$$f_R = f_1 + f_2(1-a)^{f_3}$$

$$Q \equiv \frac{f_R}{2f_I} = q_1 + q_2(1-a)^{q_3}$$

$$f_1 = 1.5251, \quad f_2 = -1.1568, \quad f_3 = 0.1292$$
$$q_1 = 0.7000, \quad q_2 = 1.4187, \quad q_3 = -0.4990.$$

$$h(t) = Ae^{-(t-t_0)/\tau}\cos(2\pi f_R(t-t_0)-\phi_0)$$

$$h(t) \sim Ae^{i2\pi f_{\rm qnm} t} = Ae^{i2\pi(f_R + i f_I)t}$$

$$a = 1 - \left(\frac{Q-q_1}{q_2}\right)^{1/q_3}$$

$$M[M_\odot] = \frac{c^3}{2\pi G}\frac{f_1 + f_2(1-a)^{f_3}}{f_{\rm qnm}[\mathrm{Hz}]}$$

BH mass and spin.

CBC: compact binary coalescence

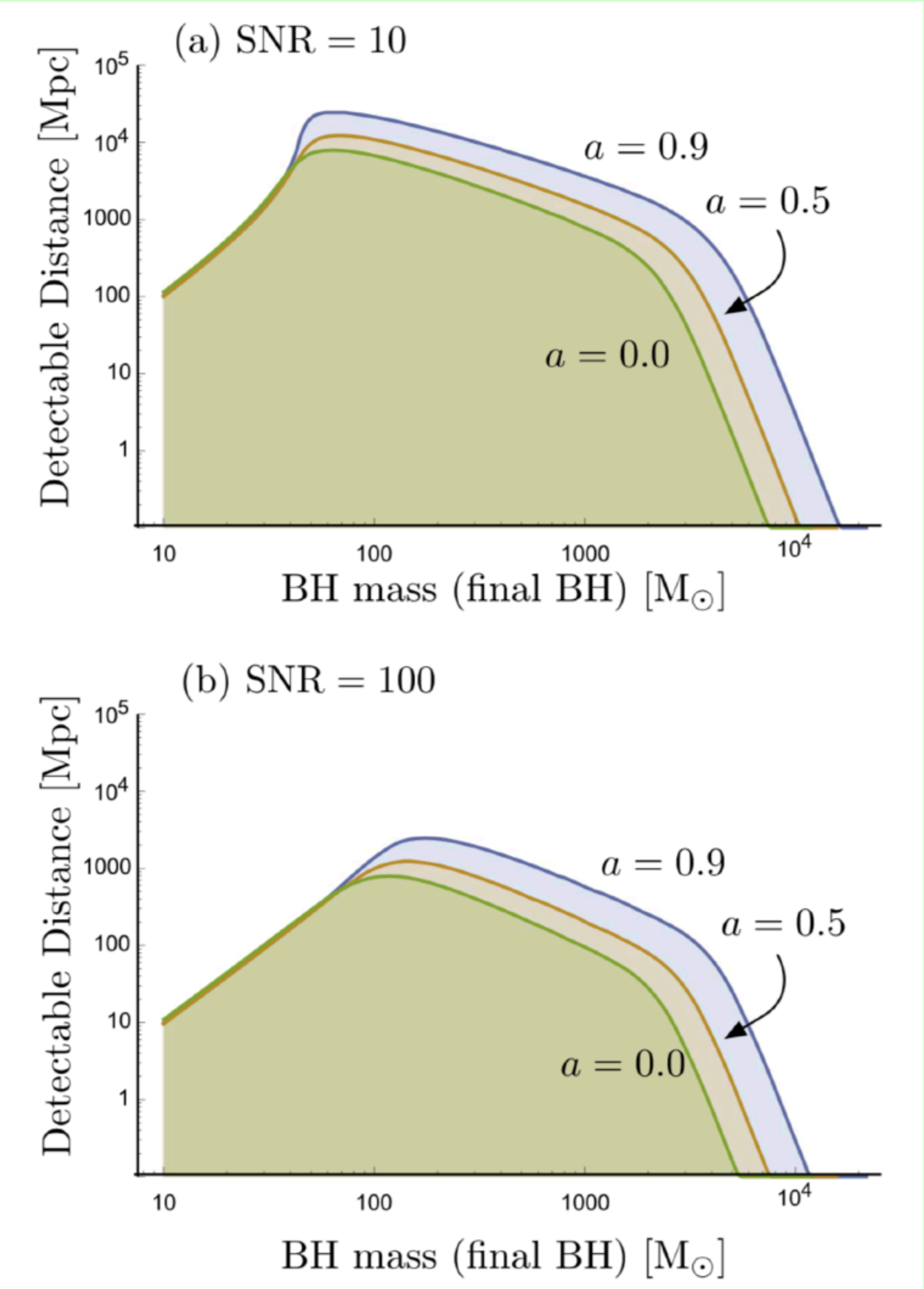

Figure 8. Detectable distance D of the ring-down signal at KAGRA. S/N is set to (a) 10 and (b) 100.

HS+, ApJ 835 (2017)276

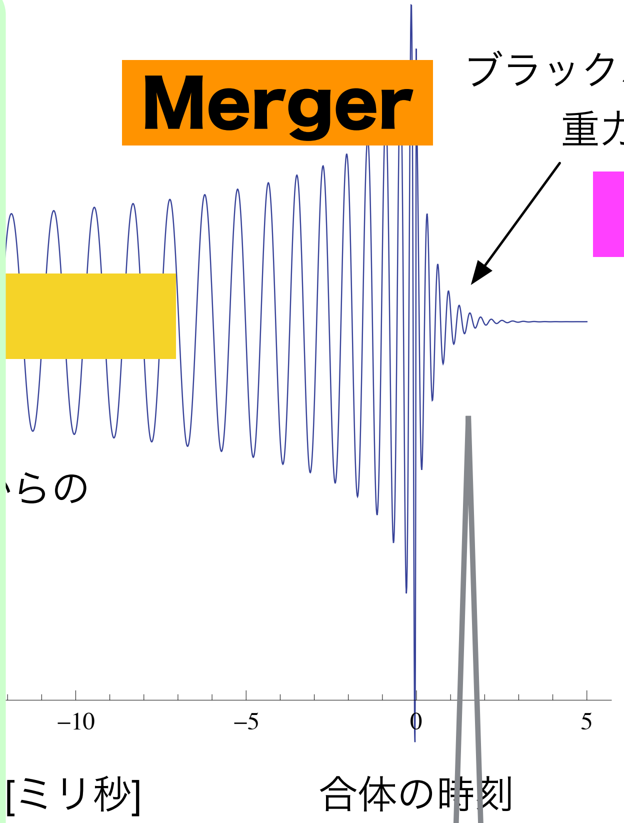

$$h(t) = Ae^{-(t-t_0)/\tau}\cos(2\pi f_R(t-t_0)-\phi_0)$$

Horizon distance (Observational range)

$$\rho^2 = \frac{8}{5}\frac{\epsilon_r(a)}{f_R^2}\frac{(1+z)M}{S_h(f_R/(1+z))} \times \left(\frac{(1+z)M}{d_L(z)}\right)^2\left(\frac{4\mu}{M}\right)^2.$$

観測スケジュール （Observation 1/2/3a/3b）

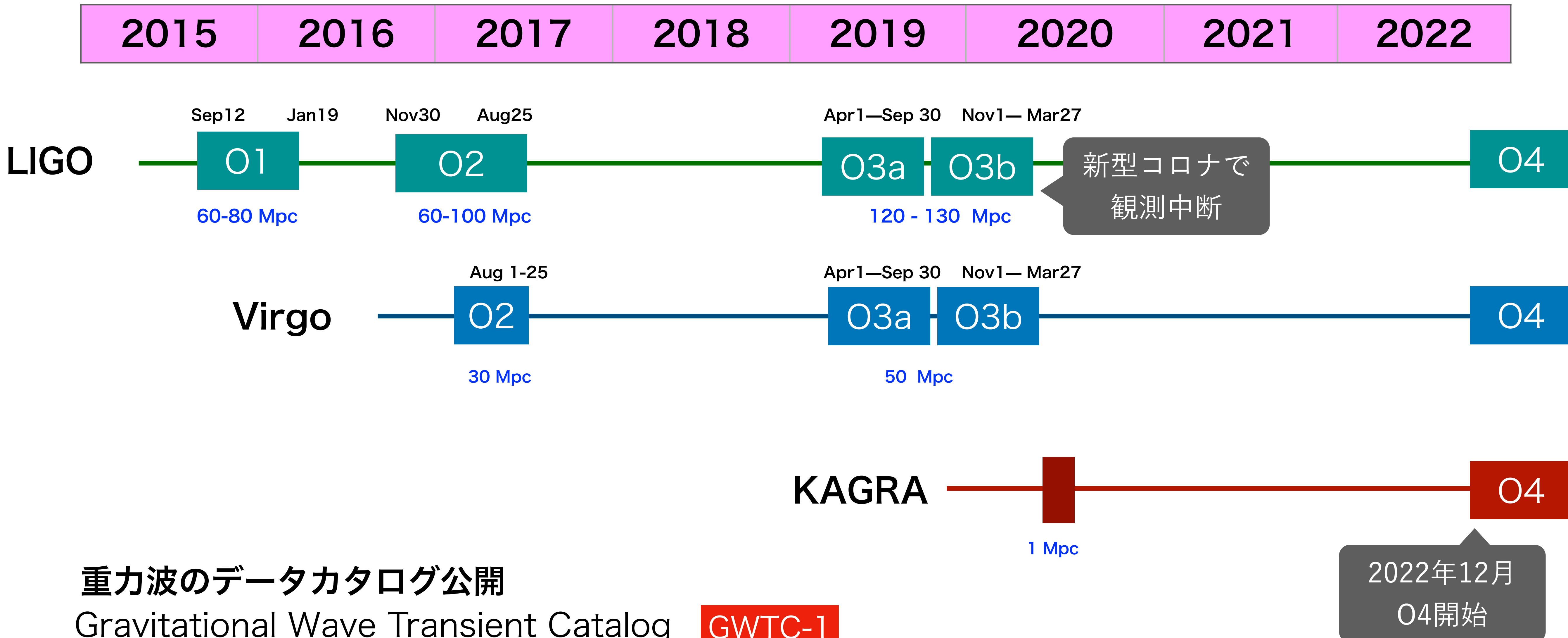

重力波のデータカタログ公開

Gravitational Wave Transient Catalog

GWTC-1
2018/12/3

GWTC-2
2020/10/28

GWTC-2.1
2021/8/2

GWTC-3
2021/11/5

https://www.gw-openscience.org

Public Alert started from O3a

https://gracedb.ligo.org

https://monitor.ligo.org/gwstatus

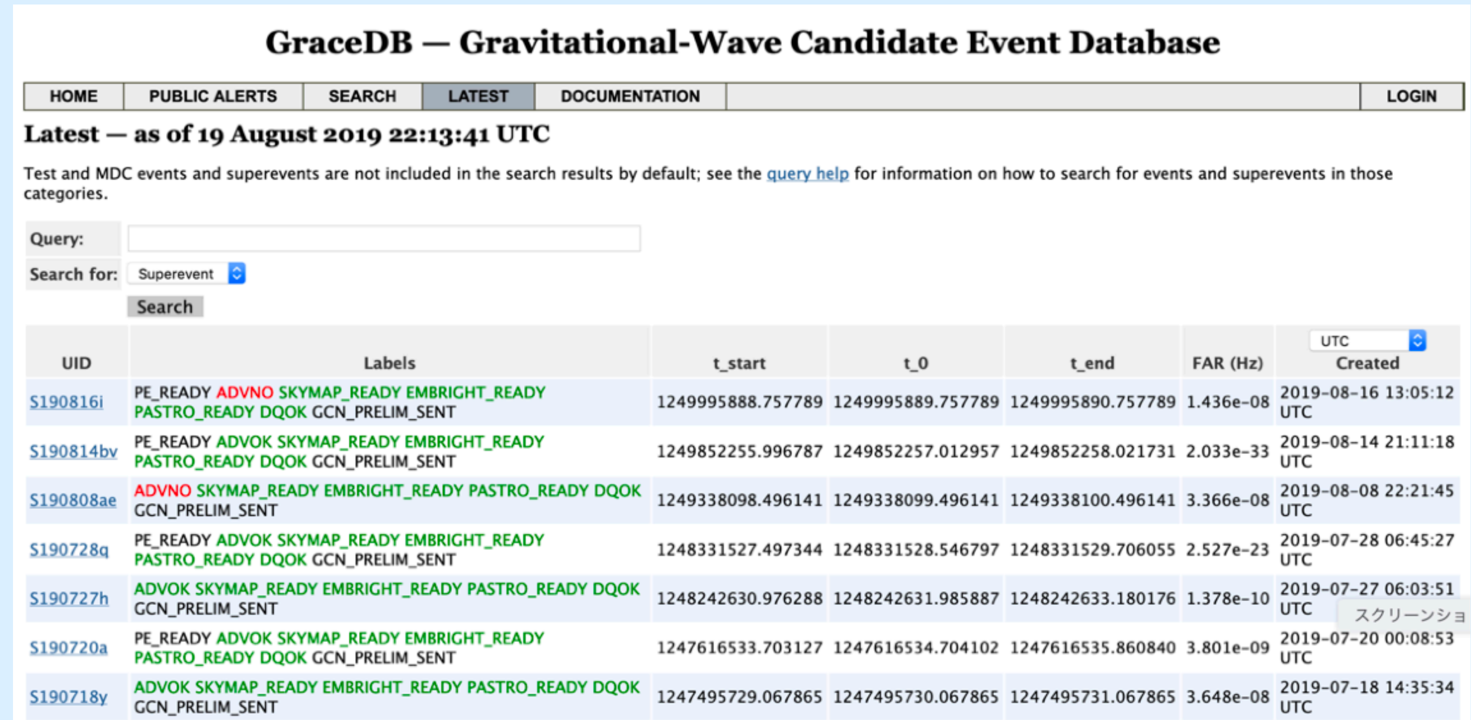

GraceDB — Gravitational-Wave Candidate Event Database

HOME | PUBLIC ALERTS | SEARCH | LATEST | DOCUMENTATION | LOGIN

Latest — as of 19 August 2019 22:13:41 UTC

Test and MDC events and superevents are not included in the search results by default; see the query help for information on how to search for events and superevents in those categories.

Query:

Search for: Superevent

Search

UID	Labels	t_start	t_0	t_end	FAR (Hz)	UTC Created
S190816i	PE_READY ADVNO SKYMAP_READY EMBRIGHT_READY PASTRO_READY DQOK GCN_PRELIM_SENT	1249995888.757789	1249995889.757789	1249995890.757789	1.436e-08	2019-08-16 13:05:12 UTC
S190814bv	PE_READY ADVOK SKYMAP_READY EMBRIGHT_READY PASTRO_READY DQOK GCN_PRELIM_SENT	1249852255.996787	1249852257.012957	1249852258.021731	2.033e-33	2019-08-14 21:11:18 UTC
S190808ae	ADVNO SKYMAP_READY EMBRIGHT_READY PASTRO_READY DQOK GCN_PRELIM_SENT	1249338098.496141	1249338099.496141	1249338100.496141	3.366e-08	2019-08-08 22:21:45 UTC
S190728q	PE_READY ADVOK SKYMAP_READY EMBRIGHT_READY PASTRO_READY DQOK GCN_PRELIM_SENT	1248331527.497344	1248331528.546797	1248331529.706055	2.527e-23	2019-07-28 06:45:27 UTC
S190727h	ADVOK SKYMAP_READY EMBRIGHT_READY PASTRO_READY DQOK GCN_PRELIM_SENT	1248242630.976288	1248242631.985887	1248242633.180176	1.378e-10	2019-07-27 06:03:51 UTC
S190720a	PE_READY ADVOK SKYMAP_READY EMBRIGHT_READY PASTRO_READY DQOK GCN_PRELIM_SENT	1247616533.703127	1247616534.704102	1247616535.860840	3.801e-09	2019-07-20 00:08:53 UTC
S190718y	ADVOK SKYMAP_READY EMBRIGHT_READY PASTRO_READY DQOK GCN_PRELIM_SENT	1247495729.067865	1247495730.067865	1247495731.067865	3.648e-08	2019-07-18 14:35:34 UTC

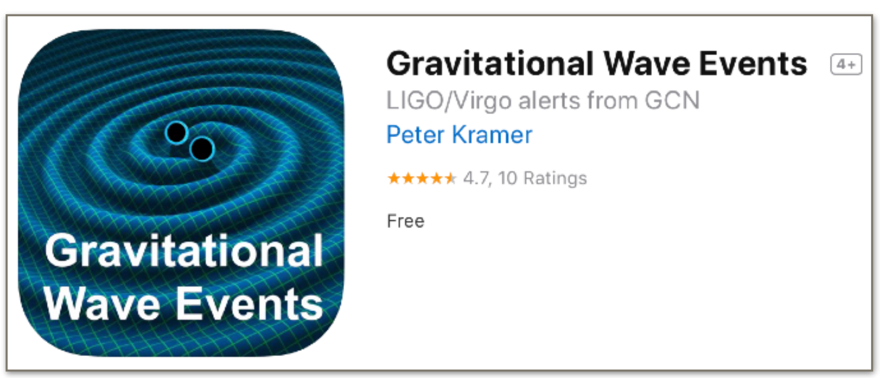

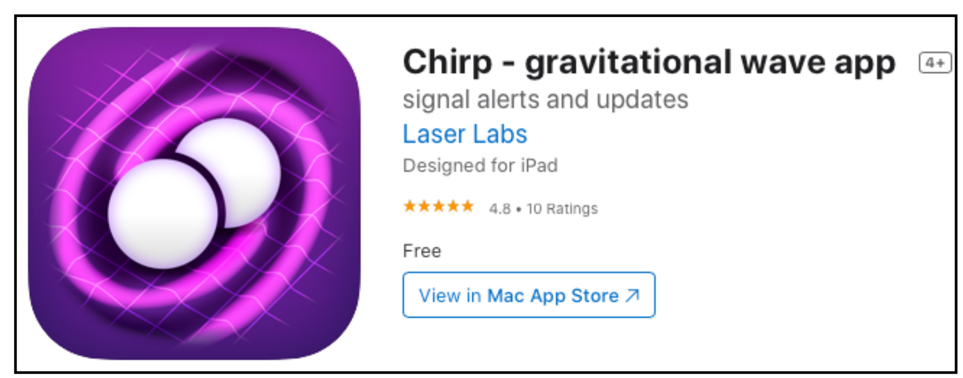

重力波観測情報は，アプリで見る時代

Public Alerts

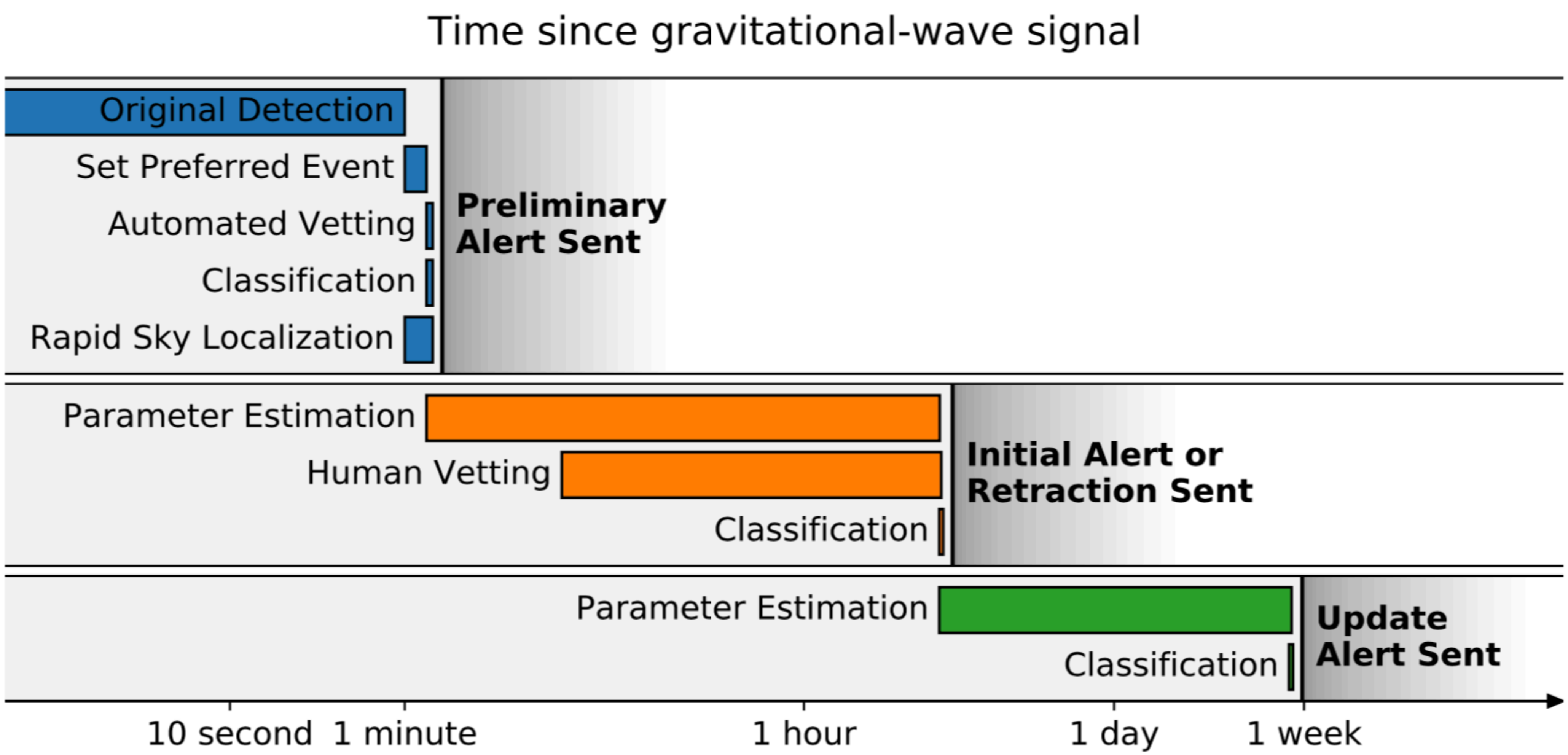

Fig. 8 Alert timeline. The *Preliminary GCN Notice* is sent autonomously within 1-10 minutes after the GW candidate trigger time. Some preliminary alerts may be retracted after human inspection for data quality, instrumental conditions, and pipeline behavior. The human vetted *Initial GCN Notice* or *Retraction GCN Notice* and associated *GCN Circular* are distributed within a few hours for BNS or NSBH sources and within one day for BBH. Update notices and circulars are sent whenever the estimate of the parameters of the signal significantly improves. Figure adapted from the LIGO/Virgo Public Alerts User Guide (see footnote 17)

https://emfollow.docs.ligo.org/userguide/

Public Alerts

GraceDB — Gravitational-Wave Candidate Event Database

HOME | PUBLIC ALERTS | SEARCH | LATEST | DOCUMENTATION | LOGIN

Latest — as of 15 February 2020 13:15:11 UTC

Test and MDC events and superevents are not included in the search results by default; see the query help for information on how to search for events and superevents in those categories.

Query:

Search for: Superevent

Search

UID	Labels	t_start	t_0	t_end	FAR (Hz)	UTC Created
S200213t	EM_READY ADVOK EM_Selected SKYMAP_READY EMBRIGHT_READY PASTRO_READY DQOK GCN_PRELIM_SENT	1265602257.327981	1265602258.327981	1265602259.327981	1.767e-08	2020-02-13 04:11:05 UTC
S200208q	EM_READY PE_READY ADVOK EM_Selected SKYMAP_READY EMBRIGHT_READY PASTRO_READY DQOK GCN_PRELIM_SENT	1265202094.944824	1265202095.991118	1265202096.991118	2.518e-09	2020-02-08 13:01:39 UTC
S200129m	EM_READY PE_READY ADVOK EM_Selected SKYMAP_READY EMBRIGHT_READY PASTRO_READY DQOK GCN_PRELIM_SENT	1264316115.411621	1264316116.435104	1264316117.460904	6.697e-32	2020-01-29 06:55:42 UTC
S200128d	EM_READY PE_READY ADVOK EM_Selected SKYMAP_READY EMBRIGHT_READY PASTRO_READY DQOK GCN_PRELIM_SENT	1264213228.897043	1264213229.903320	1264213230.953959	1.647e-08	2020-01-28 02:20:36 UTC
S200116ah	EM_READY PE_READY ADVNO EM_Selected SKYMAP_READY EMBRIGHT_READY PASTRO_READY DQOK GCN_PRELIM_SENT	1263211019.170712	1263211020.170712	1263211021.170712	2.029e-12	2020-01-16 11:57:11 UTC
S200115j	EM_READY PE_READY ADVOK EM_Selected SKYMAP_READY EMBRIGHT_READY PASTRO_READY DQOK GCN_PRELIM_SENT	1263097406.735840	1263097407.752869	1263097408.769043	2.094e-11	2020-01-15 04:23:40 UTC
S200114f	EM_READY ADVOK EM_Selected SKYMAP_READY DQOK GCN_PRELIM_SENT	1263002916.225766	1263002916.239300	1263002916.252885	1.226e-09	2020-01-14 02:11:12 UTC
S200112r	EM_READY PE_READY ADVOK EM_Selected SKYMAP_READY EMBRIGHT_READY PASTRO_READY DQOK GCN_PRELIM_SENT	1262879935.091777	1262879936.093931	1262879937.093931	1.283e-11	2020-01-12 15:59:06 UTC

https://gracedb.ligo.org/latest/

GWTC-1

PHYSICAL REVIEW X **9**, 031040 (2019)

GWTC-1: A Gravitational-Wave Transient Catalog of Compact Binary Mergers Observed by LIGO and Virgo during the First and Second Observing Runs

B. P. Abbott *et al.*[*]
(LIGO Scientific Collaboration and Virgo Collaboration)

(Received 14 December 2018; revised manuscript received 27 March 2019; published 4 September 2019)

O1: September 12, 2015 -- January 19, 2016
▶ GW150914 BHBH
O2: November 30, 2016 -- August 25, 2017
▶ GW170817 NSNS
▶ **GWTC-1 catalogue paper [arXiv:1811.12907]**
▶ **data released to public Feb, 2019**

O3a: April 1, 2019 -- September 30, 2019
▶ data released to public April, 2021
O3b: November 1, 2019 -- May 1, 2020
▶ data released to public November, 2021

Sky Localization

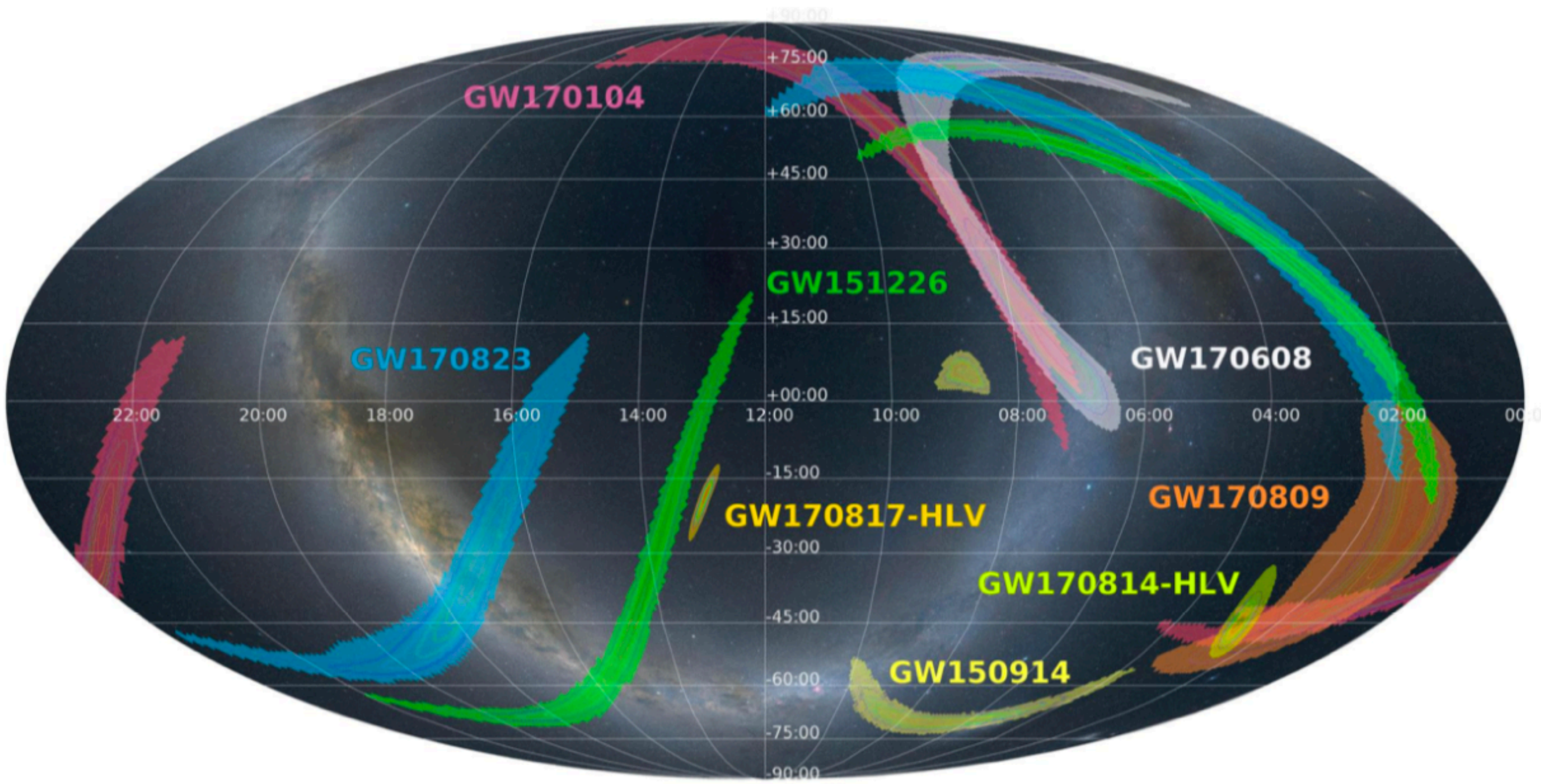

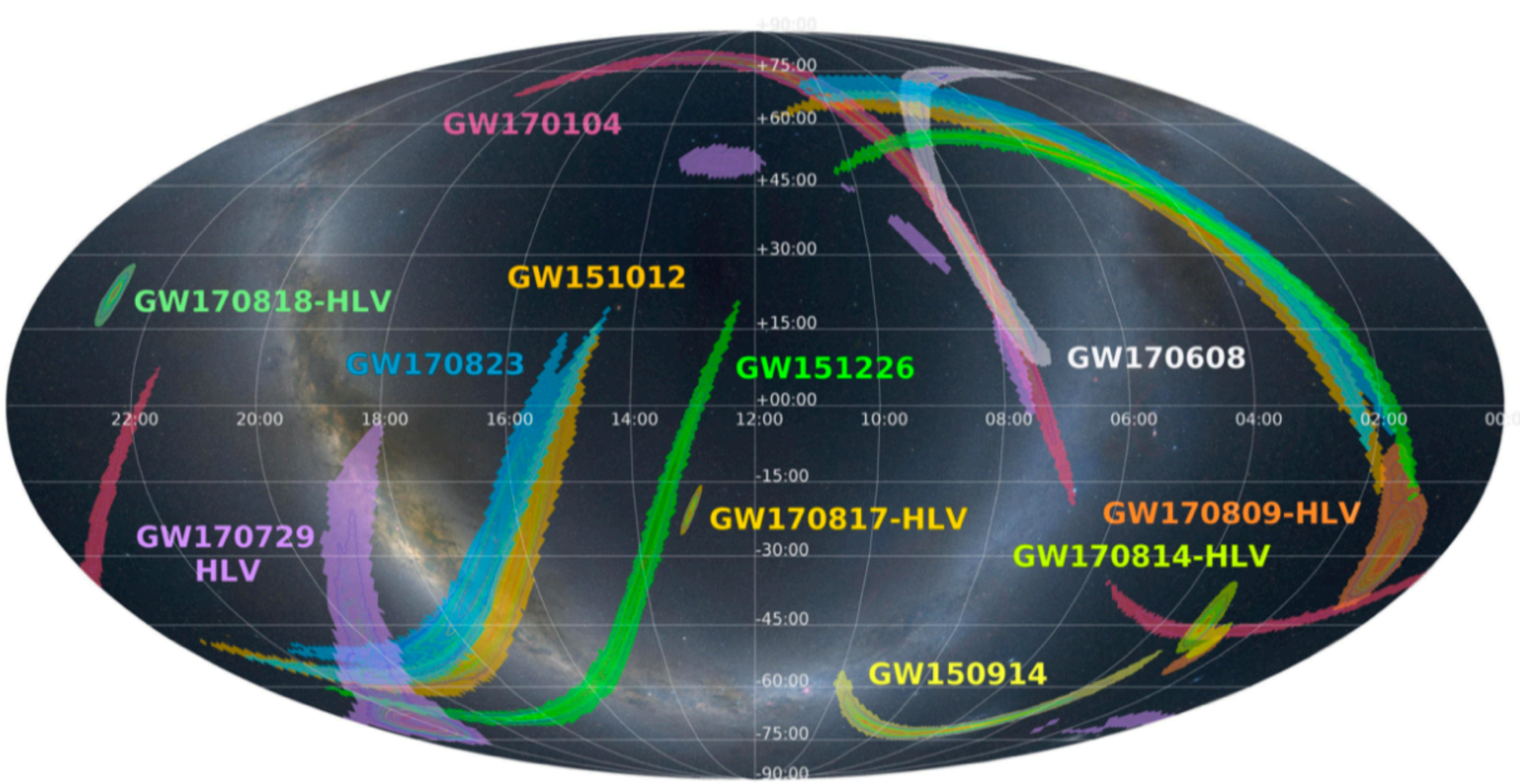

	Low-latency analysis			Refined analysis		
Event	d_L(Mpc)	$\Delta\Omega$(deg^2)	IFOs	d_L(Mpc)	$\Delta\Omega$(deg^2)	IFOs
GW150914	—	307	HL	440^{+150}_{-170}	182	HL
GW151012	—	—	—	1080^{+550}_{-490}	1523	HL
GW151226	—	1337	HL	490^{+180}_{-190}	1033	HL
GW170104	730^{+340}_{-320}	1632	HL	990^{+440}_{-430}	921	HL
GW170608	310^{+200}_{-120}	864	HL	320^{+120}_{-110}	392	HL
GW170729	—	—	—	2840^{+1400}_{-1360}	1041	HLV
GW170809	1080^{+520}_{-470}	1155	HL	1030^{+320}_{-390}	308	HLV
GW170814	480^{+190}_{-170}	97	HLV	600^{+150}_{-220}	87	HLV
GW170817	40^{+10}_{-10}	31	HLV	40^{+7}_{-15}	16	HLV
GW170818	—	—	—	1060^{+420}_{-380}	39	HLV
GW170823	1380^{+700}_{-670}	2145	HL	1940^{+970}_{-900}	1666	HL

LV event categories

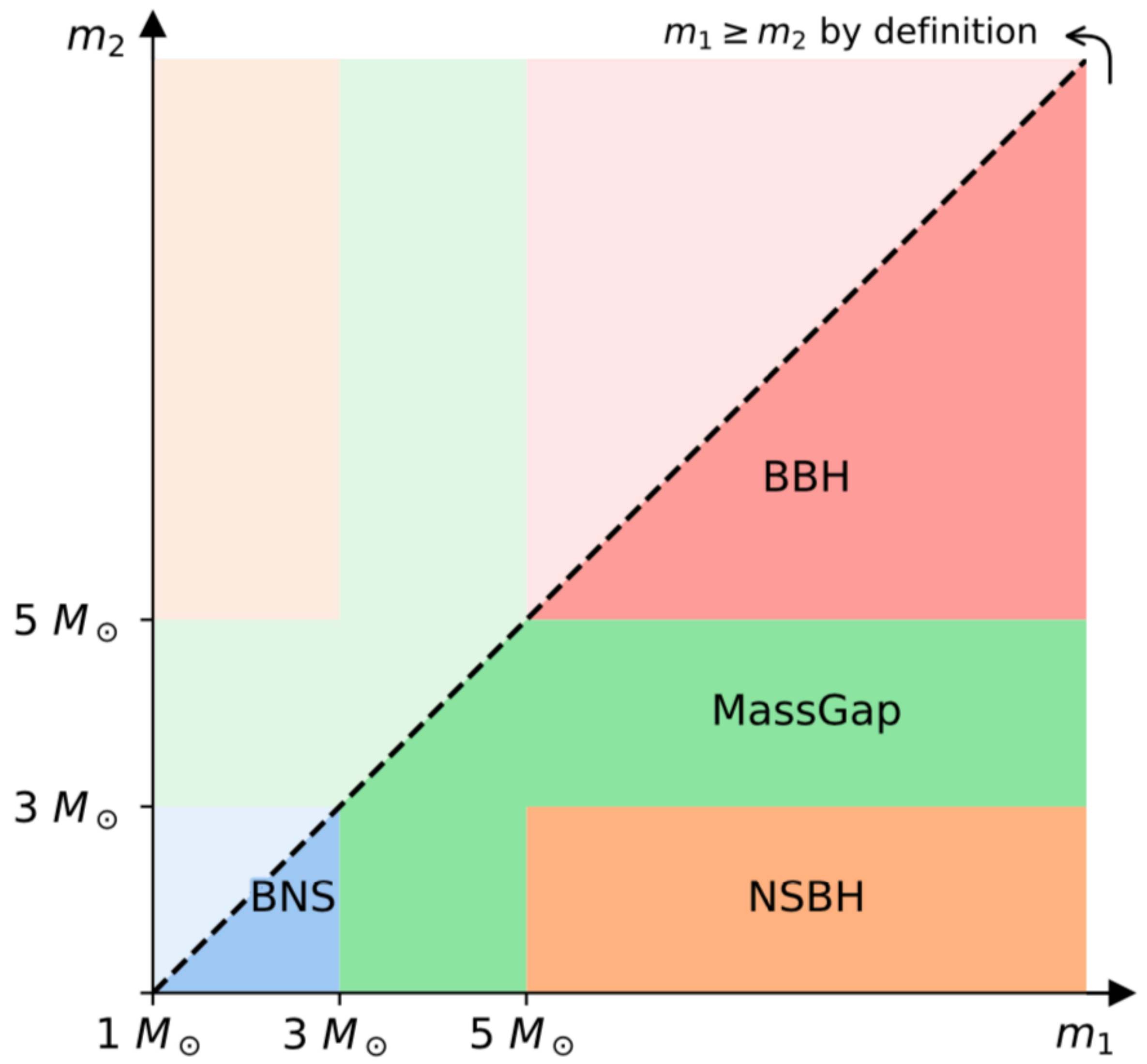

Fig. 9 The four astrophysical categories in terms (BNS, NSBH, BBH, and MassGap) of component masses *m1* and *m2*, which are used to define the source classification. By convention, the component masses are defined such that $m1 \geqslant m2$, so that the primary compact object in the binary (i.e., component 1), is always more massive than the secondary compact object (i.e., component 2). Figure adapted from the LIGO/Virgo Public Alerts User Guide (see footnote 17)

https://emfollow.docs.ligo.org/userguide/

GWTC-2

Gravitational Wave Transient Catalog 2

PHYSICAL REVIEW X **11**, 021053 (2021)

arXiv:2010.14527

GWTC-2: Compact Binary Coalescences Observed by LIGO and Virgo during the First Half of the Third Observing Run

R. Abbott *et al.**

(LIGO Scientific Collaboration and Virgo Collaboration)

(Received 30 October 2020; revised 23 February 2021; accepted 20 April 2021; published 9 June 2021)

*39 events in O3a

50 events in total

* False-Alarm Rate < 2 / 1 yr

* GWyymmdd_hhmmss for new events

- GW190412: the first BBH with definitively asymmetric component masses, which also shows evidence for higher harmonics
- GW190425: the second gravitational-wave event consistent with a BNS, following GW170817
- GW190426_152155: a low-mass event consistent with either an NSBH or BBH
- GW190514_065416: a BBH with the smallest effective aligned spin of all O3a events
- GW190517_055101: a BBH with the largest effective aligned spin of all O3a events
- GW190521: a BBH with total mass over 150 times the mass of the Sun
- GW190814: a highly asymmetric system of ambiguous nature, corresponding to the merger of a 23 solar mass black hole with a 2.6 solar mass compact object, making the latter either the lightest black hole or heaviest neutron star observed in a compact binary
- GW190924_021846: likely the lowest-mass BBH, with both black holes exceeding 3 solar masses

arXiv:2010.14529 Test of GR

arXiv:2010.14533 Population properties

Event	M ($M_\odot$)	$\mathcal{M}$ ($M_\odot$)	m_1 ($M_\odot$)	m_2 ($M_\odot$)	$\chi_{\rm eff}$	$D_{\rm L}$ (Gpc)	z	$M_{\rm f}$ ($M_\odot$)	$\chi_{\rm f}$	$\Delta\Omega$ (deg^2)	SNR
GW190408_181802	$42.9^{+4.1}_{-2.9}$	$18.3^{+1.8}_{-1.2}$	$24.5^{+5.1}_{-3.4}$	$18.3^{+3.2}_{-3.5}$	$-0.03^{+0.13}_{-0.19}$	$1.58^{+0.40}_{-0.59}$	$0.30^{+0.06}_{-0.10}$	$41.0^{+3.8}_{-2.7}$	$0.67^{+0.06}_{-0.07}$	140	$15.3^{+0.2}_{-0.3}$
GW190412	$38.4^{+3.8}_{-3.7}$	$13.3^{+0.4}_{-0.3}$	$30.0^{+4.7}_{-5.1}$	$8.3^{+1.6}_{-0.9}$	$0.25^{+0.08}_{-0.11}$	$0.74^{+0.14}_{-0.17}$	$0.15^{+0.03}_{-0.03}$	$37.3^{+3.9}_{-3.9}$	$0.67^{+0.05}_{-0.06}$	21	$18.9^{+0.2}_{-0.3}$
GW190413_052954	$56.9^{+13.1}_{-8.9}$	$24.0^{+5.4}_{-3.7}$	$33.4^{+12.4}_{-7.4}$	$23.4^{+6.7}_{-6.3}$	$0.01^{+0.29}_{-0.33}$	$4.10^{+2.41}_{-1.89}$	$0.66^{+0.30}_{-0.27}$	$54.3^{+12.4}_{-8.4}$	$0.69^{+0.12}_{-0.13}$	1400	$8.9^{+0.4}_{-0.8}$
GW190413_134308	$76.1^{+15.9}_{-10.6}$	$31.9^{+7.3}_{-4.6}$	$45.4^{+13.6}_{-9.6}$	$30.9^{+10.2}_{-9.6}$	$-0.01^{+0.24}_{-0.28}$	$5.15^{+2.44}_{-2.34}$	$0.80^{+0.30}_{-0.31}$	$72.8^{+15.2}_{-10.3}$	$0.69^{+0.10}_{-0.12}$	520	$10.0^{+0.4}_{-0.5}$
GW190421_213856	$71.8^{+12.5}_{-8.6}$	$30.7^{+5.5}_{-3.9}$	$40.6^{+10.4}_{-6.6}$	$31.4^{+7.5}_{-8.2}$	$-0.05^{+0.23}_{-0.26}$	$3.15^{+1.37}_{-1.42}$	$0.53^{+0.18}_{-0.21}$	$68.6^{+11.7}_{-8.1}$	$0.68^{+0.10}_{-0.11}$	1000	$10.7^{+0.2}_{-0.4}$
GW190424_180648	$70.7^{+13.4}_{-9.8}$	$30.3^{+5.7}_{-4.2}$	$39.5^{+10.9}_{-6.9}$	$31.0^{+7.4}_{-7.3}$	$0.15^{+0.22}_{-0.22}$	$2.55^{+1.56}_{-1.33}$	$0.45^{+0.22}_{-0.21}$	$67.1^{+12.5}_{-9.2}$	$0.75^{+0.08}_{-0.09}$	26000	$10.4^{+0.2}_{-0.4}$
GW190425	$3.4^{+0.3}_{-0.1}$	$1.44^{+0.02}_{-0.02}$	$2.0^{+0.6}_{-0.3}$	$1.4^{+0.3}_{-0.3}$	$0.06^{+0.11}_{-0.05}$	$0.16^{+0.07}_{-0.07}$	$0.03^{+0.01}_{-0.02}$	–	–	9900	$12.4^{+0.3}_{-0.4}$
GW190426_152155	$7.2^{+3.5}_{-1.5}$	$2.41^{+0.08}_{-0.08}$	$5.7^{+4.0}_{-2.3}$	$1.5^{+0.8}_{-0.5}$	$-0.03^{+0.33}_{-0.30}$	$0.38^{+0.19}_{-0.16}$	$0.08^{+0.04}_{-0.03}$	–	–	1400	$8.7^{+0.5}_{-0.6}$
GW190503_185404	$71.3^{+9.3}_{-8.0}$	$30.1^{+4.2}_{-4.0}$	$42.9^{+9.2}_{-7.8}$	$28.5^{+7.5}_{-7.9}$	$-0.02^{+0.20}_{-0.26}$	$1.52^{+0.71}_{-0.66}$	$0.29^{+0.11}_{-0.11}$	$68.2^{+8.7}_{-7.5}$	$0.67^{+0.09}_{-0.12}$	94	$12.4^{+0.2}_{-0.3}$
GW190512_180714	$35.6^{+3.9}_{-3.4}$	$14.5^{+1.3}_{-1.0}$	$23.0^{+5.4}_{-5.7}$	$12.5^{+3.5}_{-2.5}$	$0.03^{+0.13}_{-0.13}$	$1.49^{+0.53}_{-0.59}$	$0.28^{+0.09}_{-0.10}$	$34.2^{+3.9}_{-3.4}$	$0.65^{+0.07}_{-0.07}$	230	$12.2^{+0.2}_{-0.4}$
GW190513_205428	$53.6^{+8.6}_{-5.9}$	$21.5^{+3.6}_{-1.9}$	$35.3^{+9.6}_{-9.0}$	$18.1^{+7.3}_{-4.2}$	$0.12^{+0.29}_{-0.18}$	$2.16^{+0.94}_{-0.80}$	$0.39^{+0.14}_{-0.13}$	$51.3^{+8.1}_{-5.8}$	$0.69^{+0.14}_{-0.12}$	490	$12.9^{+0.3}_{-0.4}$
GW190514_065416	$64.2^{+16.6}_{-9.6}$	$27.4^{+6.9}_{-4.3}$	$36.9^{+13.4}_{-7.3}$	$27.5^{+8.2}_{-7.7}$	$-0.16^{+0.28}_{-0.32}$	$4.93^{+2.76}_{-2.41}$	$0.77^{+0.34}_{-0.33}$	$61.6^{+16.0}_{-9.2}$	$0.64^{+0.11}_{-0.14}$	2400	$8.2^{+0.3}_{-0.6}$
GW190517_055101	$61.9^{+10.0}_{-9.6}$	$26.0^{+4.2}_{-4.0}$	$36.4^{+11.8}_{-7.8}$	$24.8^{+6.9}_{-7.1}$	$0.53^{+0.20}_{-0.19}$	$2.11^{+1.79}_{-1.00}$	$0.38^{+0.26}_{-0.16}$	$57.8^{+9.4}_{-9.1}$	$0.87^{+0.05}_{-0.07}$	460	$10.7^{+0.4}_{-0.6}$
GW190519_153544	$104.2^{+14.5}_{-14.9}$	$43.5^{+6.8}_{-6.8}$	$64.5^{+11.3}_{-13.2}$	$39.9^{+11.0}_{-10.6}$	$0.33^{+0.19}_{-0.22}$	$2.85^{+2.02}_{-1.14}$	$0.49^{+0.27}_{-0.17}$	$98.7^{+13.5}_{-14.2}$	$0.80^{+0.07}_{-0.12}$	770	$15.6^{+0.2}_{-0.3}$
GW190521	$157.9^{+37.4}_{-20.9}$	$66.9^{+15.5}_{-9.2}$	$91.4^{+29.3}_{-17.5}$	$66.8^{+20.7}_{-20.7}$	$0.06^{+0.31}_{-0.37}$	$4.53^{+2.30}_{-2.13}$	$0.72^{+0.29}_{-0.29}$	$150.3^{+35.8}_{-20.0}$	$0.73^{+0.11}_{-0.14}$	940	$14.2^{+0.3}_{-0.3}$
GW190521_074359	$74.4^{+6.8}_{-4.6}$	$31.9^{+3.1}_{-2.4}$	$42.1^{+5.9}_{-4.9}$	$32.7^{+5.4}_{-6.2}$	$0.09^{+0.10}_{-0.13}$	$1.28^{+0.38}_{-0.57}$	$0.25^{+0.06}_{-0.10}$	$70.7^{+6.4}_{-4.2}$	$0.72^{+0.05}_{-0.07}$	500	$25.8^{+0.1}_{-0.2}$
GW190527_092055	$58.5^{+27.9}_{-10.6}$	$24.2^{+11.9}_{-4.4}$	$36.2^{+19.1}_{-9.5}$	$22.8^{+12.7}_{-8.1}$	$0.13^{+0.29}_{-0.28}$	$3.10^{+4.85}_{-1.64}$	$0.53^{+0.61}_{-0.25}$	$55.9^{+26.4}_{-10.1}$	$0.73^{+0.12}_{-0.16}$	3800	$8.1^{+0.4}_{-1.0}$
GW190602_175927	$114.1^{+18.5}_{-15.7}$	$48.3^{+8.6}_{-8.0}$	$67.2^{+16.0}_{-12.6}$	$47.4^{+13.4}_{-16.6}$	$0.10^{+0.25}_{-0.25}$	$2.99^{+2.02}_{-1.26}$	$0.51^{+0.27}_{-0.19}$	$108.8^{+17.2}_{-14.8}$	$0.71^{+0.10}_{-0.13}$	720	$12.8^{+0.2}_{-0.3}$
GW190620_030421	$90.1^{+17.3}_{-12.1}$	$37.5^{+7.8}_{-5.7}$	$55.4^{+15.8}_{-12.0}$	$35.0^{+11.6}_{-11.4}$	$0.34^{+0.21}_{-0.25}$	$3.16^{+1.67}_{-1.43}$	$0.54^{+0.22}_{-0.21}$	$85.4^{+15.9}_{-11.4}$	$0.80^{+0.08}_{-0.14}$	6700	$12.1^{+0.3}_{-0.4}$
GW190630_185205	$58.8^{+4.7}_{-4.8}$	$24.8^{+2.1}_{-2.0}$	$35.0^{+6.9}_{-5.7}$	$23.6^{+5.2}_{-5.1}$	$0.10^{+0.12}_{-0.13}$	$0.93^{+0.56}_{-0.40}$	$0.19^{+0.10}_{-0.07}$	$56.1^{+4.5}_{-4.6}$	$0.70^{+0.06}_{-0.07}$	1300	$15.6^{+0.2}_{-0.3}$
GW190701_203306	$94.1^{+11.6}_{-9.3}$	$40.2^{+5.2}_{-4.7}$	$53.6^{+11.7}_{-7.8}$	$40.8^{+8.3}_{-11.5}$	$-0.06^{+0.23}_{-0.28}$	$2.14^{+0.79}_{-0.73}$	$0.38^{+0.12}_{-0.12}$	$90.0^{+10.8}_{-8.6}$	$0.67^{+0.09}_{-0.12}$	45	$11.3^{+0.2}_{-0.4}$
GW190706_222641	$101.6^{+17.9}_{-13.5}$	$42.0^{+8.4}_{-6.2}$	$64.0^{+15.2}_{-15.2}$	$38.5^{+12.5}_{-12.4}$	$0.32^{+0.25}_{-0.30}$	$5.07^{+2.57}_{-2.11}$	$0.79^{+0.31}_{-0.28}$	$96.3^{+16.7}_{-13.2}$	$0.80^{+0.08}_{-0.17}$	610	$12.6^{+0.2}_{-0.4}$
GW190707_093326	$20.0^{+1.9}_{-1.3}$	$8.5^{+0.6}_{-0.4}$	$11.5^{+3.3}_{-1.7}$	$8.4^{+1.4}_{-1.6}$	$-0.05^{+0.10}_{-0.08}$	$0.80^{+0.37}_{-0.38}$	$0.16^{+0.07}_{-0.07}$	$19.2^{+1.9}_{-1.3}$	$0.66^{+0.03}_{-0.04}$	1300	$13.3^{+0.2}_{-0.4}$
GW190708_232457	$30.8^{+2.5}_{-1.8}$	$13.1^{+0.9}_{-0.6}$	$17.5^{+4.7}_{-2.3}$	$13.1^{+2.0}_{-2.7}$	$0.02^{+0.10}_{-0.08}$	$0.90^{+0.33}_{-0.40}$	$0.18^{+0.06}_{-0.07}$	$29.4^{+2.5}_{-1.7}$	$0.69^{+0.04}_{-0.04}$	14000	$13.1^{+0.2}_{-0.3}$
GW190719_215514	$55.8^{+16.3}_{-10.0}$	$22.7^{+5.9}_{-3.7}$	$35.2^{+16.9}_{-9.9}$	$20.2^{+8.1}_{-6.5}$	$0.35^{+0.28}_{-0.32}$	$4.61^{+2.84}_{-2.17}$	$0.73^{+0.35}_{-0.30}$	$52.9^{+15.6}_{-9.5}$	$0.80^{+0.10}_{-0.16}$	2300	$8.3^{+0.3}_{-1.0}$
GW190720_000836	$21.3^{+4.3}_{-2.3}$	$8.9^{+0.5}_{-0.8}$	$13.3^{+6.6}_{-3.0}$	$7.8^{+2.2}_{-2.2}$	$0.18^{+0.14}_{-0.12}$	$0.81^{+0.71}_{-0.33}$	$0.16^{+0.12}_{-0.06}$	$20.3^{+4.5}_{-2.3}$	$0.72^{+0.06}_{-0.05}$	510	$11.0^{+0.3}_{-0.8}$
GW190727_060333	$65.8^{+10.9}_{-7.4}$	$28.1^{+4.9}_{-3.4}$	$37.2^{+9.4}_{-5.9}$	$28.8^{+6.6}_{-7.9}$	$0.12^{+0.26}_{-0.25}$	$3.60^{+1.56}_{-1.51}$	$0.60^{+0.20}_{-0.22}$	$62.6^{+10.2}_{-7.0}$	$0.73^{+0.10}_{-0.10}$	860	$11.9^{+0.3}_{-0.5}$
GW190728_064510	$20.5^{+4.5}_{-1.3}$	$8.6^{+0.5}_{-0.3}$	$12.2^{+7.1}_{-2.2}$	$8.1^{+1.7}_{-2.6}$	$0.12^{+0.19}_{-0.07}$	$0.89^{+0.25}_{-0.37}$	$0.18^{+0.05}_{-0.07}$	$19.5^{+4.6}_{-1.3}$	$0.71^{+0.04}_{-0.04}$	410	$13.0^{+0.2}_{-0.4}$
GW190731_140936	$67.1^{+15.3}_{-10.2}$	$28.4^{+6.8}_{-4.5}$	$39.3^{+11.8}_{-8.2}$	$28.0^{+8.9}_{-8.4}$	$0.08^{+0.24}_{-0.24}$	$3.97^{+2.56}_{-2.07}$	$0.65^{+0.32}_{-0.30}$	$63.9^{+14.4}_{-9.8}$	$0.71^{+0.10}_{-0.12}$	3000	$8.6^{+0.2}_{-0.5}$
GW190803_022701	$62.7^{+11.8}_{-8.4}$	$26.7^{+5.2}_{-3.8}$	$36.1^{+10.2}_{-6.7}$	$26.7^{+7.1}_{-7.6}$	$-0.01^{+0.25}_{-0.26}$	$3.69^{+2.04}_{-1.69}$	$0.61^{+0.26}_{-0.24}$	$59.9^{+11.2}_{-7.9}$	$0.69^{+0.10}_{-0.11}$	1500	$8.6^{+0.3}_{-0.5}$
GW190814	$25.8^{+1.0}_{-0.9}$	$6.09^{+0.06}_{-0.06}$	$23.2^{+1.1}_{-1.0}$	$2.59^{+0.08}_{-0.09}$	$0.00^{+0.06}_{-0.06}$	$0.24^{+0.04}_{-0.05}$	$0.05^{+0.009}_{-0.010}$	$25.6^{+1.0}_{-0.9}$	$0.28^{+0.02}_{-0.02}$	19	$24.9^{+0.1}_{-0.2}$
GW190828_063405	$57.5^{+7.5}_{-4.4}$	$24.8^{+3.3}_{-2.0}$	$31.8^{+5.8}_{-3.9}$	$25.9^{+4.4}_{-4.6}$	$0.19^{+0.15}_{-0.16}$	$2.22^{+0.63}_{-0.95}$	$0.40^{+0.09}_{-0.15}$	$54.5^{+6.9}_{-4.0}$	$0.76^{+0.06}_{-0.07}$	520	$16.2^{+0.2}_{-0.3}$
GW190828_065509	$34.1^{+5.5}_{-4.5}$	$13.3^{+1.2}_{-0.9}$	$23.8^{+7.2}_{-7.0}$	$10.2^{+3.5}_{-2.1}$	$0.08^{+0.16}_{-0.16}$	$1.66^{+0.63}_{-0.61}$	$0.31^{+0.10}_{-0.10}$	$32.9^{+5.7}_{-4.5}$	$0.65^{+0.09}_{-0.08}$	640	$10.0^{+0.3}_{-0.5}$
GW190909_114149	$71.2^{+54.3}_{-15.0}$	$29.5^{+17.5}_{-6.3}$	$43.2^{+50.7}_{-12.2}$	$27.6^{+13.0}_{-10.9}$	$-0.03^{+0.44}_{-0.36}$	$4.77^{+3.70}_{-2.66}$	$0.75^{+0.45}_{-0.37}$	$68.3^{+52.5}_{-14.5}$	$0.68^{+0.16}_{-0.18}$	4200	$8.1^{+0.4}_{-0.7}$
GW190910_112807	$78.7^{+9.5}_{-9.0}$	$33.9^{+4.3}_{-3.9}$	$43.5^{+7.6}_{-6.2}$	$35.1^{+6.3}_{-7.0}$	$0.02^{+0.19}_{-0.18}$	$1.57^{+1.07}_{-0.64}$	$0.29^{+0.17}_{-0.11}$	$75.0^{+8.7}_{-8.5}$	$0.70^{+0.08}_{-0.07}$	10000	$14.1^{+0.2}_{-0.3}$
GW190915_235702	$59.5^{+7.5}_{-6.2}$	$25.1^{+3.1}_{-2.6}$	$34.9^{+9.5}_{-6.2}$	$24.4^{+5.5}_{-6.0}$	$0.03^{+0.19}_{-0.24}$	$1.70^{+0.71}_{-0.64}$	$0.32^{+0.11}_{-0.11}$	$56.8^{+7.1}_{-5.8}$	$0.71^{+0.09}_{-0.11}$	380	$13.6^{+0.2}_{-0.3}$
GW190924_021846	$13.9^{+5.1}_{-0.9}$	$5.8^{+0.2}_{-0.2}$	$8.8^{+7.0}_{-2.0}$	$5.0^{+1.3}_{-1.9}$	$0.03^{+0.30}_{-0.09}$	$0.57^{+0.22}_{-0.22}$	$0.12^{+0.04}_{-0.04}$	$13.3^{+5.2}_{-1.0}$	$0.67^{+0.05}_{-0.05}$	380	$11.5^{+0.3}_{-0.4}$
GW190929_012149	$90.6^{+21.2}_{-14.1}$	$34.3^{+8.6}_{-6.5}$	$64.7^{+22.4}_{-18.9}$	$25.7^{+14.4}_{-9.7}$	$0.03^{+0.27}_{-0.27}$	$3.68^{+2.98}_{-1.68}$	$0.61^{+0.38}_{-0.24}$	$87.5^{+20.7}_{-14.1}$	$0.64^{+0.17}_{-0.23}$	1800	$9.8^{+0.8}_{-0.6}$
GW190930_133541	$20.3^{+9.0}_{-1.5}$	$8.5^{+0.5}_{-0.5}$	$12.3^{+12.5}_{-2.3}$	$7.8^{+1.7}_{-3.3}$	$0.14^{+0.31}_{-0.15}$	$0.78^{+0.37}_{-0.33}$	$0.16^{+0.07}_{-0.06}$	$19.3^{+9.3}_{-1.5}$	$0.72^{+0.07}_{-0.06}$	1800	$9.5^{+0.3}_{-0.5}$

GWTC-2

Gravitational Wave Transient Catalog 2

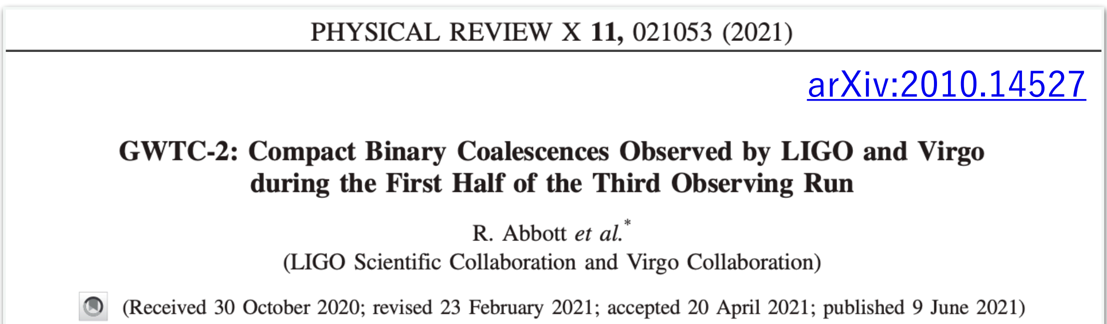
PHYSICAL REVIEW X **11**, 021053 (2021)

arXiv:2010.14527

GWTC-2: Compact Binary Coalescences Observed by LIGO and Virgo during the First Half of the Third Observing Run

R. Abbott *et al.**

(LIGO Scientific Collaboration and Virgo Collaboration)

(Received 30 October 2020; revised 23 February 2021; accepted 20 April 2021; published 9 June 2021)

*39 events in O3a

50 events in total

* False-Alarm Rate < 2 / 1 yr
* GWyymmdd_hhmmss for new events

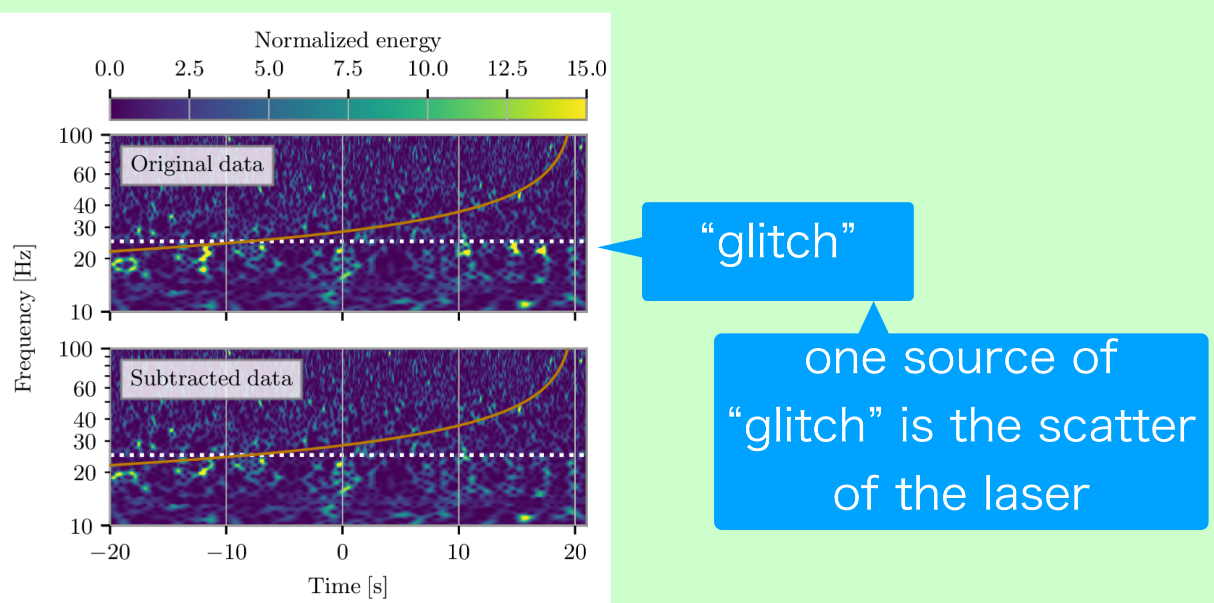

GWTC-2.1

Gravitational Wave Transient Catalog 2.1

arXiv:2108.01045

* re-calibrated data in O3a
* includes 1201 events of FAR < 2 / 1 day
* 44 events P_{astro} > 0.5 （8 new in O3a)
* 3 events retracted since P_{astro} < 0.5

55 events in total

$P_{astro}+P_{terre}=1$

noise

- GW190917 _114630 (P_{astro} = 0.77) potentially NSBH
- GW190426 _190642 (P_{astro} = 0.75) total mass 185 M -> 175M final (maximum ever)
- GW190403 _051519 (P_{astro} = 0.61) & GW190805 _211137(P_{astro} = 0.95) have χ > 0.8 BH

	GWTC-2	GWTC-2.1
BHBH	add 36 (total 46)	+8 -3 (51)
NSNS	+1 (2)	+0 (2)
NSBH		
BH+unknown	+ 2 (2)	+0 (2)
Total	+ 39 (50)	+5 (55)

GW190521 Discovery of IMBH（1）

PRL 125 (2020) 101102

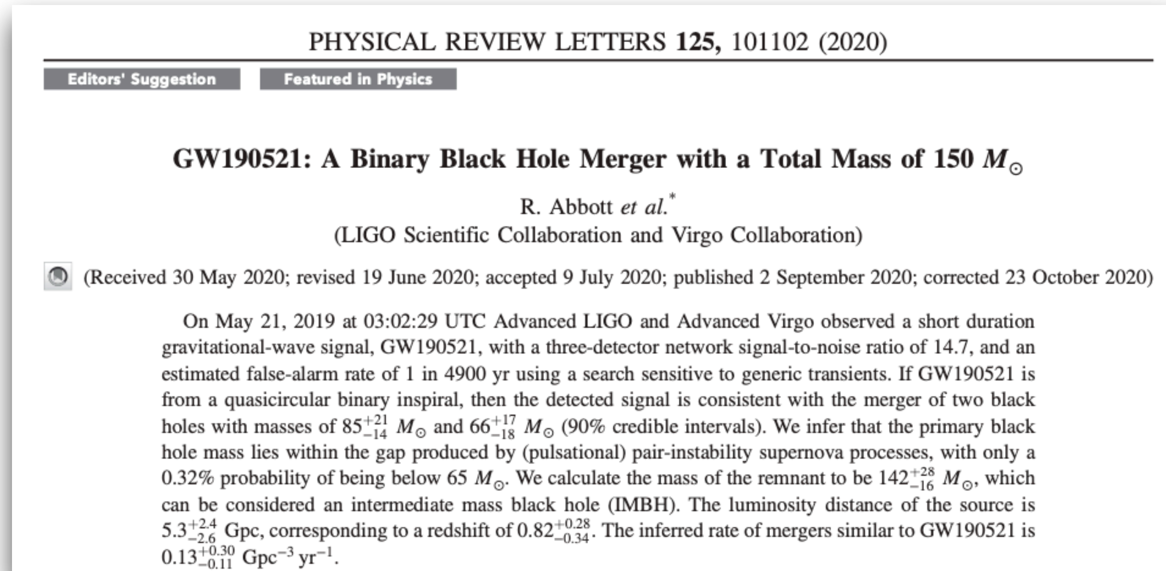
PHYSICAL REVIEW LETTERS 125, 101102 (2020)

Editors' Suggestion Featured in Physics

GW190521: A Binary Black Hole Merger with a Total Mass of 150 $M_\odot$

R. Abbott *et al.**

(LIGO Scientific Collaboration and Virgo Collaboration)

(Received 30 May 2020; revised 19 June 2020; accepted 9 July 2020; published 2 September 2020; corrected 23 October 2020)

On May 21, 2019 at 03:02:29 UTC Advanced LIGO and Advanced Virgo observed a short duration gravitational-wave signal, GW190521, with a three-detector network signal-to-noise ratio of 14.7, and an estimated false-alarm rate of 1 in 4900 yr using a search sensitive to generic transients. If GW190521 is from a quasicircular binary inspiral, then the detected signal is consistent with the merger of two black holes with masses of $85^{+21}_{-14}\,M_\odot$ and $66^{+17}_{-18}\,M_\odot$ (90% credible intervals). We infer that the primary black hole mass lies within the gap produced by (pulsational) pair-instability supernova processes, with only a 0.32% probability of being below 65 $M_\odot$. We calculate the mass of the remnant to be $142^{+28}_{-16}\,M_\odot$, which can be considered an intermediate mass black hole (IMBH). The luminosity distance of the source is $5.3^{+2.4}_{-2.6}$ Gpc, corresponding to a redshift of $0.82^{+0.28}_{-0.34}$. The inferred rate of mergers similar to GW190521 is $0.13^{+0.30}_{-0.11}$ Gpc^{-3} yr^{-1}.

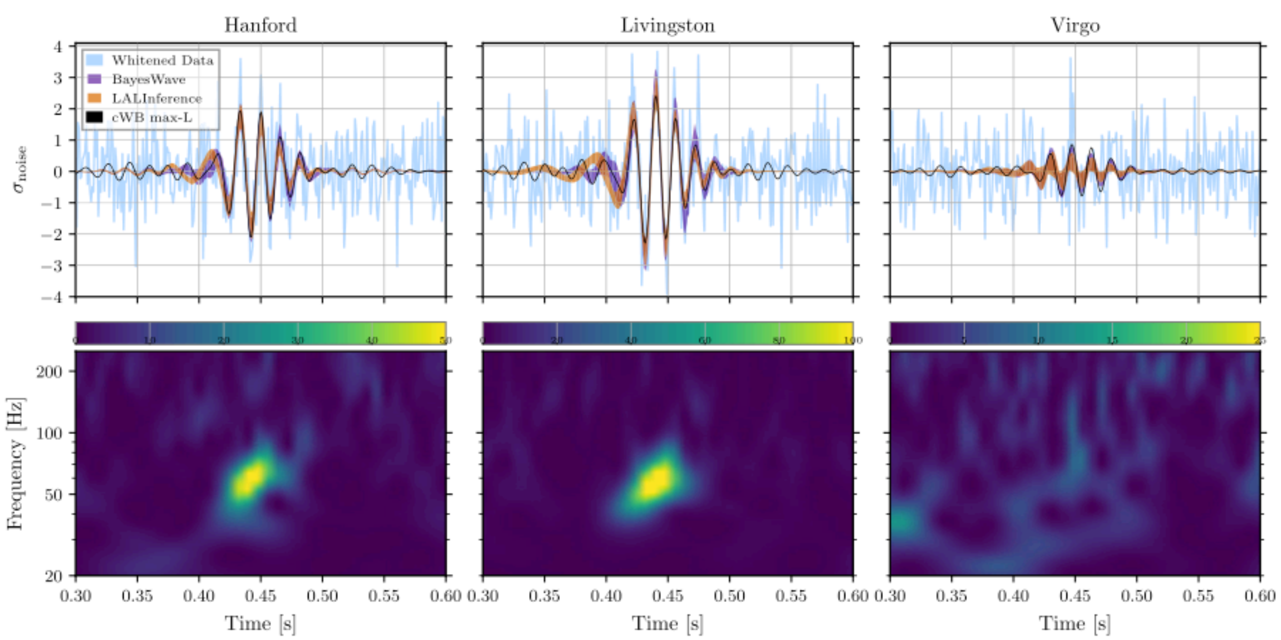

Mass $85^{+21}_{-14}\,M_{sun} + 66^{+17}_{-18}\,M_{sun} \rightarrow 142^{+28}_{-16}\,M_{sun}$

Distance $5.3^{+2.4}_{-2.6}$ Gpc, $z = 0.82^{+0.28}_{-0.34}$

100 10^5 M_{sun}

Stellar-mass BH **Intermediate-massBH** **Super-massive BH**

Existence of BH over 100 M_{sun} !

No formation scenario for BH over 65 M_{sun} in the standard model.

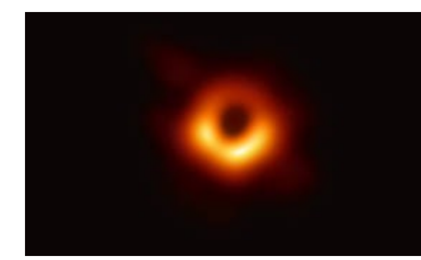

M87 by EHT

mass $6.5\ 10^9 M_{sun}$

distance

55 Mly

16.9 Mpc

GW190521　Discovery of IMBH（2）

PRL 125 (2020) 101102

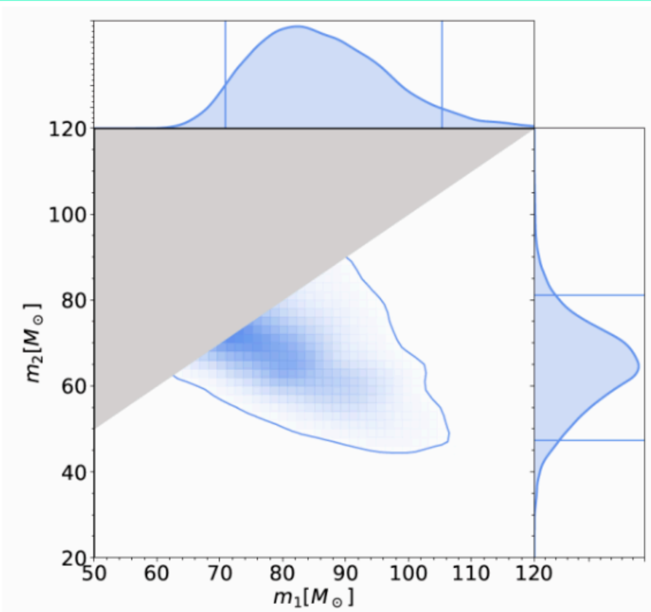

Mass　　$85^{+21}_{-14}\ M_{sun} + 66^{+17}_{-18}\ M_{sun}$ -> $142^{+28}_{-16}\ M_{sun}$

Distance　$5.3^{+2.4}_{-2.6}$ Gpc, $z = 0.82^{+0.28}_{-0.34}$

100　　　10^5　　　M_{sun}

Stellar-mass BH　**Intermediate-massBH**　**Super-massive BH**

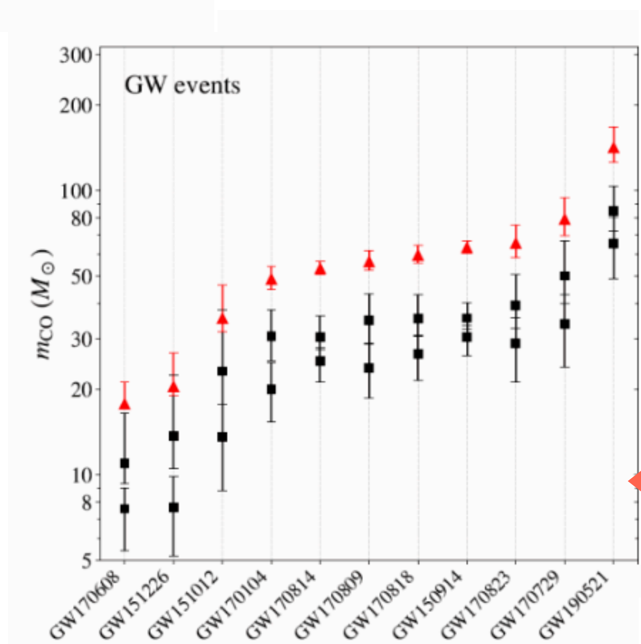

Existence of BH over 100 M_{sun} !

No formation scenario for BH over 65 M_{sun} in the standard model.

Second generation of mergers

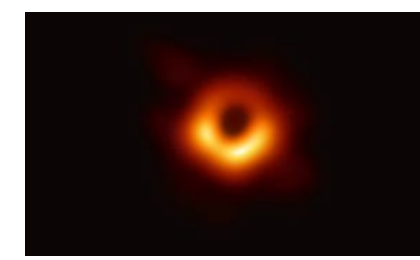

M87　by EHT
mass　$6.5\ 10^9 M_{sun}$
distance
55 Mly
16.9 Mpc

LVK papers http://www.oit.ac.jp/is/shinkai/linkGW.html

Only for selected ones before O3a, and all for after O3b.

	abbrev	title	arXiv, publ	Science Summary
LVK	O3bAstroDist	The population of merging compact binaries inferred using gravitational waves through GWTC-3	arXiv:2111.03634	Eng , Jap Nov 5, 2021
LVK	O3bGRB	Search for Gravitational Waves Associated with Gamma-Ray Bursts Detected by Fermi and Swift During the LIGO-Virgo Run O3b	arXiv:2111.03608	Eng , Jap Nov 5, 2021
LVK	O3bCatalog	GWTC-3: Compact Binary Coalescences Observed by LIGO and Virgo During the Second Part of the Third Observing Run	arXiv:2111.03606	Eng , Jap Nov 5, 2021
LVK	O3Cosmology	Constraints on the cosmic expansion history from GWTC-3	arXiv:2111.03604	Eng , Jap Nov 5, 2021
LVK	O3Radiometer	All-sky, all-frequency directional search for persistent gravitational-waves from Advanced LIGO's and Advanced Virgo's first three observing runs	arXiv:2110.09834	Eng , Jap Oct 27, 2021
LV	O3aSSM	Search for subsolar-mass binaries in the first half of Advanced LIGO and Virgo's third observing run	arXiv:2109.12197	Eng , Jap Sep 28, 2021
LVK	O3LMXBsAMXPs	Search for continuous gravitational waves from 20 accreting millisecond X-ray pulsars in O3 LIGO data	arXiv:2109.09255	Eng , Jap Sep 20, 2021
LV	GWTC2.1	GWTC-2.1: Deep Extended Catalog of Compact Binary Coalescences Observed by LIGO and Virgo During the First Half of the Third Observing Run	arXiv:2108.01045	Eng , Jap Aug 2, 2021
LVK	O3LongBurst	All-sky search for long-duration gravitational-wave bursts in the third Advanced LIGO and Advanced Virgo run	arXiv: 2107.13796	Eng , Jap July 30, 2021
LVK	O3ShortBurst	All-sky search for short gravitational-wave bursts in the third Advanced LIGO and Advanced Virgo run	arXiv: 2107.03701	Eng , Jap July 9, 2021
LVK	O3ShortBurst	All-sky Search for Continuous Gravitational Waves from Isolated Neutron Stars in the Early O3 LIGO Data	arXiv: 2107.00600	Eng , Jap July 1, 2021
LVK	NSBH	Observation of Gravitational Waves from Two Neutron Star–Black Hole Coalescences	ApJL 915; L5 (2021)	Eng , Jap June 30, 2021
LVK	O3IMBH	Search for intermediate mass black hole binaries in the third observing run of Advanced LIGO and Advanced Virgo	arXiv:2105.15120 submitted to	Eng , Jap May 31, 2021
LVK	O3DarkPhoton	Constraints on dark photon dark matter using data from LIGO's and Virgo's third observing run	arXiv:2105.13085 submitted to	Eng , Jap May 27, 2021
LVK	O3DirectedSNR	Searches for continuous gravitational waves from young supernova remnants in the early third observing run of Advanced LIGO and Virgo	arXiv:2105.11641 submitted to	Eng , Jap May 26, 2021
LV	O3aLensing	Search for lensing signatures in the gravitational-wave observations from the first half of LIGO-Virgo's third observing run	arXiv:2105.06384 submitted to	Eng , Jap May 13, 2021
LVK	O3aRmode	Constraints from LIGO O3 data on gravitational-wave emission due to r-modes in the glitching pulsar PSR J0537-6910	arXiv:2104.14417 submitted to	Eng , Jap Apr 30, 2021
LV	O2H0	A Gravitational-wave Measurement of the Hubble Constant Following the Second Observing Run of Advanced LIGO and Virgo	arXiv: ApJ 909:218 (2021)	Eng , Jap Mar 19, 2021
LVK	O3StochDirectional	Search for anisotropic gravitational-wave backgrounds using data from Advanced LIGO's and Advanced Virgo's first three observing runs	arXiv:2103.08520 submitted to	Eng , Jap Mar 16, 2021
LVK	O3StochIso	Upper Limits on the Isotropic Gravitational-Wave Background from Advanced LIGO's and Advanced Virgo's Third Observing Run	arXiv:2101.12130 submitted to PRD	Eng, Jap Feb 01, 2021
LVK	O3CosmicString	Constraints on cosmic strings using data from the third Advanced LIGO-Virgo observing run	arXiv:2101.12248 PRL126, 241102 (2021)	Eng, Jap Feb 01, 2021
LVK	PSR J0537-6910	Diving below the spin-down limit: Constraints on gravitational waves from the energetic young pulsar PSR J0537-6910	arXiv:2012.12926 ApJL 913 L27 (2021)	Eng, Jap Dec 25, 2020

LVK-EPO (Education & Public Outreach) provides Science Summaries

LIGO Scientific Collaboration

News | Detections | Our science explained | Multimedia | Educational resources | For researcher

Intro to LIGO & Gravitational Waves | Science Summaries | Popular Articles | Frequently Asked

SUMMARIES OF LSC/LVK SCIENTIFIC PUBLICATIONS

For each of our new research articles, we feature a summary of the paper's key points written for the general public. Simply click on any of the titles for an online version, or on the '[flyer]' links for a downloadable file in PDF format. Translations into several languages are also available for some of these summaries. Where not noted separately, translations can be accessed through their language acronyms (e.g. 'es' for Spanish, also see details in the sidebar) or from the top of the English online versions. Most recent papers, and their summaries, are written together by the LIGO Scientific Collaboration (LSC), the Virgo Collaboration and the KAGRA Collaboration, forming the LVK collaboration.

LATEST DETECTIONS

GWTC-3 (Nov 07, 2021) GWTC-3, a third catalog of gravitational-wave detections [**flyer**]

Also in: Chinese (simplified) [zh-Hans] | Chinese (traditional) [zh-Hant] | French [fr] | German [de] | Japanese [ja] | Polish [pl] | Spanish [es]

Companion papers: (also available in some other languages):

- Uncovering the population properties of black holes and neutron stars following LIGO and Virgo's third observing run [**flyer**] | [fr] | [ja] | [pl] | [zh-Hant]
- Improving measurements of the cosmic expansion with gravitational waves [**flyer**] | [fr] | [el] | [ja] | [zh-Hant]
- Searching for quiet gravitational waves produced by gamma-ray bursts in O3b [**flyer**] | [fr] | [zh-Hant]

https://www.ligo.org/science/outreach.php

1. Auto-Regressive model (Method, general) I

Fitting data with linear func.

$$
\begin{aligned}
x_n &= a_1 x_{n-1} + a_2 x_{n-2} + \cdots + a_M x_{n-M} + \varepsilon \\
&= \sum_{j=1}^{M} a_j x_{n-j} + \varepsilon
\end{aligned}
$$

e.g. $x_n = A e^{-rn\Delta t} \cos(\omega n \Delta t)$

$$Z_1 = e^{-(r-j\omega)\Delta t}$$
$$Z_2 = e^{-(r+j\omega)\Delta t}$$

→ $x_n = \frac{A}{2}(Z_1^n + Z_2^n) = (Z_1 + Z_2)x_{n-1} - Z_1 Z_2 x_{n-2}$

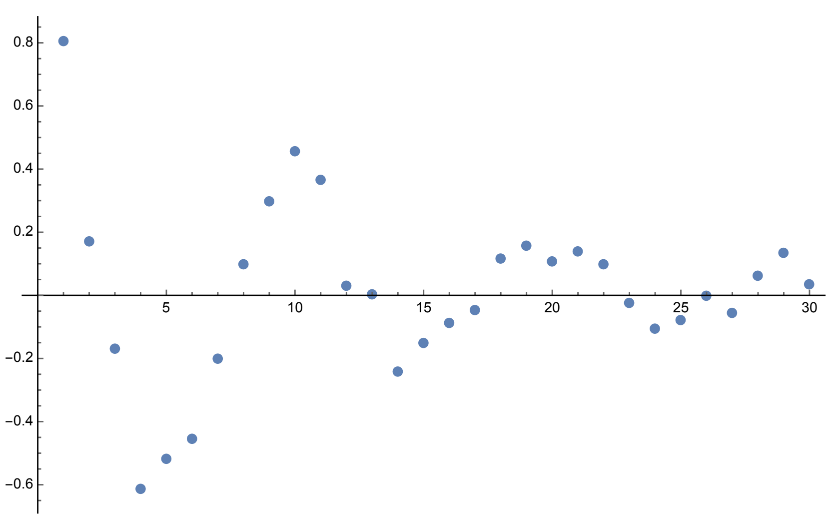

→

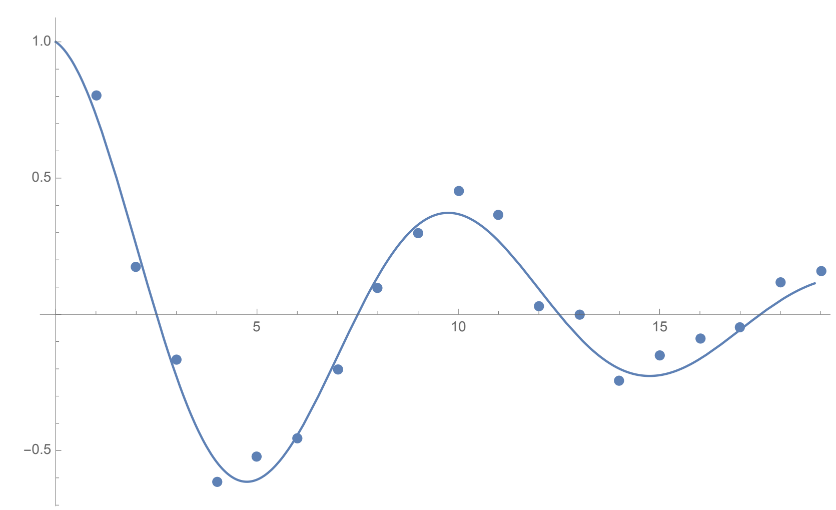

can be applied also to noisy data by adjusting *M*

1. Auto-Regressive model (Method, general) II

Fitting data with linear func.

$$x_n = a_1 x_{n-1} + a_2 x_{n-2} + \cdots + a_M x_{n-M} + \varepsilon$$
$$= \sum_{j=1}^{M} a_j x_{n-j} + \varepsilon$$

- find a_j (Burg method)
- find M (FPE final prediction error method)
- re-construct wave signal from fitted function
- apply FFT with arbitrary precision.

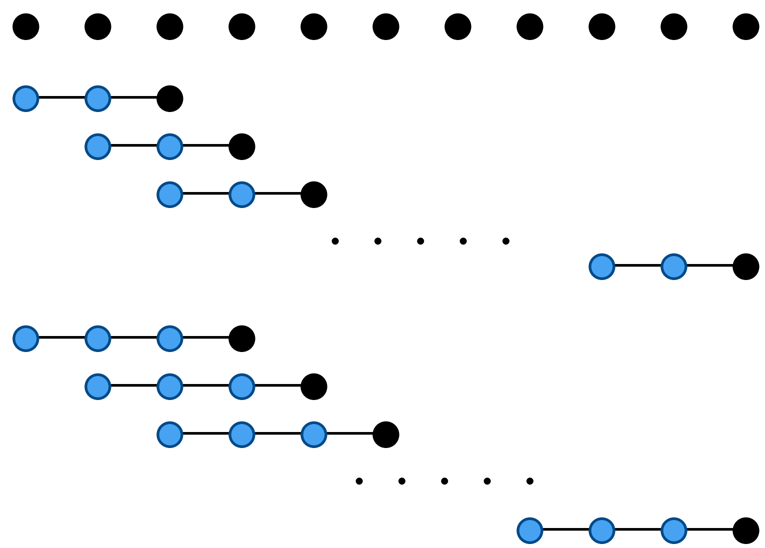

power spectrum

$$p(f) = \frac{\sigma^2}{\left| 1 - \sum_{j=1}^{M} a_j e^{-I 2\pi j f \Delta t} \right|^2}$$

Auto-Regressive model　vs　Short FFT

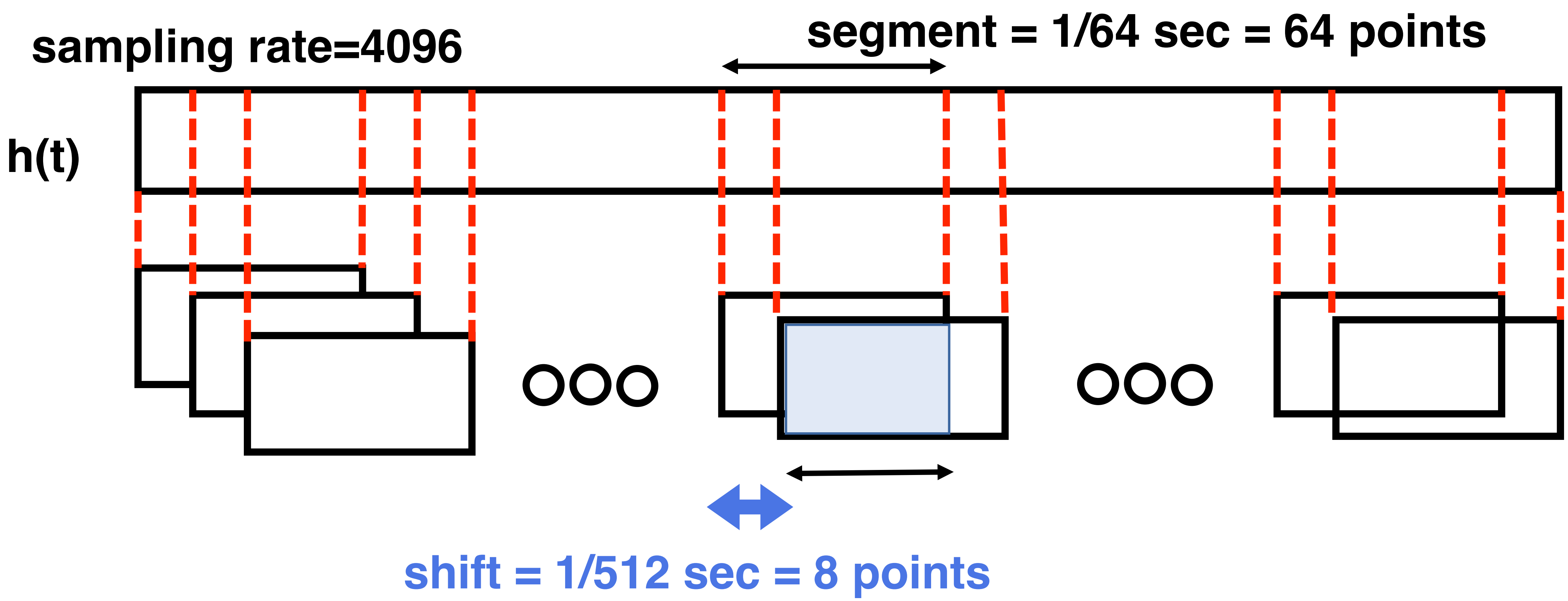

P(f)

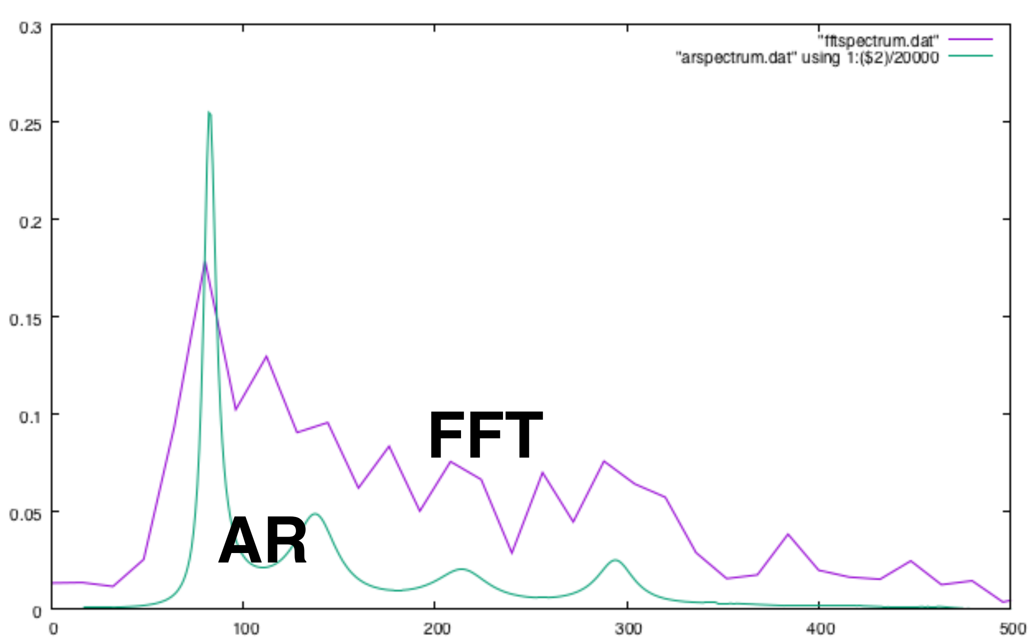

freq.　　[mock data, SNR=40, inspiral part]

The order *M* can be fixed at 2〜8.

Even for short segment,
AR model shows precise power-spectrum.

1. Auto-Regressive model (Method, general) III

Fitting data with linear func.

$$
\begin{aligned}
x_n &= a_1 x_{n-1} + a_2 x_{n-2} + \cdots + a_M x_{n-M} + \varepsilon \\
&= \sum_{j=1}^{M} a_j x_{n-j} + \varepsilon
\end{aligned}
$$

- find a_j (Burg method)
- find M (FPE final prediction error method)
- re-construct wave signal from fitted function
- apply FFT with arbitrary precision.

power spectrum

$$
p(f) = \frac{\sigma^2}{\left| 1 - \sum_{j=1}^{M} a_j e^{-I 2\pi j f \Delta t} \right|^2}
$$

characteristic eq.

$$
f(z) = 1 - \sum_{j=1}^{M} a_j z^j = 0
$$

$|z_k|$ says amplitude,
$\arg(z_k)$ says frequency.

Ringdown Search by Auto-Regressive Approach (O1/O2 public data, GWTC1 catalogue)

GW150914

LIGO paper

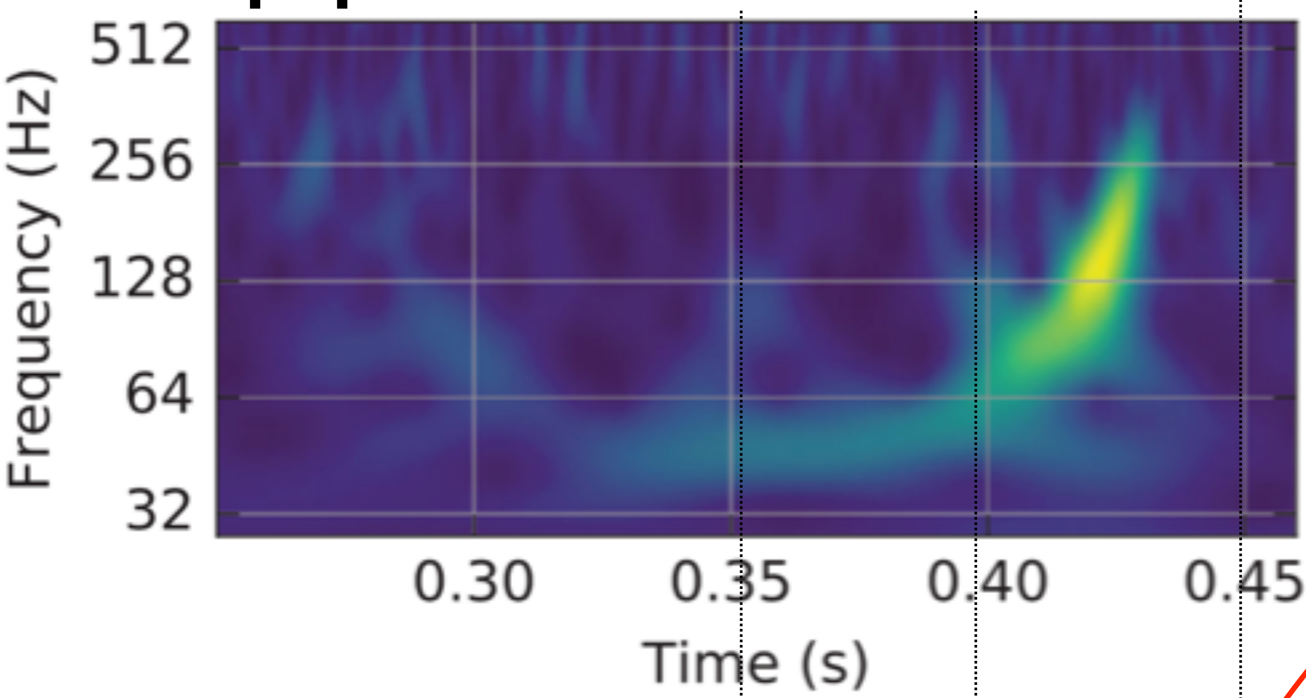

AR model

Hanford

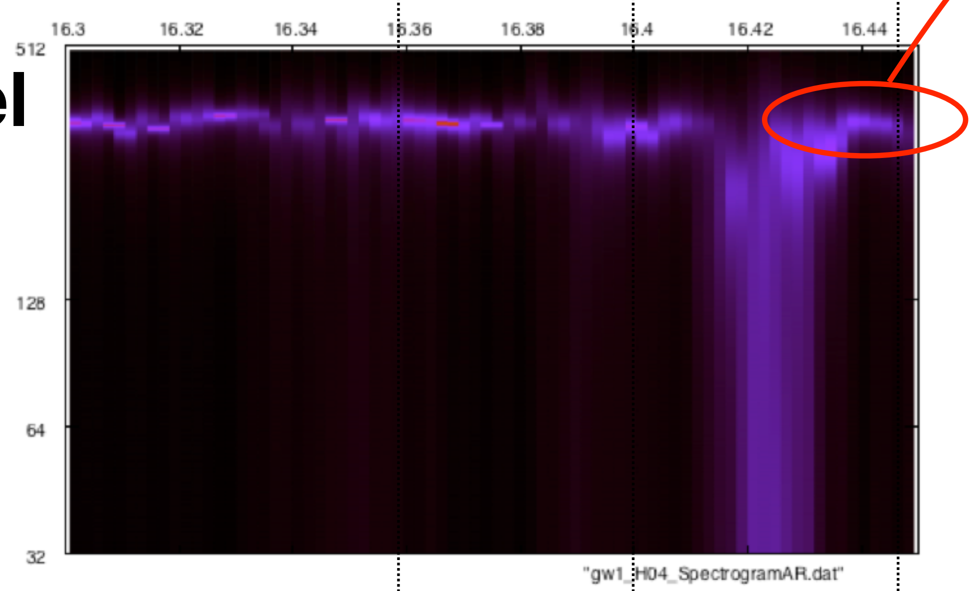

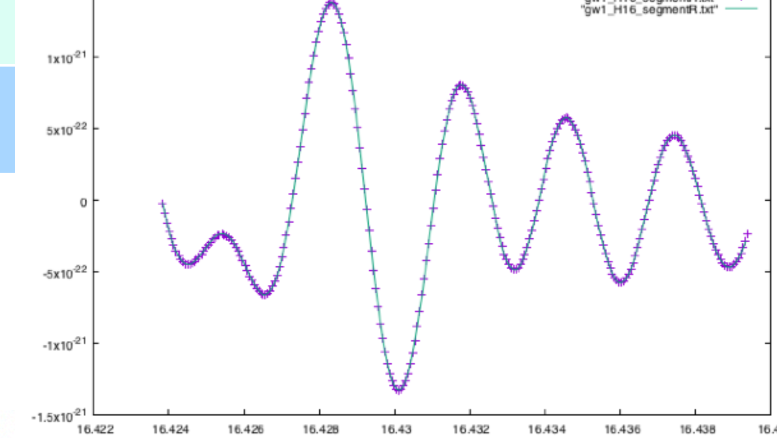

freq [Hz]

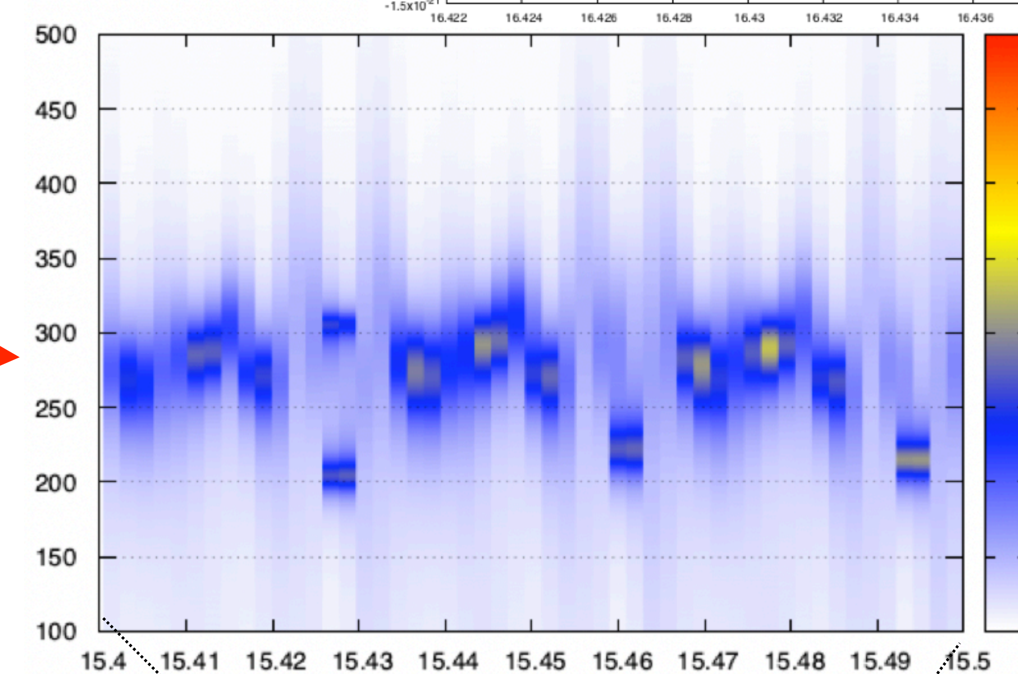

▲merger time

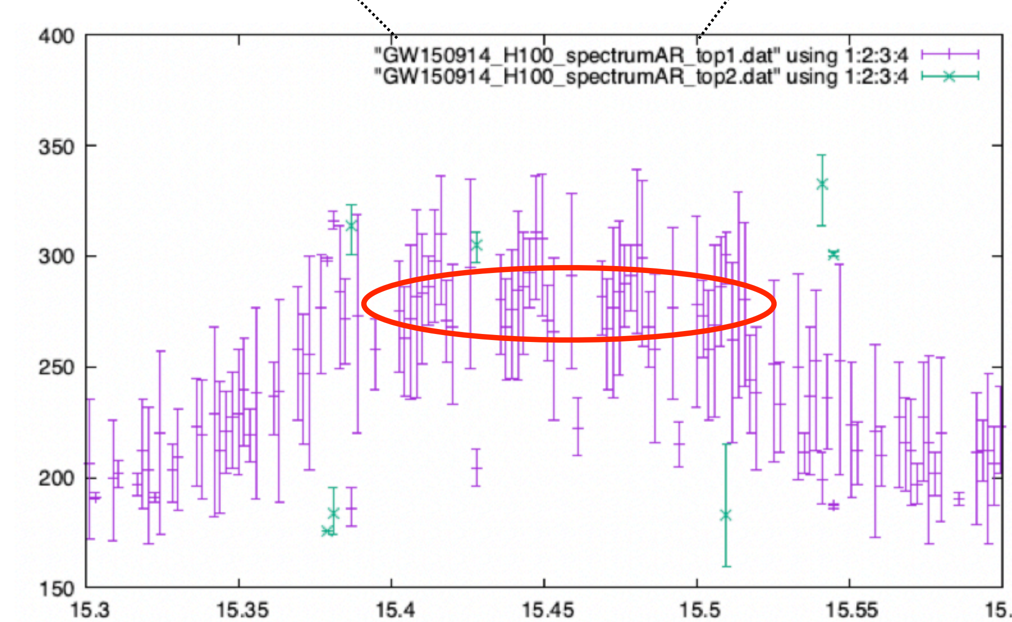

$f_{220} = 249.4$ Hz, $f_{221} = 244.0$ Hz, $f_{222} = 233.7$ Hz

$f_{210} = 349.3$ Hz, $f_{211} = 207.1$ Hz, $f_{200} = 231.9$ Hz

$f_{330} = 395.3$ Hz, $f_{331} = 392.1$ Hz, $f_{332} = 386.3$ Hz

$f_{320} = 355.9$ Hz, $f_{310} = 322.1$ Hz, $f_{300} = 293.9$ Hz

4096 sampling rate
150-450 Hz filter
1 segment = 1/64 sec= 64 points
1 shift = 1/512 sec = 8 points

Summary & Outlook

自己回帰モデル *x(t)*

$$x_n = a_1 x_{n-1} + a_2 x_{n-2} + \cdots + a_M x_{n-M} + \varepsilon$$
$$= \sum_{j=1}^{M} a_j x_{n-j} + \varepsilon$$

短いデータ (〜 60 pts) に対しても精度よく周波数・減衰率を特定できる.
シグナルを見つけるのにテンプレートは不要.

LIGO/Virgo の O1/O2イベントデータに適用，リングダウン部分の抽出を試みた.
SN比が高ければ，独立にリングダウン部分が取り出せそうだ.

★ノイズ除去の方法や，他の方法と組み合わせ，より精密な周波数特定法を検討中.
★higher modesの検出へ，BHの特長量の特定へ，相対論検証へ.
★テンプレートを使わない方法は，今後，未知の重力波シグナルの候補検出に役立つかも.

GW observatory plans in space

http://gwplotter.com

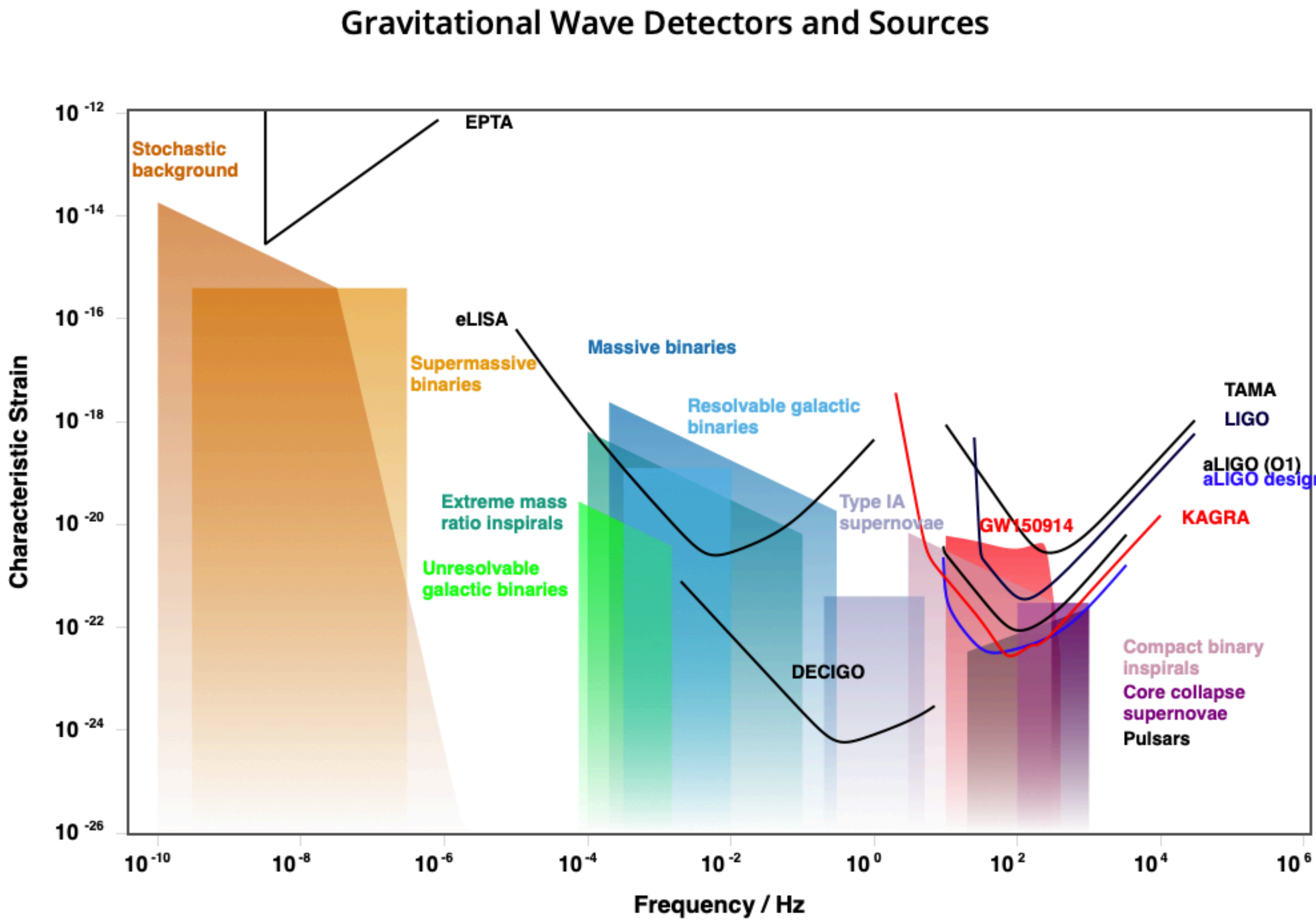

GW observatory plans in space

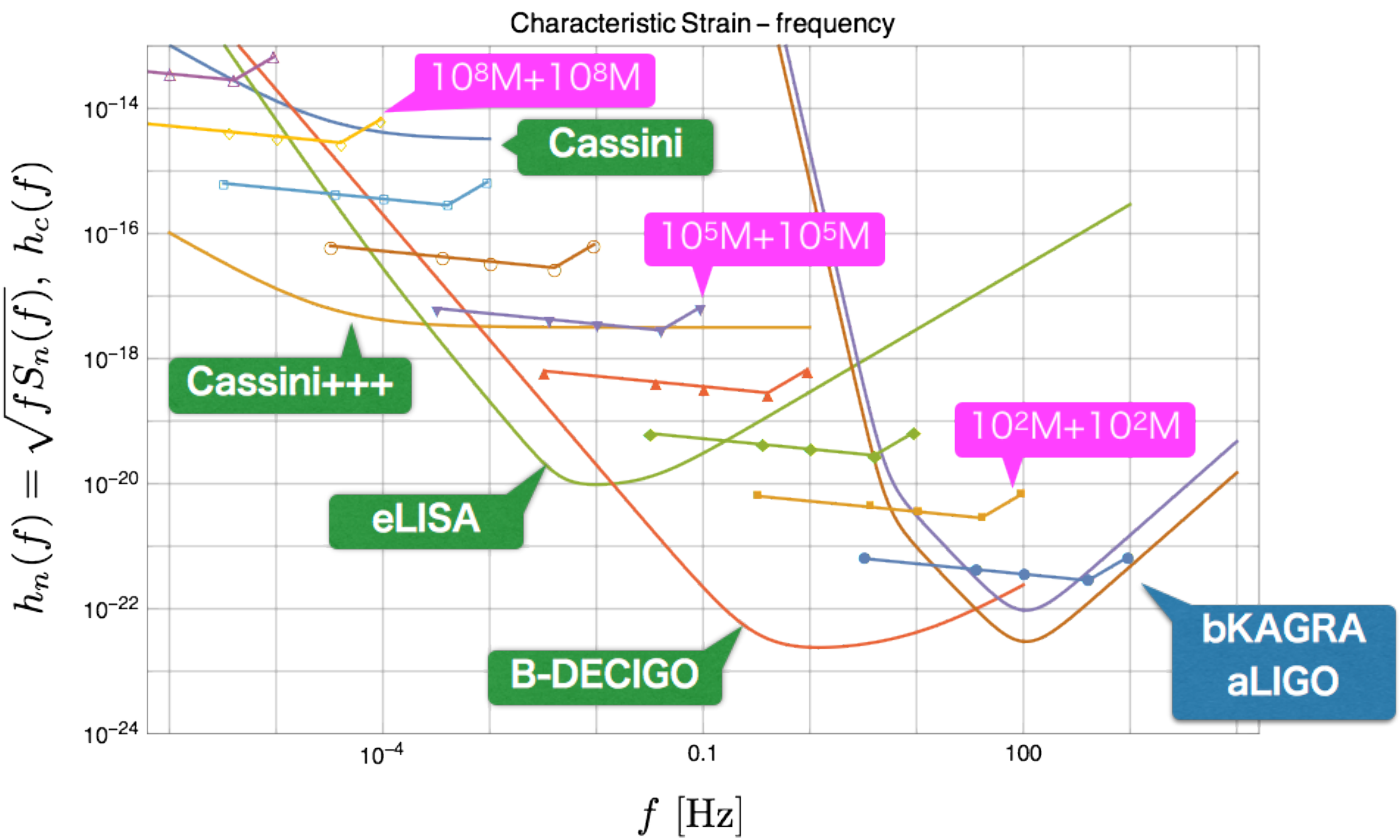

重力波宇宙干渉計LISA（リサ）　ESA予算承認
2017/6/20
Laser Interferometer Space Antenna

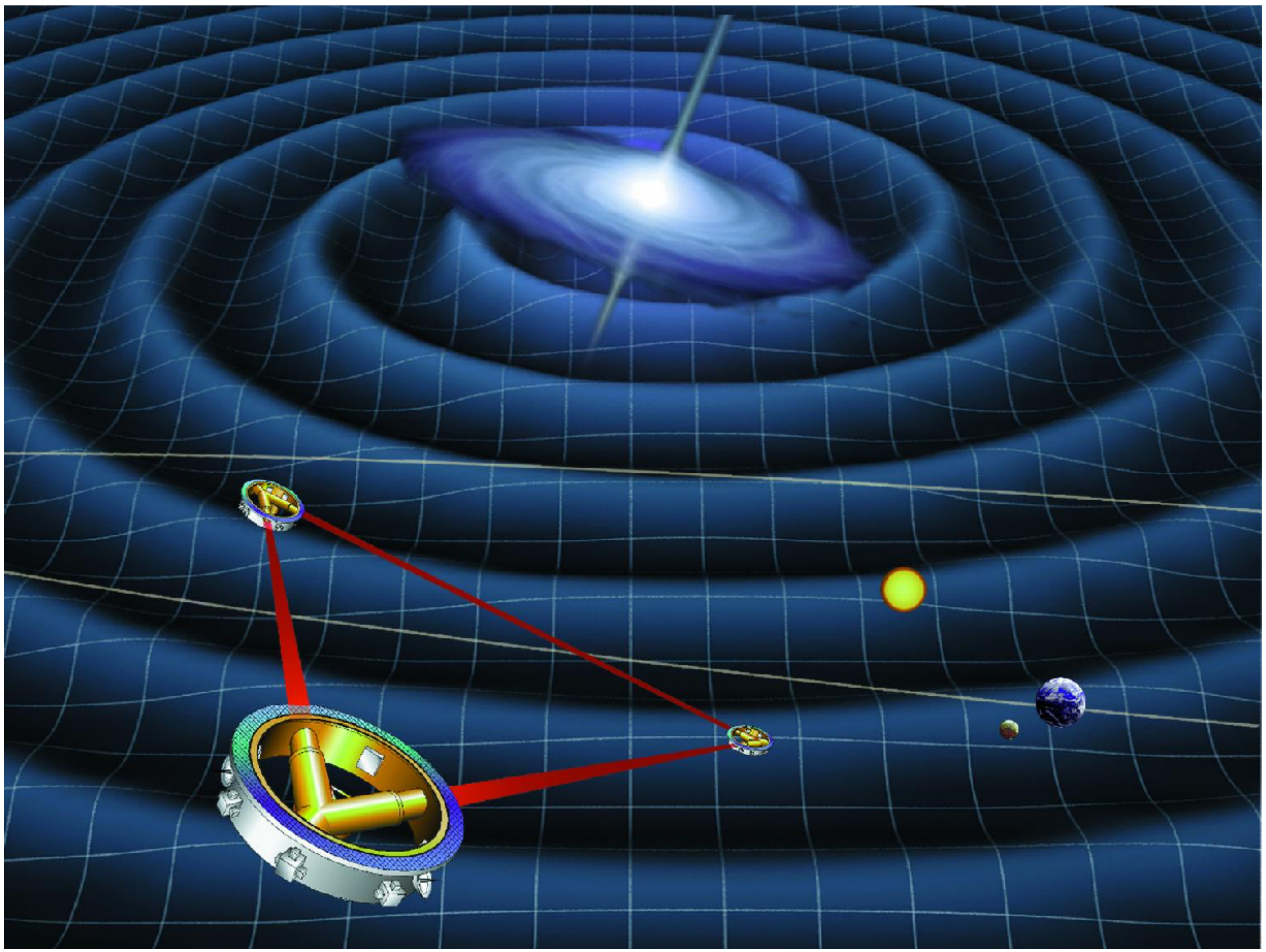

2034年に打ち上げ予定
250万kmの腕の長さ
地球の公転軌道のL4
低周波数帯（mHzからHz帯）

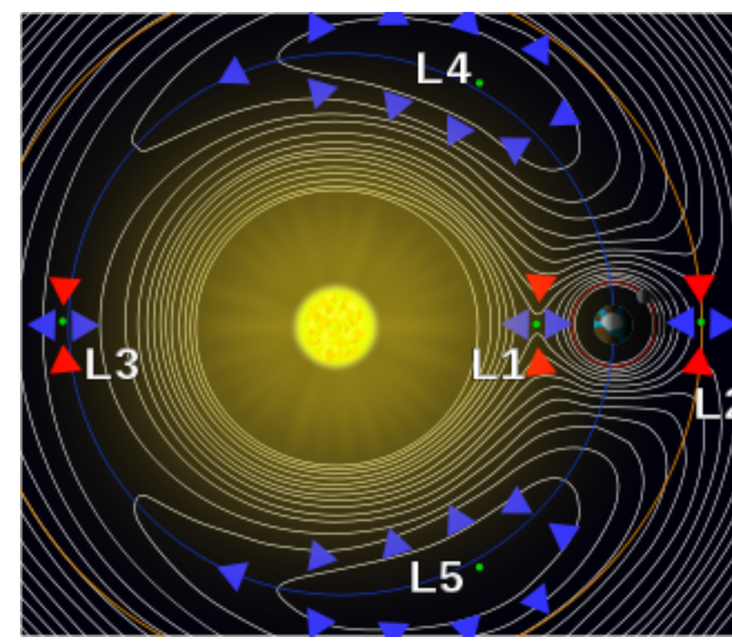

重力波宇宙干渉計DECIGO（ディサイゴ）

Deci-hertz Interferometer Gravitational wave Observatory

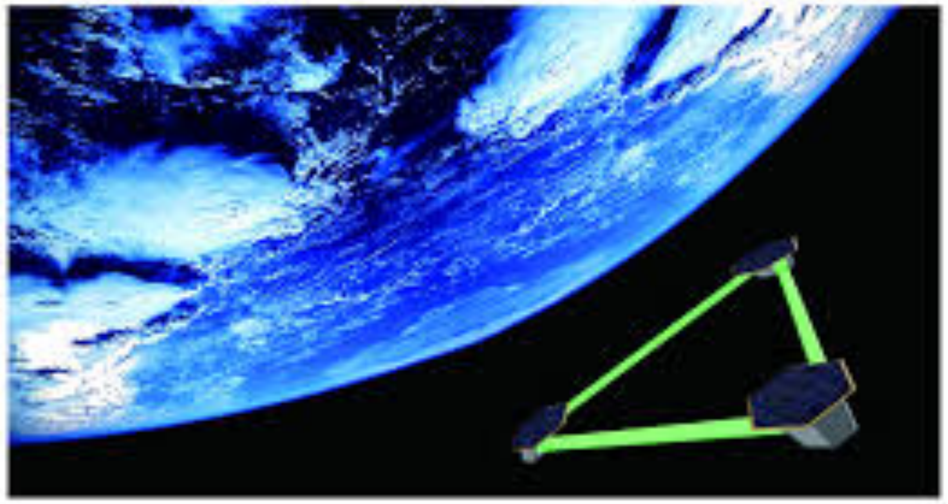

1000kmの腕の長さ
低周波数帯（deciHzからHz帯）

重力波の検出感度

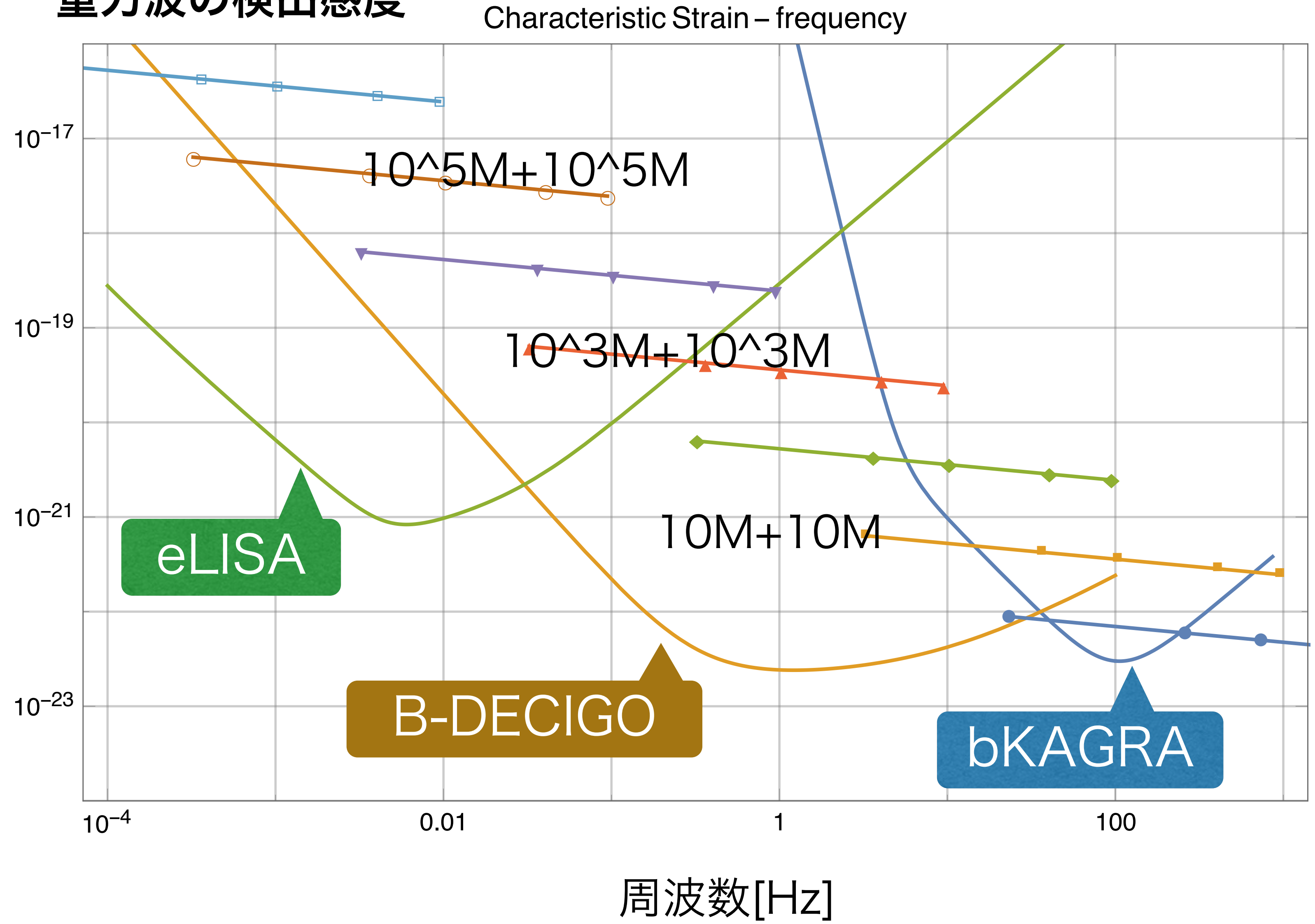

宇宙全体スケールで
巨大ブラックホール連星合体の
重力波が検出できる

↓

銀河中心の超巨大ブラックホール
形成過程がわかる

宇宙の膨張速度がわかる

宇宙空間光格子時計ネットワーク INO

Interplanetary Network of Optical Lattice Clocks

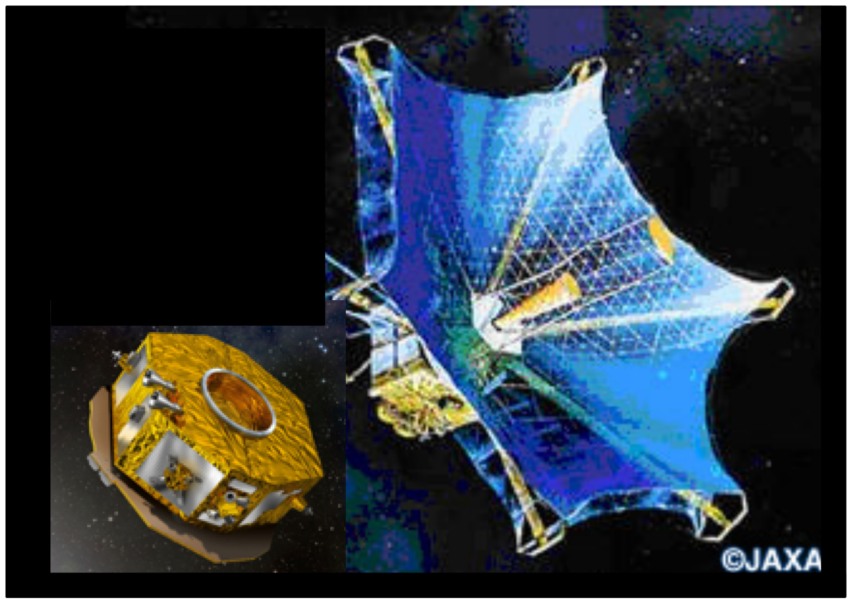

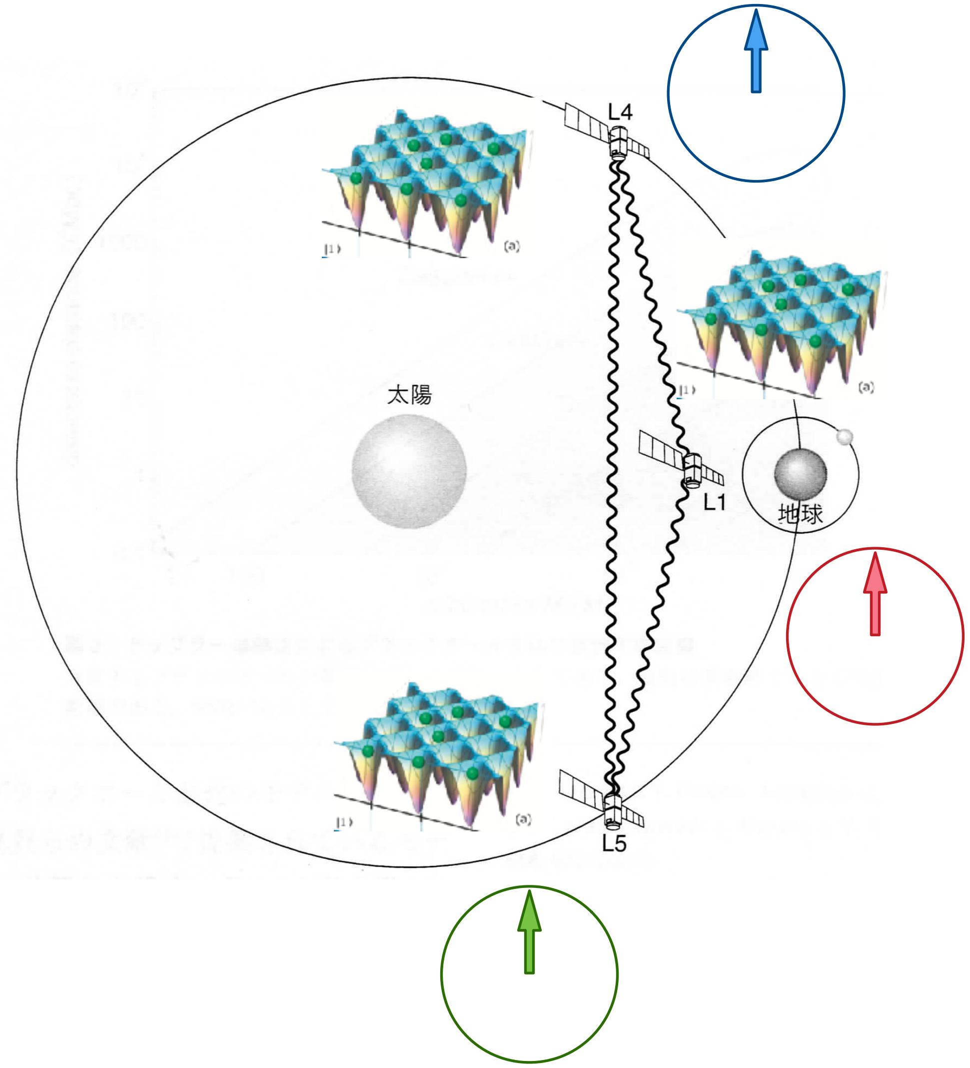

「数理科学」2018-12

「科学」2017-12

Int. J. Mod. Phys.
D 28 (2019) 1940002
arXiv:1809.10317

宇宙全体スケールで
巨大ブラックホール連星合体の
重力波が検出できる

↓

銀河中心の超巨大ブラックホール
形成過程がわかる

伊能忠敬

江戸時代，日本中で
精密な測量をして地図を作成

BH連星合体から銀河中心SMBHの形成シナリオを決める

★BH連星合体が繰り返されて，SMBHが形成されると考える
★1つの銀河にいくつBH連星合体があるかを数える
★宇宙にいくつ銀河があるかを数える
★LIGOやKAGRAの検出器感度で，1年にいくつ観測できるのか予想する

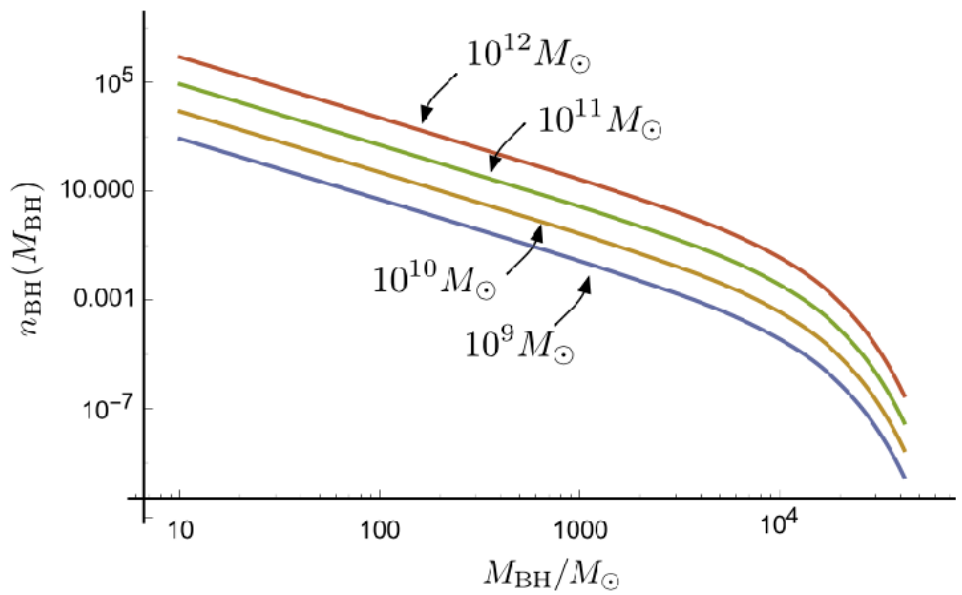

Figure 5. Number density of BHs per galaxy as a function of BH mass for different total mass of galaxies $M_{\rm galaxy} = 10^9 M_\odot, \cdots, 10^{12} M_\odot$.

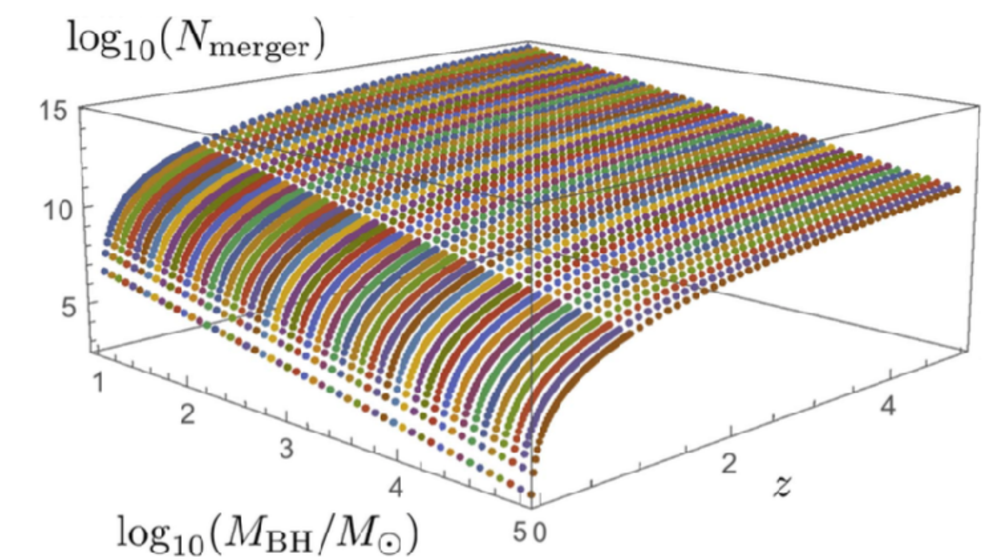

Figure 6. Cumulative distribution function of the number of BH mergers $N_{\rm merger}(M_{\rm BH})$ as a function of the redshift z. $N_{\rm merger}$ is expressed with binned one, of which we binned 20 for one order in $M_{\rm BH}$.

The Astrophysical Journal, 835:276 (8pp), 2017 February 1
doi:10.3847/1538-4357/835/2/276

Gravitational Waves from Merging Intermediate-mass Black Holes. II. Event Rates at Ground-based Detectors

Hisa-aki Shinkai[1], Nobuyuki Kanda[2], and Toshikazu Ebisuzaki[3]

BH連星合体から銀河中心SMBHの形成シナリオを決める

★BH連星合体が繰り返されて，SMBHが形成されると考える
★1つの銀河にいくつBH連星合体があるかを数える
★宇宙にいくつ銀河があるかを数える
★LIGOやKAGRAの検出器感度で，1年にいくつ観測できるのか予想する

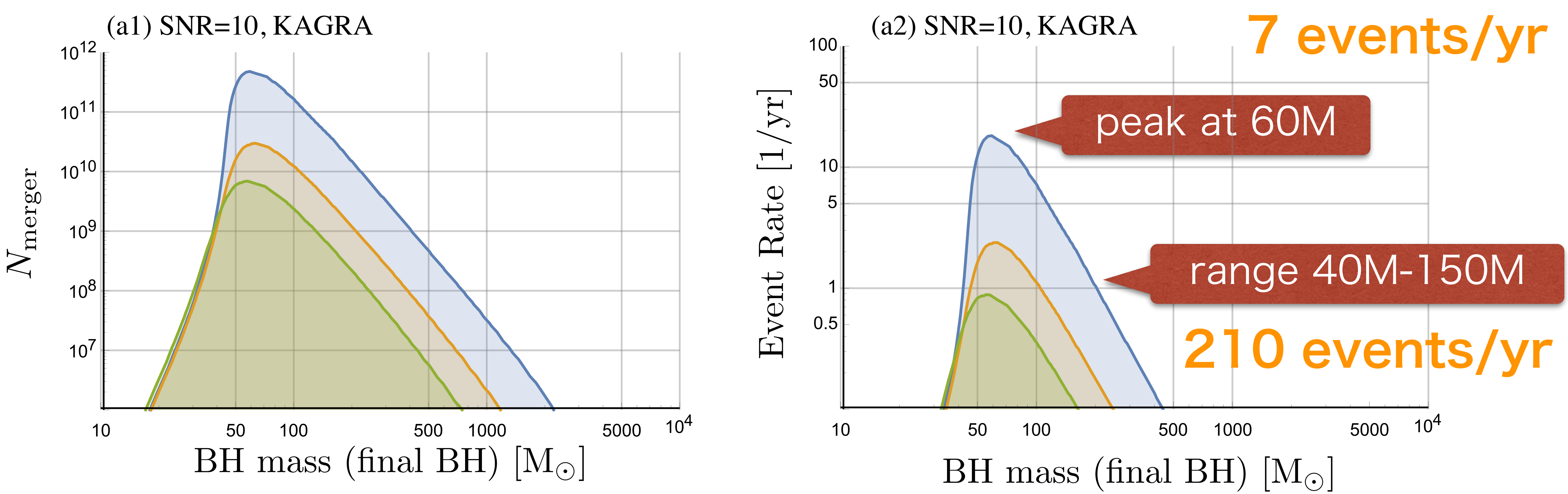

The Astrophysical Journal, 835:276 (8pp), 2017 February 1
doi:10.3847/1538-4357/835/2/276

CrossMark

Gravitational Waves from Merging Intermediate-mass Black Holes. II. Event Rates at Ground-based Detectors

Hisa-aki Shinkai[1], Nobuyuki Kanda[2], and Toshikazu Ebisuzaki[3]

Event Rates at bKAGRA/aLIGO

Mass distribution	PyCBC	GstLAL	Combined
	$R/(\mathrm{Gpc}^{-3}\ \mathrm{yr}^{-1})$		
	Event based		
GW150914	$3.2^{+8.3}_{-2.7}$	$3.6^{+9.1}_{-3.0}$	$3.4^{+8.8}_{-2.8}$
LVT151012	$9.2^{+30.3}_{-8.5}$	$9.2^{+31.4}_{-8.5}$	$9.1^{+31.0}_{-8.5}$
GW151226	35^{+92}_{-29}	37^{+94}_{-31}	36^{+95}_{-30}
All	53^{+100}_{-40}	56^{+105}_{-42}	55^{+103}_{-41}
	Astrophysical		
Flat in log mass	31^{+43}_{-21}	29^{+43}_{-21}	31^{+42}_{-21}
Power law (−2.35)	100^{+136}_{-69}	94^{+137}_{-66}	97^{+135}_{-67}

LIGO group PRX6(2016)041015

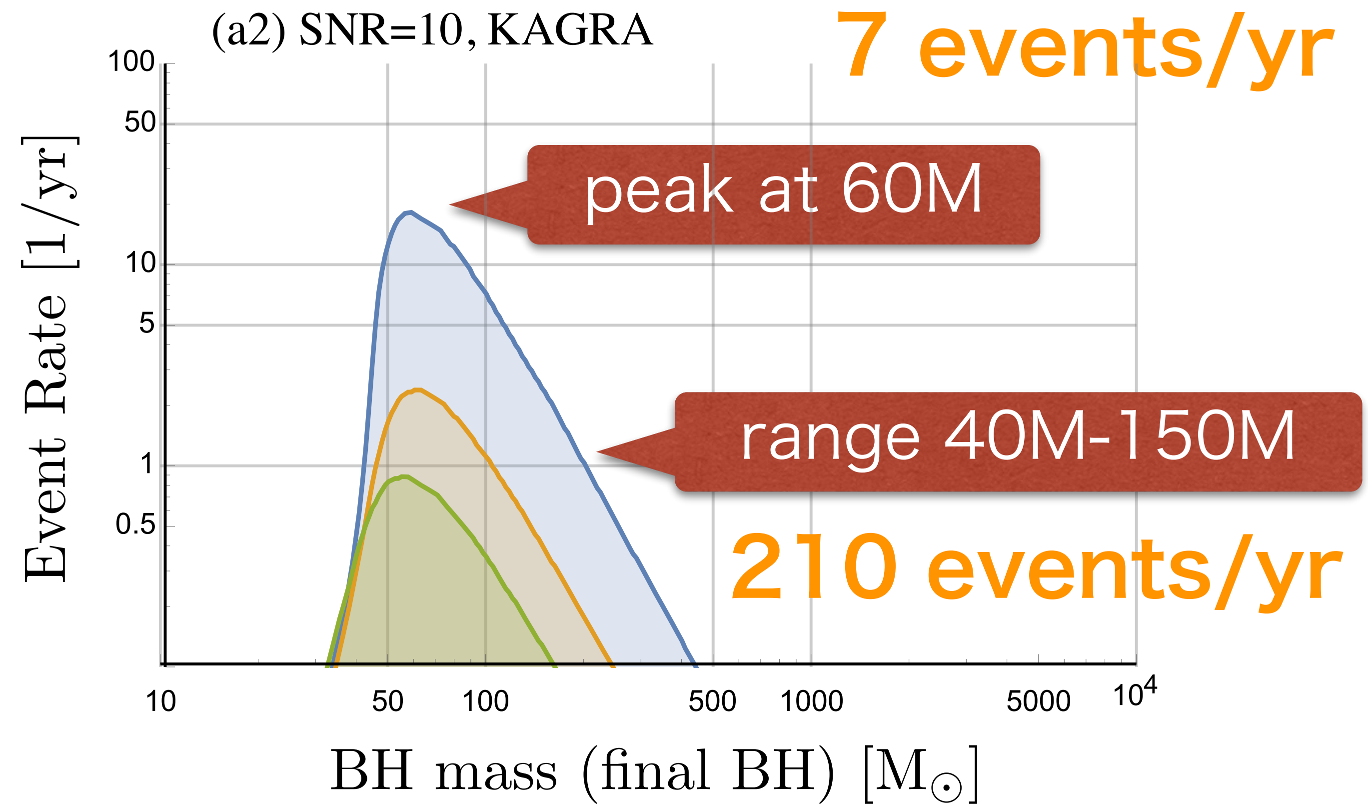

Shinkai+ ApJ 835(2017)276

Inoue+ MNRAS461(2016)4329

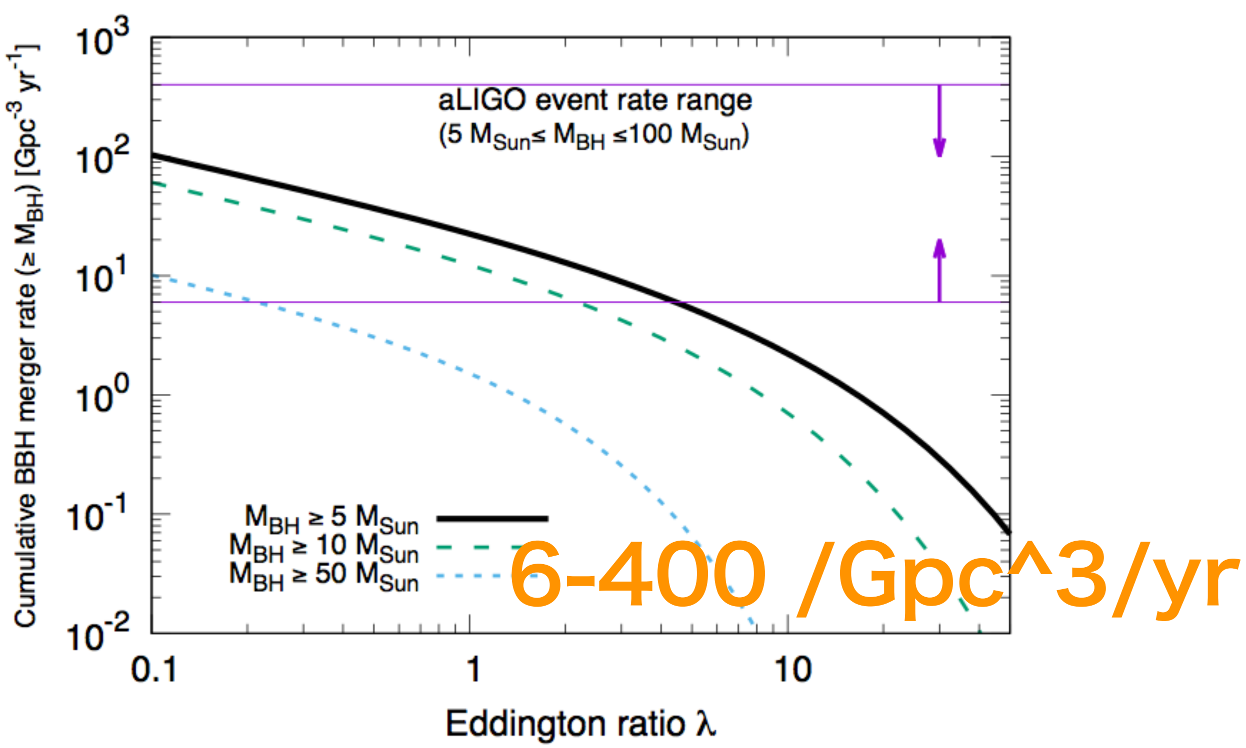

Kinugawa+ MNRAS456(2015)1093

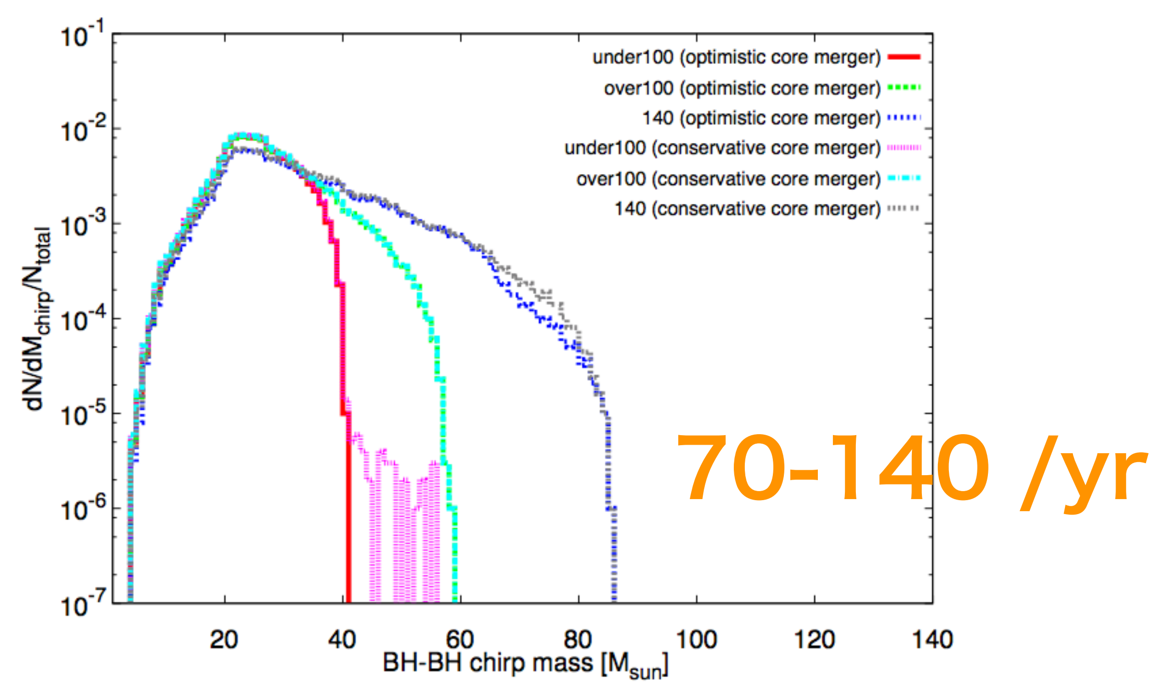

重力波観測の将来計画

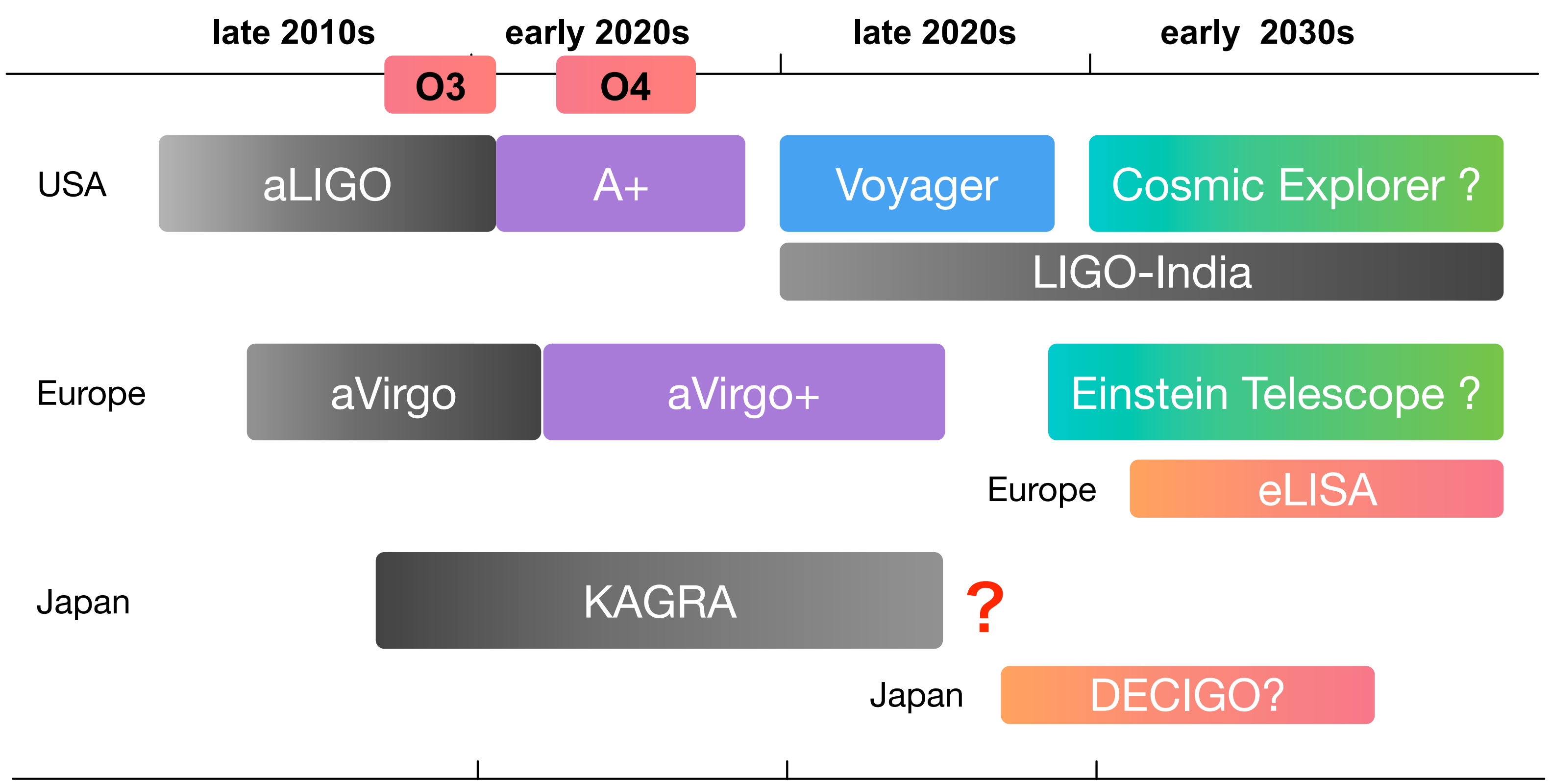

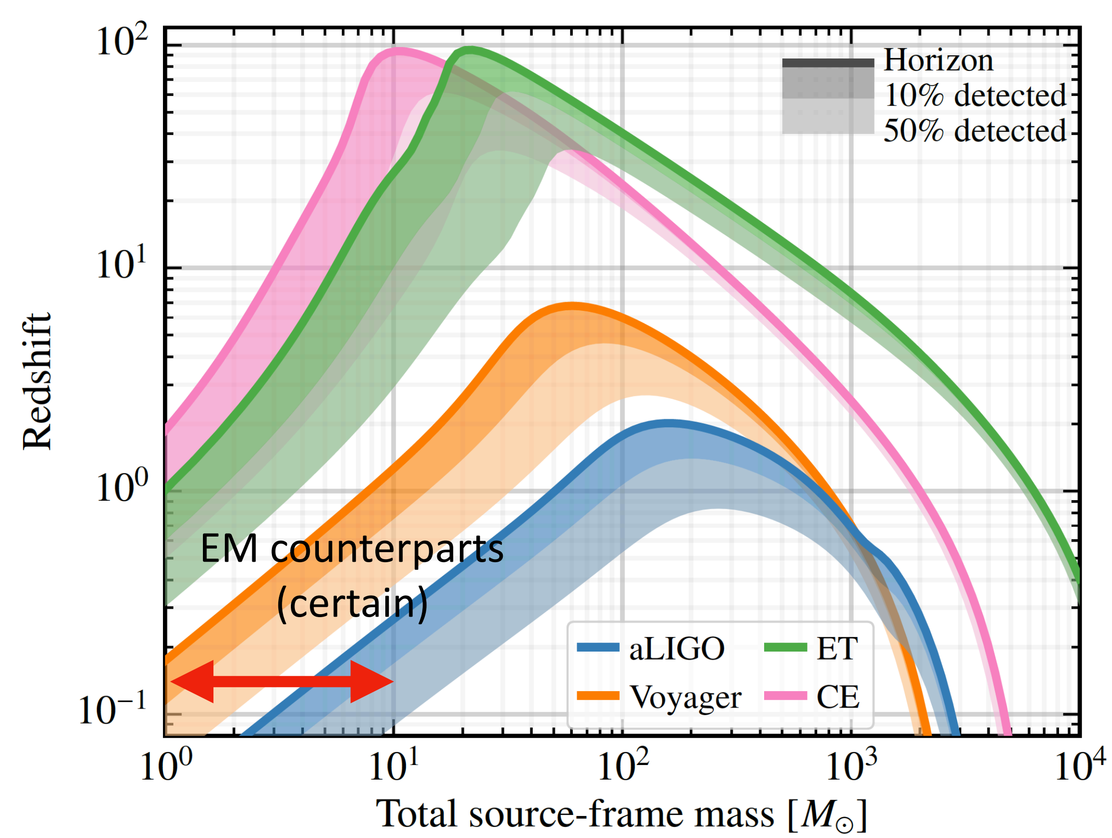

Evan Hall, MIT

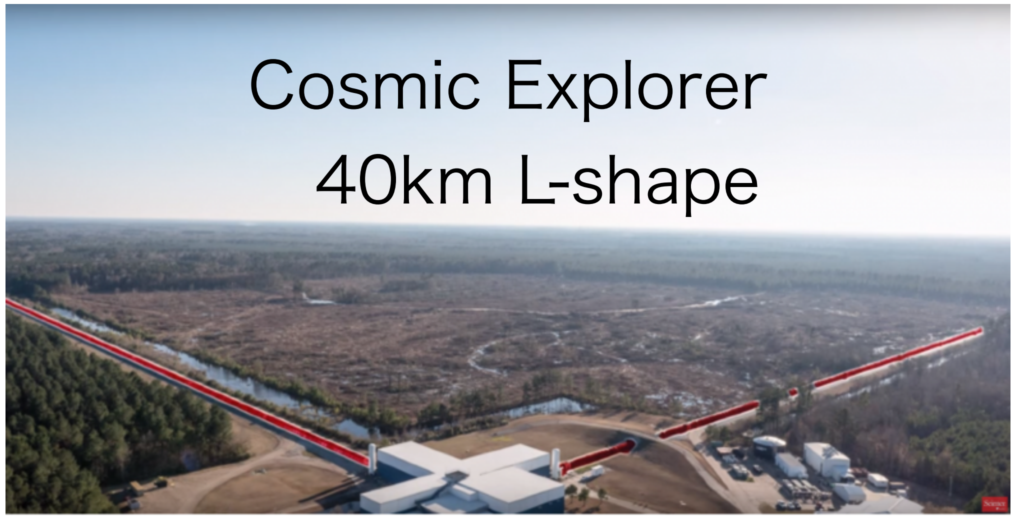

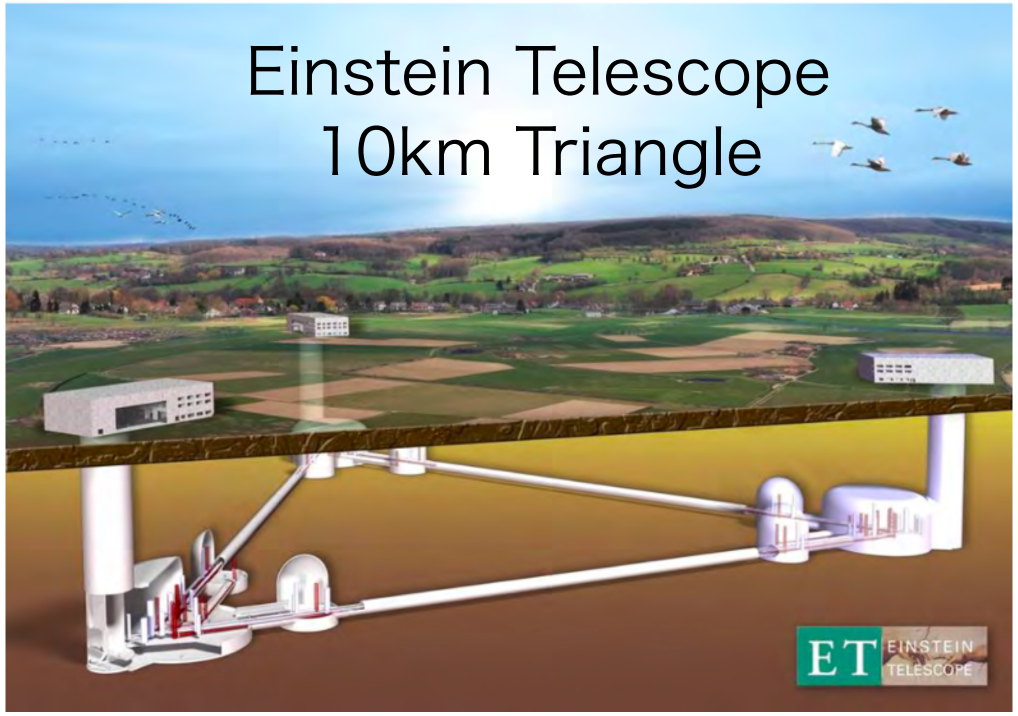

2018/10

Fermi衛星チーム，ガンマ線バースト天体
カタログで21星座を命名

https://fermi.gsfc.nasa.gov/science/constellations/

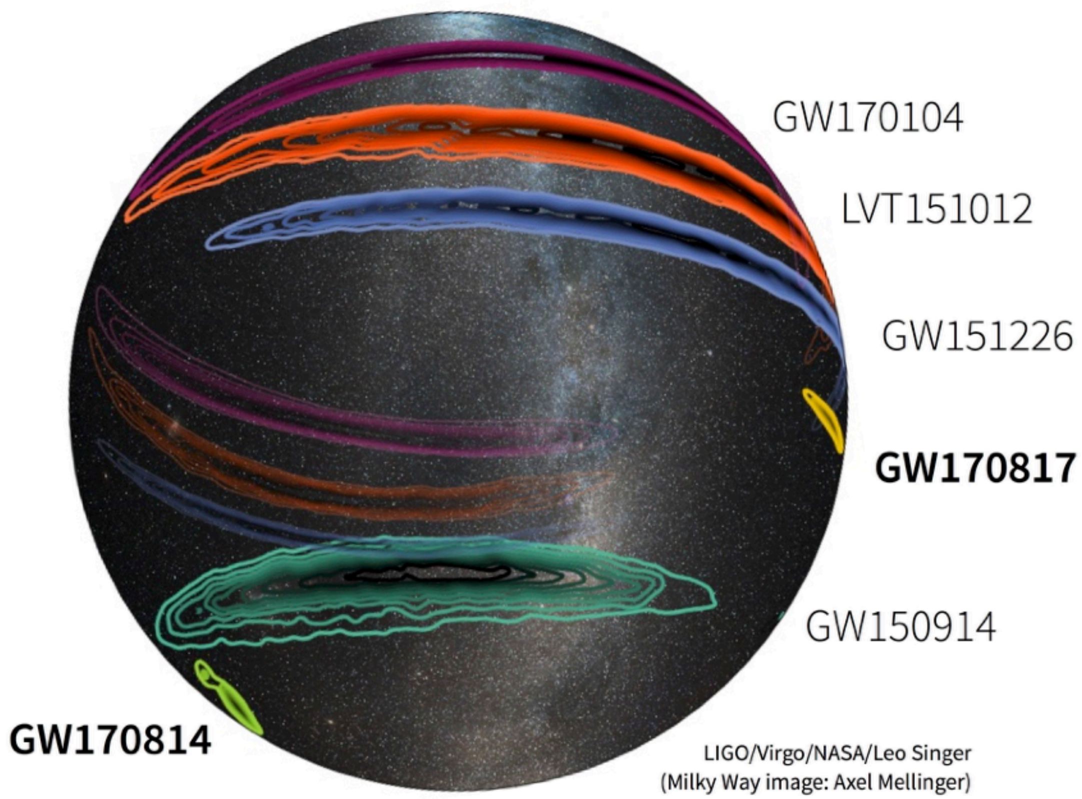

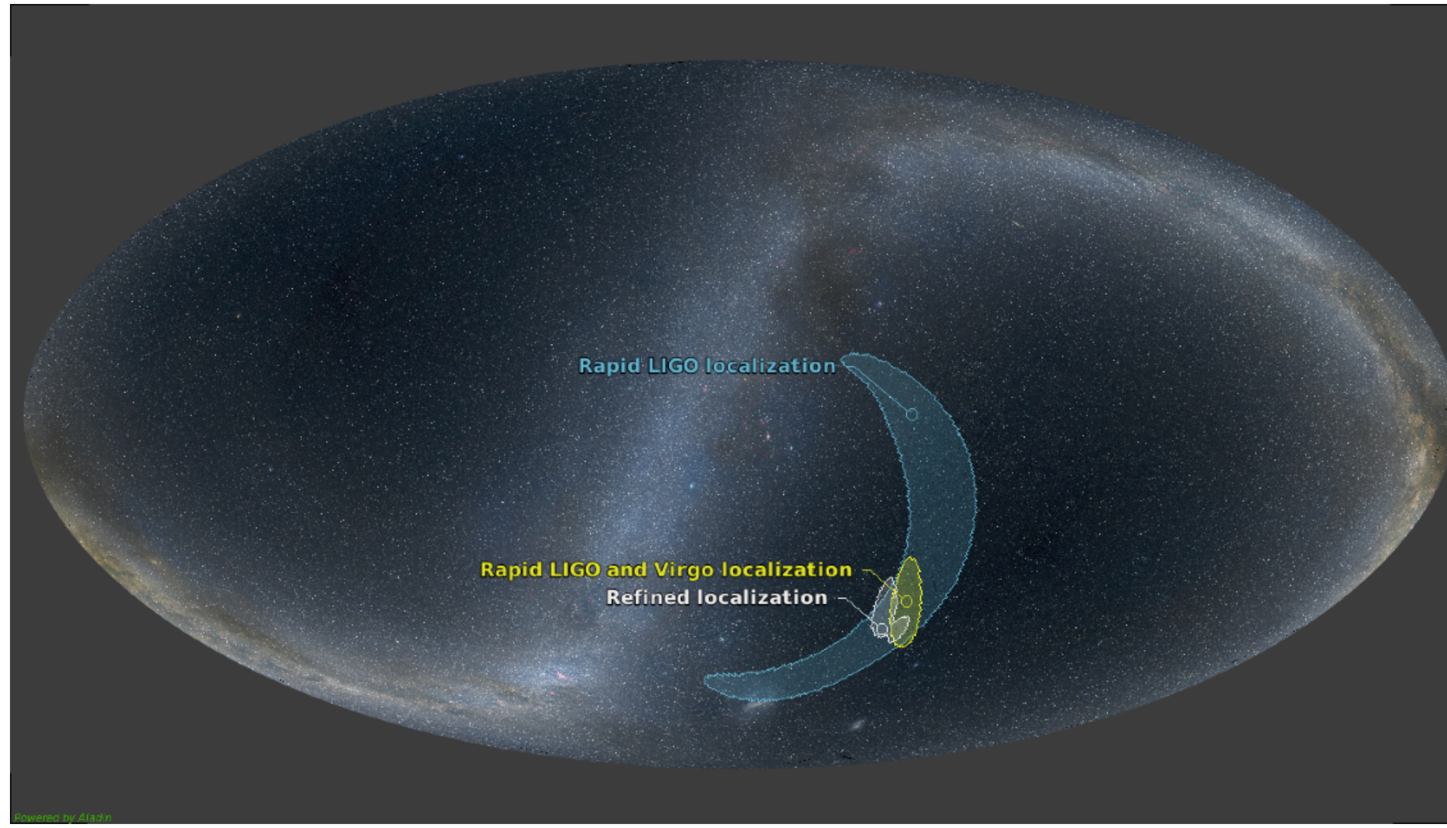

http://www.virgo-gw.eu/skymap.html

重力波源が特定されたのは，まだ１つ.

202x/xx
LIGO/Virgo/KAGRAチーム,
重力波天体カタログで108星座を命名

しかし
2020年12月から始まる観測で,
週に数回，BH-BH？
月に１回，NS-NS？

宇宙空間での観測がはじまれば,
1日に10回，BH-BH ??